Study on Three-level DC/DC Converter with Coupled Inductors

Ruiyang Qin

Thesis submitted to the faculty of the
Virginia Polytechnic Institute and State University
in partial fulfillment of the requirements for the degree of

Master of Science
In
Electrical Engineering

Fred C. Lee, Chair
Qiang Li
Rolando Burgos

September 6th, 2016
Blacksburg, Virginia

Keywords: Coupled inductors, Magnetic Integration, Multi-phase Three-level DC/DC, Interleaving

Study on Three-level DC/DC Converter with Coupled Inductors

Ruiyang Qin

(Abstract)

High power multi-level converters are deemed as the mainstay power conversion technology for renewable energy systems including the battery storage system, PV farm and electrical vehicle charge station. This thesis is focused on the study of three-level DC/DC converter with multi-phase interleaved structure, with coupled and integrated magnetics to achieve high power density. The proposed interleaved phased legs offer the benefit of output current ripple reduction, while inversed coupled inductors can suppress the circulating current between phase legs. Compared with conventional non-interleaving three-level DC/DC converter with non-coupling inductors, both inductor current ripple and output current ripple are largely reduced by interleaving with inverse-coupled inductors.

Because of the non-linearity of the inductor coupling, the equivalent circuit model is developed for the proposed interleaving structure. The model identifies the existence of multiple equivalent inductances during one switching cycle. A combination of them determines the inductor current ripple and dynamics of the system. By virtue of inverse coupling and means of controlling the coupling coefficients, one can minimize the current ripple and the unwanted circulating current.

To further reduce the magnetic volume, the four inductors in two-phase three-level DC/DC converter are integrated into one common structure, incorporating the negative coupling effects. The integrated magnetic structure can effectively suppress the circulating current and reduce the inductor current ripple and it is easy to manufacture. This thesis provides an equivalent circuit model to facilitate the design optimization of the integrated system.

A prototype of integrated coupled inductors is assembled with nano-crystalline C-C core and powder block core. It is tested with both impedance analyzer and single pulse tester, to guarantee proper mutual inductance for inductor current ripple and output current ripple target. With a two-phase three-level DC/DC converter hardware, the concept of integrated coupled inductors is verified, showing its good performance in high-voltage, high-power conversion applications.

Study on Three-level DC/DC Converter with Coupled Inductors

Ruiyang Qin

(General Audience Abstract)

With the demanding energy consumption globally, there is an increasing trend for the requirement of high efficiency power converters with high power density. The application for renewable energies including the PV farm, battery storage system and electrical vehicle become more and more important for the sustainable development of society. High-power, high-voltage DC/DC converters can fulfill the role for such renewable energy power conversion. In this paper, a multi-phase multi-level DC/DC converter solution suitable for high-power, high-voltage application is analyzed and designed. With the techniques including interleaving operation and inverse coupled inductors, the power density for the power conversion is increased while keeping a high system efficiency.

The discussed power converter in this thesis demonstrated a solution for high-power, high-voltage DC/DC power conversion with high efficiency. And the concept is verified with real hardware experimental results, showing its good performance for a 200kW power conversion system.

Acknowledgement

First of all, I would like to express my deepest gratitude for my advisor, Professor Fred C. Lee, for his generous and inspiring instruction, guidance and support for my study at Center for Power Electronics System for the past three years. Dr. Lee's instruction is a precious treasure for me, and I am benefited not only in intellectual aspect, but also for logic thinking and earnest attitude toward research and everything in everyday life. I believe I'll be blessed in the future work because of my experience studying with Dr. Lee in CPES.

I also would like to thank Dr. Dushan Boroyevich, Dr. Rolando Burgos, and Dr. Qiang Li, for their instructions and guidance within the Renewable Energy and Nanogrids (REN) group. Their kind and honest suggestions for my work gives me more in-depth understanding and idea of research.

I would like to appreciate all the colleagues and students from CPES: Dr. Yang Jiao, Dr. Mingkai Mu, Dr. Lingxiao Xue, Mr. Wei Zhang, Dr. Zhemin Zhang, Mr. Xiucheng Huang, Mr. Zhengyang Liu, Mr. Jun Wang, Mr. Ming Lv, Mr. Yuchen Yang, Mr. Dongbin Hou, Mr. Chao Fei, Mr. Qiong Wang, Mr. Fang Chen, Mr. Chi Li, Ms. Rashidi Mehrabadi Niloofar, Mr. Yadong Lv, Mr. Yi-Hsun Hsieh. I also want to thank Mr. Bin Li, Mr. Shishuo Zhao, Mr. Chen Li, Mr. Tinge Ge, Ms. Bingyao Sun, Mr. Zichen Miao, Mr. Tao Liu, Mr. Kai Li for their help. It's my great honor working with all the colleagues above.

I want to thank all the CPES staffs, for their great help making it possible for me to study at CPES: Ms. Teresa Shaw, Mr. David Gilham, Ms. Linda Long, Ms. Teresa Rose, and Ms. Marianne Hawthorne.

At last, I will give my greatest appreciation for my parents Dr. Li Qin and Ms. Juhong Hu. Thank you for your selfless understanding, support and love for my career and life.

This work was supported by the WBG High-Power Converters & Systems (WBG-HPCS, formerly REN) at CPES (ABB, Delta Electronics, GE Power Conversion, Huawei Technologies, Keysight Technologies, Rockwell)

Table of Contents

Table of Figures

Chapter 1 Introduction

1.1 Research Background

There is a growing interest on the application of renewable energy systems with the PV farm, energy storage system or electrical vehicle charge station in recent years [1][2][3][4]. Due to the limitation on voltage rating, switching frequency and cost of semiconductor devices [5], multilevel converters have been widely used in the area of high-voltage, high-power renewable energy systems. It gives lower harmonic distortion such that a smaller out filter is needed with improved power density. Another main advantage is that the voltage stress on the switches will be reduced and a high-voltage, high-power converter can be implemented with lower voltage rating semiconductor devices. A typical multilevel power conversion system with renewable energy applications is shown in Figure 1.1, where there are two-stage AC/DC and DC/DC converters connected by a high voltage DC-link.

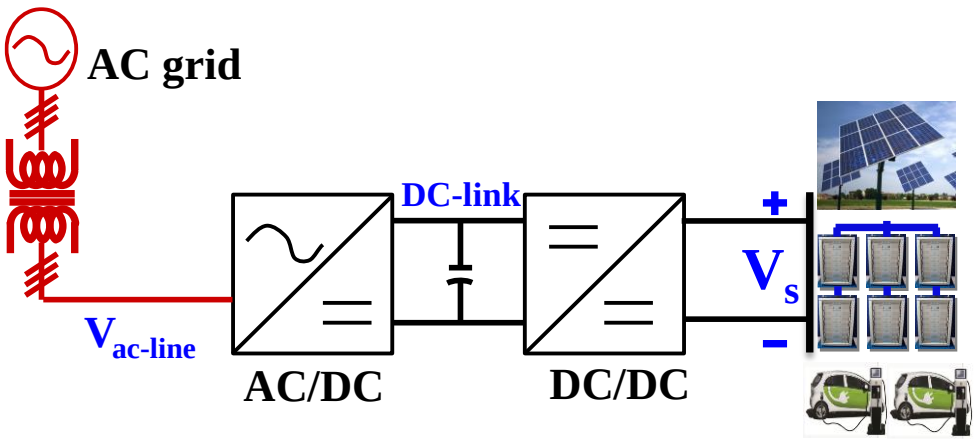

Figure 1.1 Two-stage power conversion system with renewable energy systems

In Figure 1.2, state-of-the-art high power device rating is demonstrated. For the IGBT, the single module can handle only several kilo volt voltage. And for other higher voltage rating devices like GTO, the rating can be up to 12kV and 1500A. However, because of high switching losses, typical operating frequency is up to 500 Hz. We can also connect the device in serial for higher voltage rating, but the voltage sharing for each device cannot be easily achieved because of parameter mismatch. As a result, it is difficult to satisfy the high-voltage, high-power density requirement only by applying higher voltage rating devices.

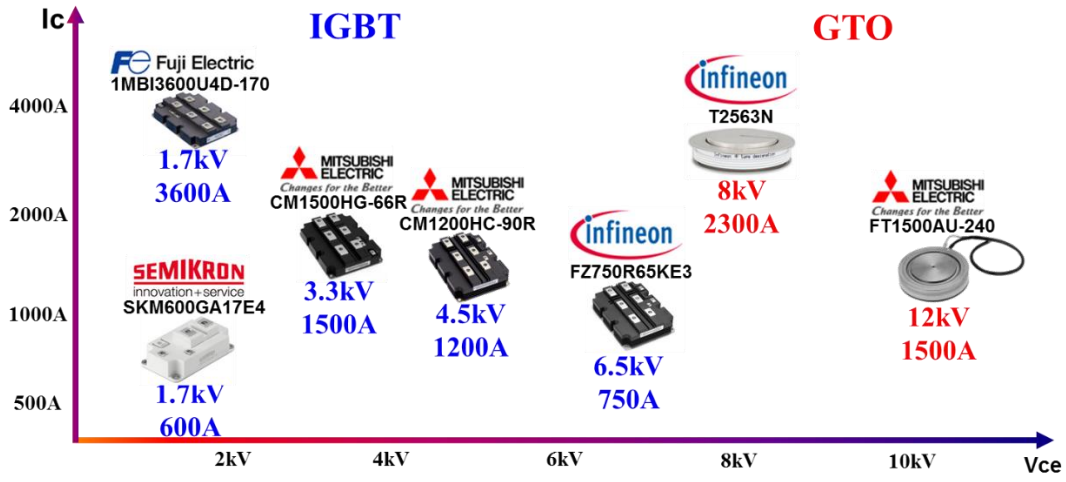

Figure 1.2 State-of-art high voltage device rating

The multilevel converter concept was first proposed by Nabae [6], which was a neutral-point-clamped (NPC) three-level inverter that can generate the neutral-point voltage besides the positive and negative bus voltages. The advantages of this multilevel converter include lower voltage stress on switches, lower EMI issue and less harmonic distortion. In terms of DC/DC application with NPC topology, Pinheiro and Barbi [7] used a three-level NPC leg in DC/DC converters with galvanic isolation. Okui and Irie [8] used two three-level diode-clamp inverters to build a five-level DC/DC converter. Foch [9] first applied the multi-level flying-capacitor converter in DC/DC applications. Ruan [10] applied the bidirectional flying capacitor converter

for the hybrid fuel cell power system where a bidirectional converter needs to be employed between DC bus and battery to control the charge and discharge current. In terms of multi-level buck/boost topology, Lee [11] mentioned the application of three-level boost converter for high power and/or high voltage applications and the three-level bidirectional DC/DC converter can be used in the renewable energy system where the power flow is bidirectional [12]. A generalized multilevel converter topology is reported that can balance each dc voltage level automatically without any assistance from other circuits [13]. Ruan [14][15] gives a systematic method to derive a family of six non-isolated three-level DC/DC converters: buck, boost, buck-boost, Cuk, sepic and zeta from the standard buck and boost converters.

The three-level NPC circuit can be extended to higher levels, thus a lower voltage stress on semiconductor components and better harmonic performance [16][17]. [18] explored the application of two back-to-back connected five-level diode-clamped converter legs. Fang Z. Peng [19][20] used the four-level flying capacitor topology based DC/DC converter for PHEVs. The inductance required can be largely reduced with a fixed duty cycle, thus power density can be increased as well as the overall efficiency. Huang [21] applied five-level flying capacitor topology for high-voltage, high-frequency DC/DC converter with solid state transformer. Barbi [22][23][24][25] proposed the non-isolated five-level structure for buck-type, boost-type and the bidirectional type suitable for high power applications. However, a large number of devices will be needed and the system structure and control scheme will become more complex as the level increases. Capacitor voltage balancing control will also become unattainable with higher levels.

The subject of multi-level converters has been widely pursued over the last three decades. In principle, the concept can be extended to many levels for very high voltage applications. However, due to the inherent complexity in topological structure, capacitor voltage balancing, and

associated controls, commercialization of the multilevel converters have been limited only to five level to date.

1.2 Configuration of Multi-phase Three-level DC/DC Converter

In terms of non-isolated three-level DC/DC converter, there are two major suitable candidates, flying-capacitor and three-level buck, which are shown in the Figure 1.3 and Figure 1.4, respectively. For flying-capacitor, there is 180 degree phase shift between switch S1 and S2, and gate signals for S4 and S3 are complimentary to S1 and S2, respectively. For three-level buck, the 180 degree phase shift is between switch S1 and S4.

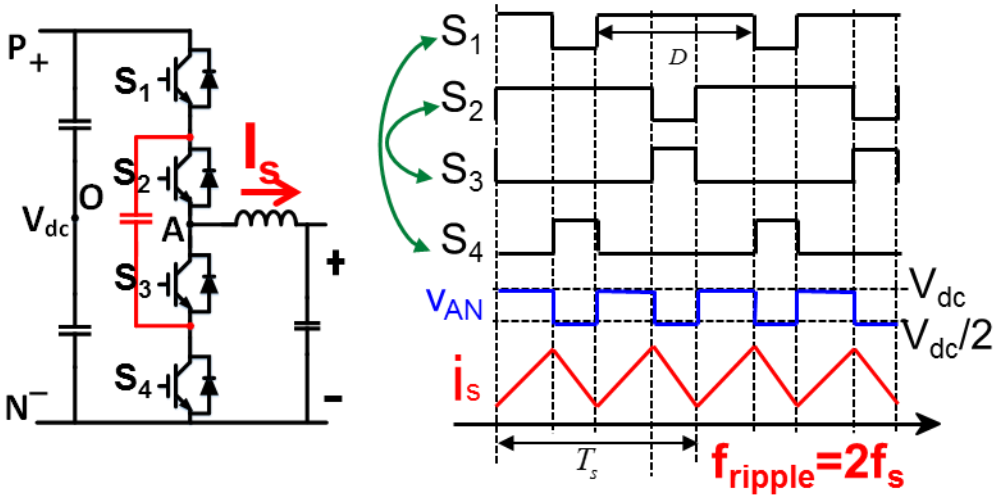

Figure 1.3 Three-level flying-capacitor topology

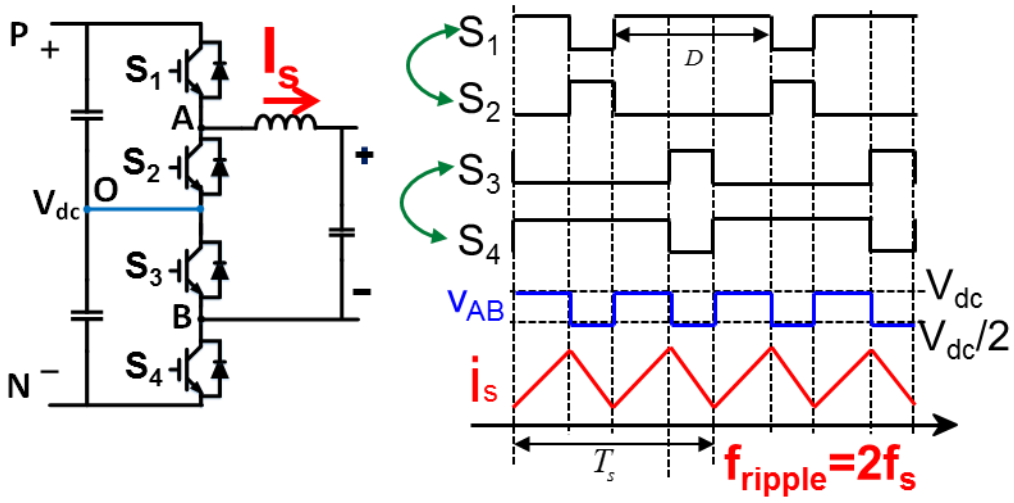

Figure 1.4 Three-level buck topology

For these two types of topologies, the voltage polarity of both input and output sides are fixed while the current can flow in both directions, such that the power can also flow bidirectional. With the three-level structure, the inductor current ripple frequency will be twice the switching frequency and size of passive components can be reduced. For capacitor voltage balance issue, flying-capacitor needs to keep the voltage of flying cap at half of the dc link voltage Vdc [26] while for three-level buck, neutral point voltage should be balanced. For flying-capacitor, it gives common ground for input and output sides, but one more flying capacitor is required compared with the three-level buck if considering the part number count. Based on these comparisons, the three-level buck topology is chosen and analyzed in the rest of this paper for its simplicity and low part number count.

For the power conversion system shown in the Figure 1.1, the AC/DC stage has been built with three-level active neutral-point-clamped topology to achieve good performance and high power density with 1200V/400A IGBT at the power rating of 200kW [27]. Taking safe margin of the semiconductor device into consideration, a 1200V DC link is applied to connect AC/DC and DC/DC stages. To have a modularized structure for the whole system, the same device is desired

to be employed for the DC/DC stage as AC/DC stage. Under the 200kW power rating, the lower the voltage of DC application side, the more phase legs are needed to be paralleled at DC/DC stage because of the higher possible RMS current. Assuming that the range of DC application side voltage is 500V-800V, at least two paralleled three-level buck phase legs are needed to handle the 200kW power rating with enough safe margin considering 400A current rating.

Figure 1.5 gives the complete three-level power conversion system structure with 200kW power rating with bidirectional power flow.

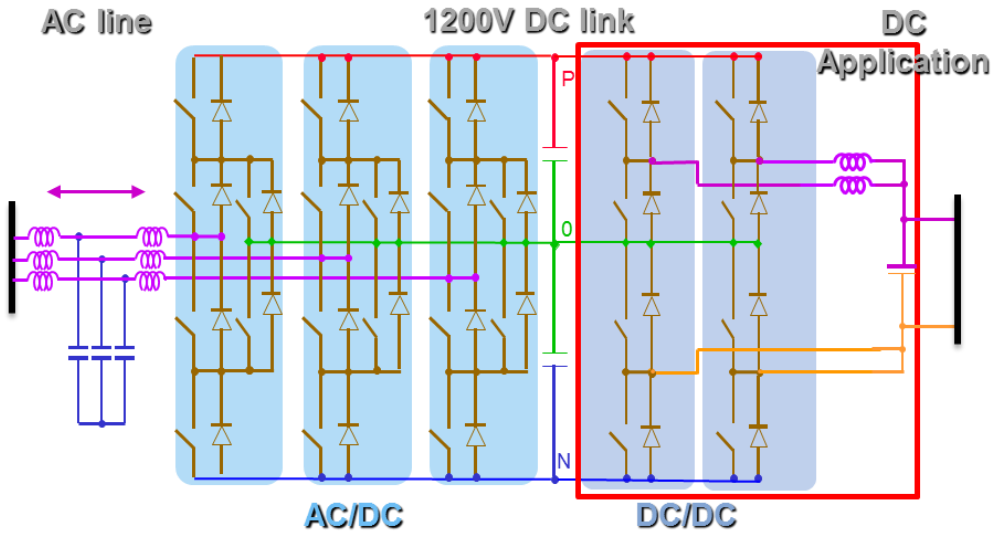

Figure 1.5 Three-level power conversion system

1.3 Objectives and Thesis Outline

With the configuration of the two-phase paralleled three-level DC/DC determined, this paper focuses on the study to improve the power density and efficiency of the three-level DC/DC conversion by addressing the magnetic design and integration process.

Chapter 1 provides the fundamental introduction for the two-stage three-level power conversion system with its application for renewable energy systems. Possible topology candidates

for DC/DC conversion are compared and a two-phase three-level buck converter is applied as the DC/DC conversion stage within the conversion system based on the power rating and performance requirements. The conversion system aims at the power rating of 200kW, with bidirectional power flow.

In chapter 2, non-interleaving and two types of interleaving methods are compared for the paralleled three-level DC/DC converter. Interleaving operation can reduce the output current ripple, but may cause significant inductor current ripple. This phenomenon is analyzed using equivalent circuit of the converter. By applying the inverse coupling of two inductors, the circulating current caused by interleaving can be suppressed. Three different scenarios for DC/DC converter, including non-interleaving with non-coupling inductors, N-type interleaving with inversed coupled inductors and Z-type interleaving with inversed coupled inductors, are analyzed carefully in terms of current ripple and common-noise comparison.

Chapter 3 addresses the design issues concerning the inverse coupling of the two inductors in two-phase interleaved three-level DC/DC converter. Because of the coupling of two inductors, together with their associated switching networks, inductors act like nonlinear devices. It offers additional benefits of containing the circulating current and minimizing total output current ripple. This chapter presents the mathematical model for such coupled system and decouple it based on the equivalent inductance concept. Design guidelines for coupling are provided according to inductor current ripple and total output current ripple requirements.

Chapter 4 presents further improvement by integrating all the magnetics in a common structure. An integrated coupled inductors structure was proposed, and it is hard to analyze the coupling directly. Again, equivalent inductance analysis is applied, and can provide the guideline for coupling design based on the current ripple target. The benefit of magnetic integration is

demonstrated by comparing with inverse coupling of two inductors. The concept of integrated coupled inductors is verified with a prototype built with nano-crystalline magnetic material. Hardware experiment results are demonstrated and discussed.

In the last chapter, the conclusion for the paper is summarized, emphasizing the benefit of integrated coupled inductors with interleaved phase legs to push for high-power, high-performance DC/DC conversion in renewable energy systems. Possible future work is introduced.

Chapter 2 Evaluation on Method of Interleaving for Paralleled Three-level DC/DC Converter

As introduced in the previous chapter, two phase legs are employed for the DC/DC stage considering the high-power, high-current rating requirements. This chapter will present an overview of possible interleaving methods for the paralleled phase legs in the three-level DC/DC converter, including non-interleaving, N-type interleaving and Z-type interleaving methods. The comparison of different methods will be based on their effects on inductor current ripple and output current ripple. An equivalent circuit is used to analyze the difference on ripple and give more physical insight into why inverse coupled inductors can be beneficial with interleaving. In addition, the common-mode voltage for all three cases are compared. The optimal interleaving method is selected with trade-off between ripple reduction effect and common-mode voltage magnitude.

2.1 Interleaving Methods

2.1.1 In-phase Method

As for in-phase method [28], the two phase legs will have the same switching sequence and there is no phase shift between the two legs. Figure 2.1 gives the circuit diagram and corresponding waveforms. For both phase leg A and B, there will be 180 degree phase shift between outer switches, S_{1a} and S_{4a}, or S_{1b} and S_{4b}. The corresponding inner switches, S_{2a} and S_{3a}, or S_{2b} and S_{3b}, have the complementary gate signals with the outer switches to avoid shoot through across the DC bus. Because of the non-interleaving method, two phase legs share the identical

output voltage and inductor current waveform. Clearly, this method is good for its simplicity. However, since the output current is the summation of two inductor currents, the output current ripple is large. Considering the possible scenario that the number of phase legs would increase as the system power rating requirement increases, the output current ripple would become unacceptable.

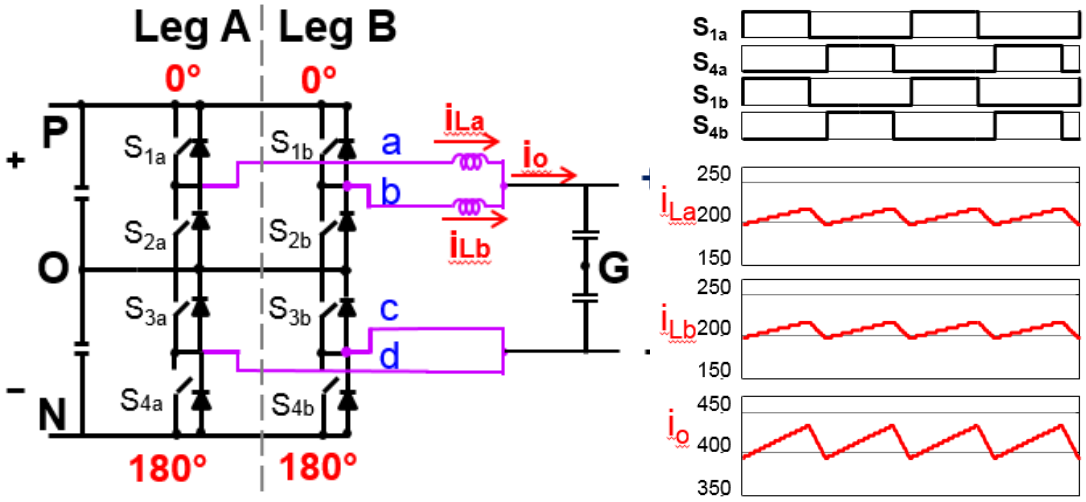

Figure 2.1 In-phase method

2.1.2 N-type Interleaving Method

In comparison with non-interleaving, interleaving methods were introduced to reduce the output current ripple. Figure 2.2 gives the circuit diagram and waveforms of N-type [29]. Since the sequence of switching is S_{1a}-S_{4a}-S_{1b}-S_{4b}, there is 90 degree phase shift between every switch. The name N-type comes from its switching sequence. Because of the ripple-cancelling effect, the output current ripple can be reduced for both types of interleaving. However, it can be noticed from the waveforms that inductor current ripple is huge, and causes problems including much

higher switching loss and conduction loss on the switches, and also potential saturation of the magnetics. As a result, interleaving methods cannot be applied directly with the phase legs.

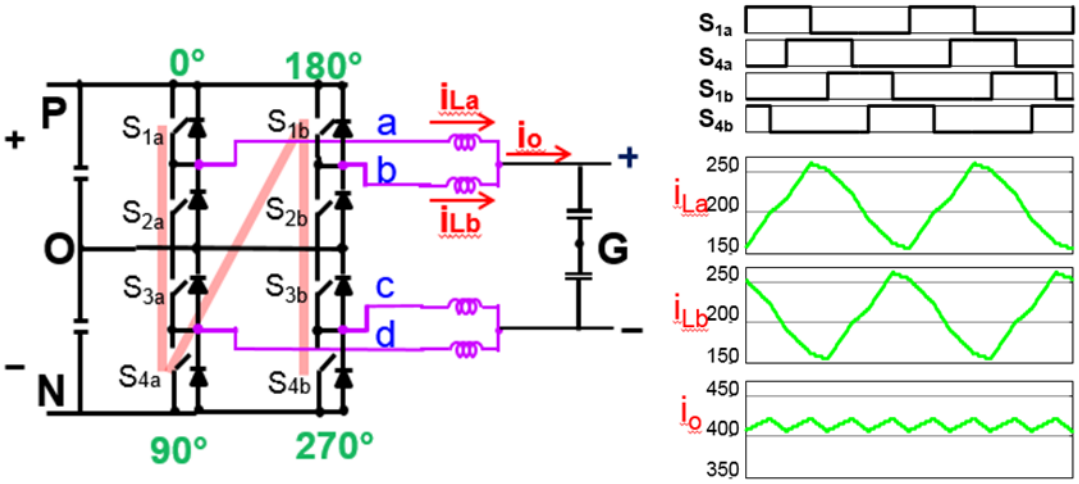

Figure 2.2 N-type interleaving method

2.1.3 Z-type Interleaving Method

The other type of interleaving for two-phase paralleled three-level DC/DC conversion is called Z-type. Figure 2.3 gives the circuit diagram and waveforms of Z-type interleaving [30]. The sequence of switching is S_{1a}-S_{1b}-S_{4a}-S_{4b}, with 90 degree phase shift between every switch. Similar as N-type interleaving, it can be noticed that there are reduced output current ripple and large inductor current ripple.

Figure 2.4 compared the output current ripple and inductor current ripple of the three methods introduced above, with input voltage V_{in}=1200V, duty ratio D=0.4, switching frequency f_{sw}=20kHz, four arm inductors L_a=L_b=L_c=L_d=60μH. Clearly, interleaving has the benefit of reduced output current ripple, with increased inductor current ripple.

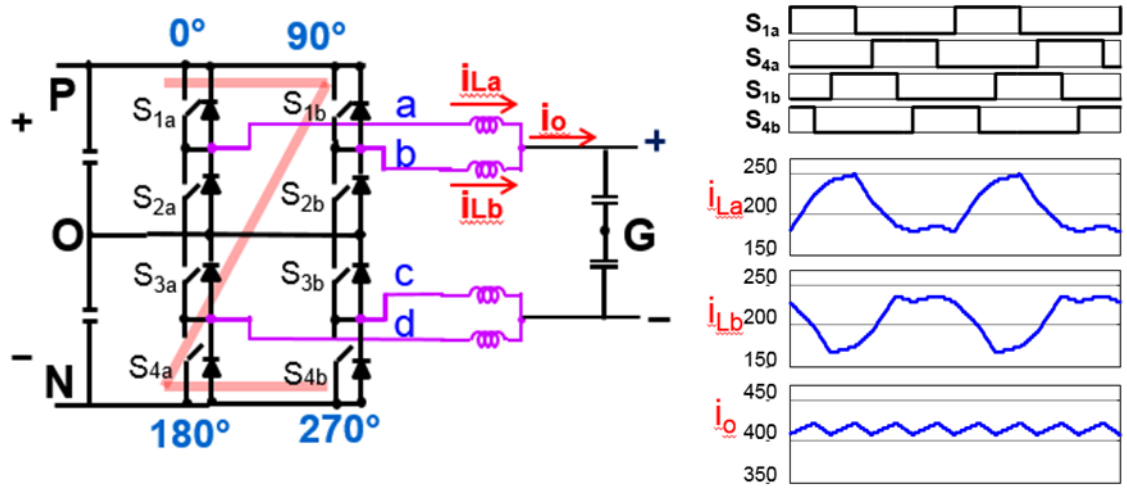

Figure 2.3 Z-type interleaving method

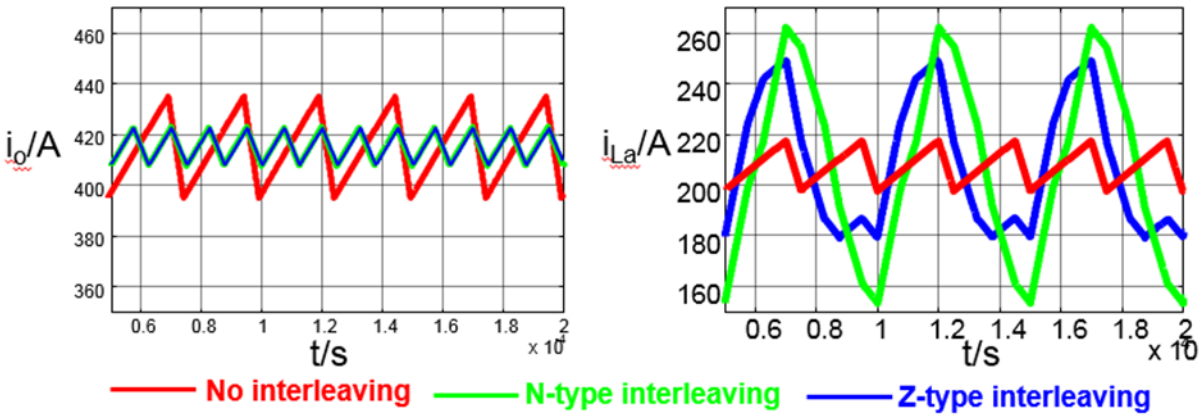

Figure 2.4 Current ripple comparison of different interleaving method

2.2 Inductor Current Ripple Analysis of Different Interleaving Methods

2.2.1 Equivalent Circuit of the Converter

To analyze the difference of inductor current ripples, the equivalent circuit of the converter is first derived. For the paralleled phase legs, there are in fact four three-terminal switches, S_{1a} and S_{2a}, or S_{3a} and S_{4a}, or S_{1b} and S_{2b}, or S_{3b} and S_{4b}. And for each of the three-terminal switches, it can be represented by one controlled voltage source in the equivalent circuit for the simplicity of

analysis, namely v_{ao}, v_{bo}, v_{co} and v_{do}. As shown in the Figure 2.5, the inductor current i_{La} and i_{Lb} can be decomposed by two parts. In detail, the inductor current i_{La} can be separated as common-mode current i_{cm} and differential-mode current i_{dm}, and the relationship can be described as,

$$i_{La} = i_{cm} + i_{dm} \tag{2.1}$$

Similarly, the inductor current i_{Lb} can be seen as the difference between common-mode current i_{cm} and differential-mode current i_{dm}.

$$i_{Lb} = i_{cm} - i_{dm} \tag{2.2}$$

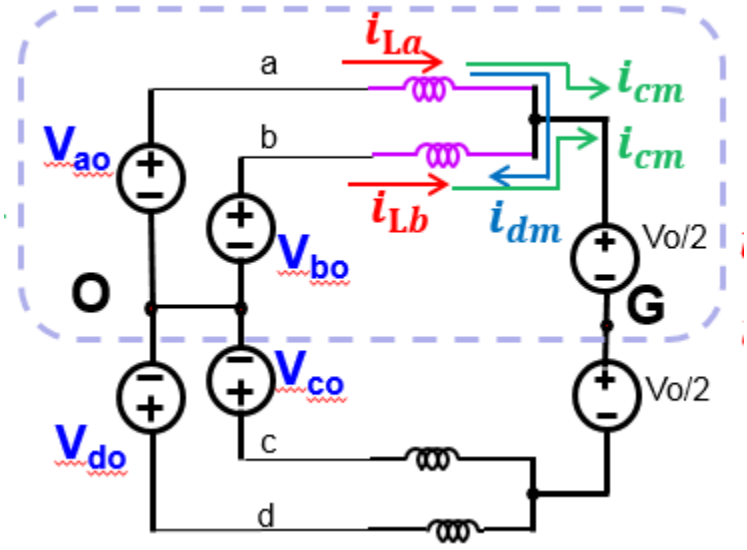

Figure 2.5 Equivalent circuit of the converter

By superposition, one can divide the circuit into two parts, depending on the common-mode and differential-mode current difference defined by (2.1) and (2.2) [30]. Figure 2.6 gives the equivalent circuits for i_{cm} and i_{dm}. And together, these two circuits are equivalent to the upper part of the circuit in Figure 2.5, as shown in the dashed square. Following this chapter, analysis will focus on the equivalent circuit for the upper part of the circuit, and corresponding inductor current

i_{La} and i_{Lb}. The analysis process and result is similar for inductor current i_{Lc} and i_{Ld} in the lower part of the circuit. For the simplicity of the content, it will not be discussed in detail.

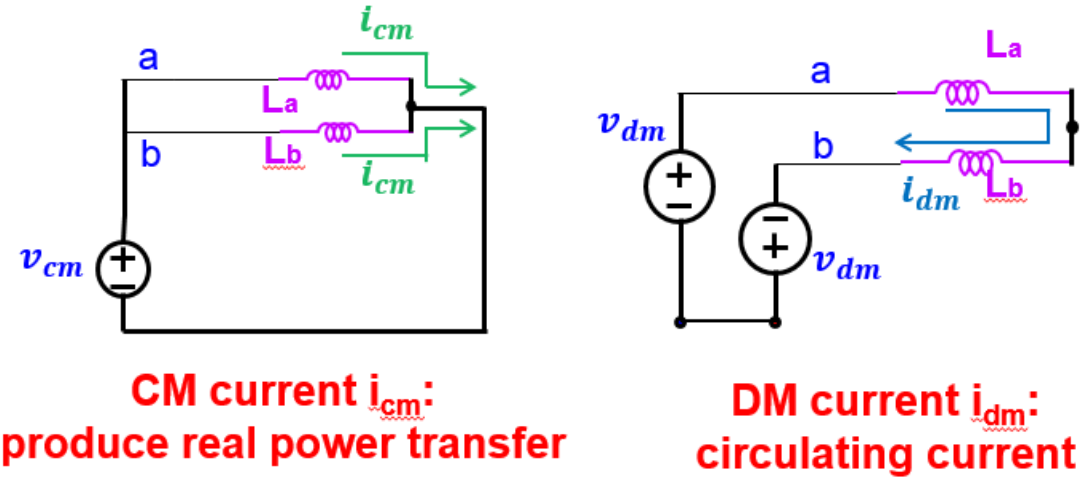

Figure 2.6 Equivalent circuits for common-mode current and differential-mode current

In the equivalent circuit for common-mode current, only a common-mode voltage source is included,

$$v_{cm} = \frac{v_{ao} + v_{bo} - v_{co} - v_{do}}{4} - \frac{v_o}{2} \tag{2.3}$$

And it will generate the same common-mode current i_{cm} in inductor L_a and L_b. Since common-mode current flows to the output side, it produces real power transfer from input to output.

In comparison, the differential-mode voltage source v_{dm} will produce the differential-mode current in the equivalent circuit. And generated i_{dm} is circulating between inductor L_a and L_b. As a result, the differential-mode current i_{dm} can be viewed as a circulating current between the two phase legs, and it should be avoided.

$$v_{dm} = \frac{v_{ao} - v_{bo}}{2} \tag{2.4}$$

Figure 2.7 compares the common-mode current and differential-mode current among different methods including non-interleaving, N-type interleaving and Z-type interleaving. And the simulation condition for the waveform is, V_{in}=1200V, D=0.4, f_{sw}=20kHz, L_a=L_b=L_c=L_d=60uH. From the waveforms for common-mode voltage and current, one can conclude that due to the difference of interleaving, the four controlled voltage sources v_{ao}, v_{bo}, v_{co} and v_{do} in Figure 2.5 will have different voltage sequences, thus causing the difference in common-mode voltage v_{cm} according to (2.3). For non-interleaving, the magnitude of the v_{cm} is large and the frequency is twice the switching frequency. For both N-type and Z-type interleaving, the magnitudes of the v_{cm} are identical and relatively small compared with non-interleaving case. Also the frequency of v_{cm} is four times the switching frequency. Accordingly, the current ripple i_{cm} is smaller in both N-type and Z-type interleaving compared with non-interleaving case.

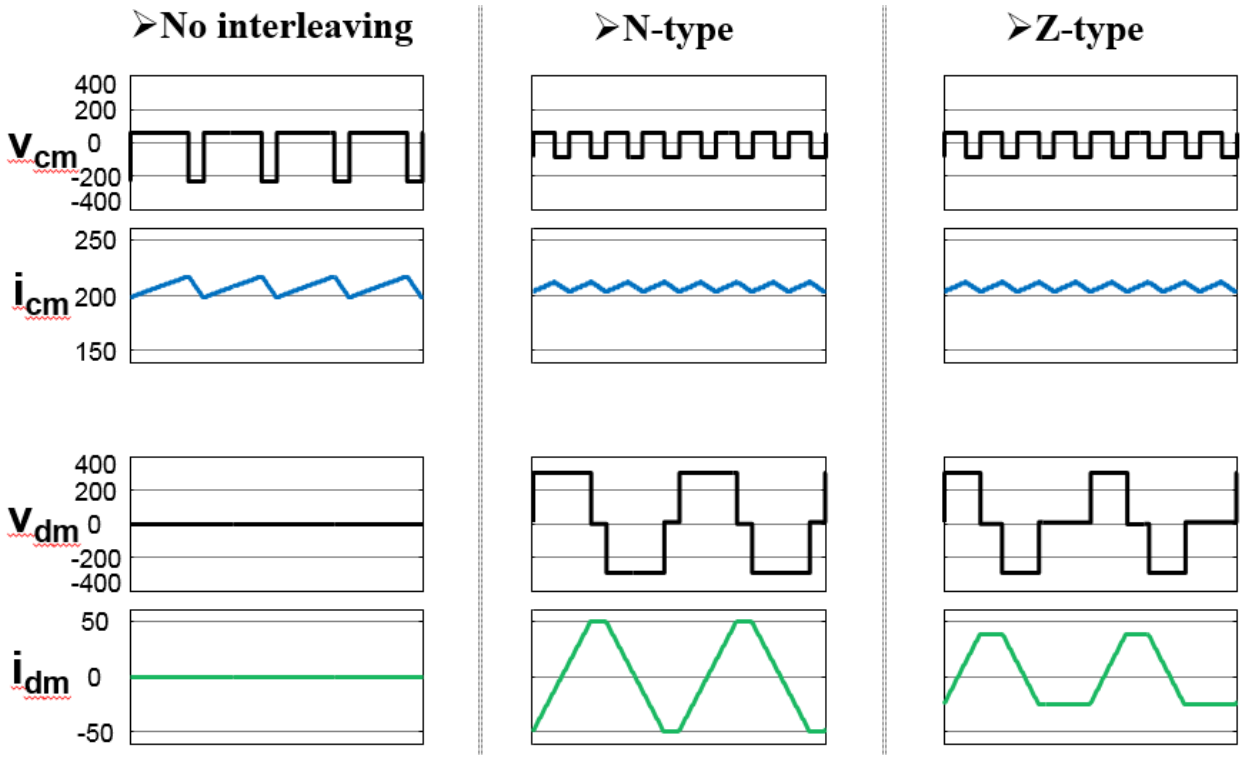

Figure 2.7 Common-mode current and differential-mode current comparison

In terms of differential-mode voltage and current, the two phase legs have identical switching sequences for non-interleaving and v_{dm} will remain zero by (2.4). Since no differential-mode current exists in the non-interleaving case, only current ripple of i_{cm} will contribute to the inductor current ripple. In contrast, because of the interleaving, both N-type and Z-type interleaving will have differential-mode voltage with large magnitude, causing huge differential-mode current ripple, as illustrated in the bottom line of the Figure 2.7. Due to this huge circulating current between the two phase legs, the current ripple on the inductors is not acceptable.

2.2.2 Inductor Current Ripple Reduction by Inverse Coupled Inductors

To suppress the huge inductor current ripple caused by interleaving, the method of applying inverse coupled inductors with the converter was proposed [30]. Figure 2.8 shows the converter with the inverse coupled inductors and two coupled inductors are needed for the two phase legs. For example, the inverse coupling between L_{aa} and L_{bb} is used to suppress the circulating current between them.

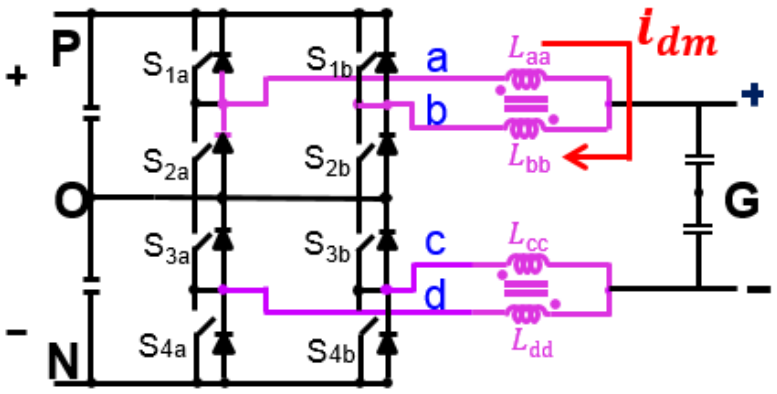

Figure 2.8 Applying inverse coupled inductors with the converter

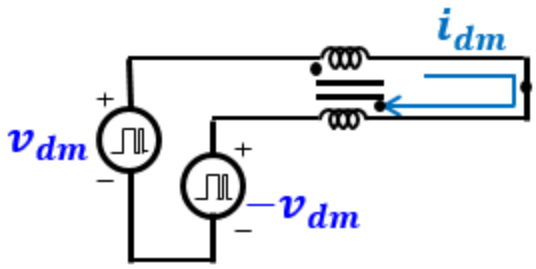

Figure 2.9 Equivalent circuit for differential-mode current with coupled inductors

Following the analysis method in 2.2.1, one can also give the equivalent circuit for the differential-mode current with coupled inductors, as shown in Figure 2.9. Because of the inverse coupling, the differential-mode current sees high impedance in the equivalent circuit, and the differential-mode current ripple will become small.

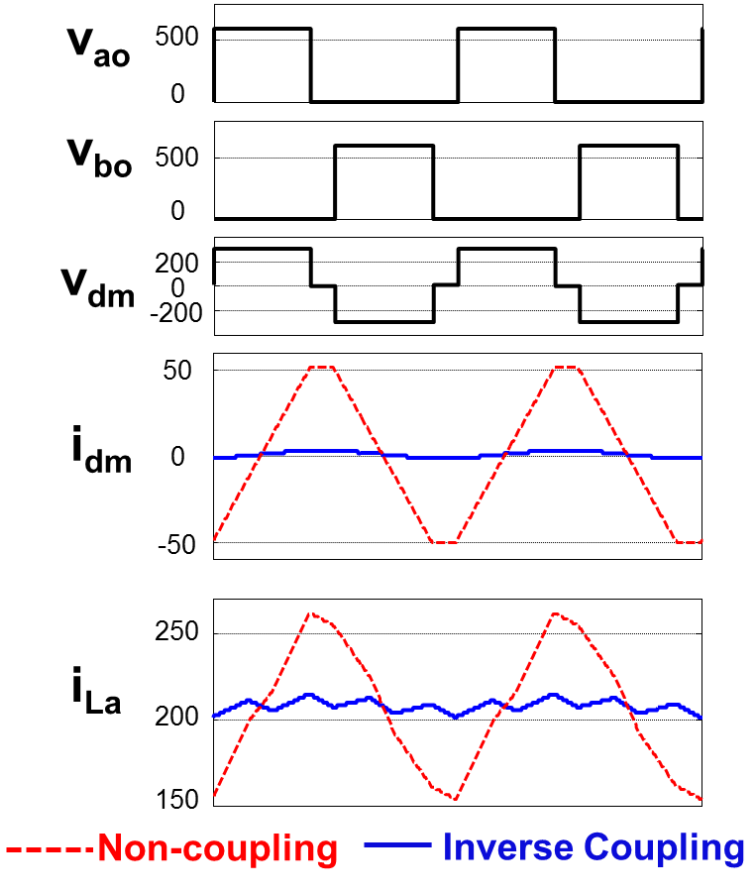

Figure 2.10 Differential-mode current ripple reduction for N-type interleaving

Based on the simulated waveforms in Figure 2.10, for N-type interleaving, the differential-mode current decreases largely by applying inverse coupled inductors. Since the contribution of differential-mode current ripple to the inductor current ripple drops, the overall inductor current ripple drops accordingly by applying the coupled inductors instead of single inductors. The same conclusion can be drawn for Z-type interleaving, as shown in Figure 2.11. The inductor current ripple drops as the differential-mode current ripple is suppressed by inverse coupling.

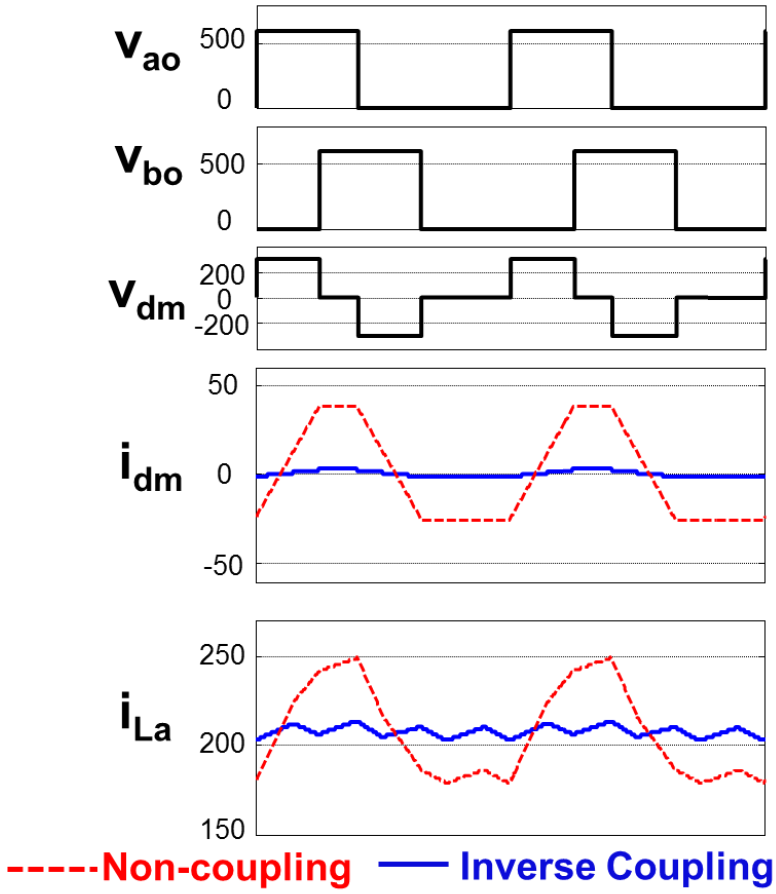

Figure 2.11 Differential-mode current ripple reduction for Z-type interleaving

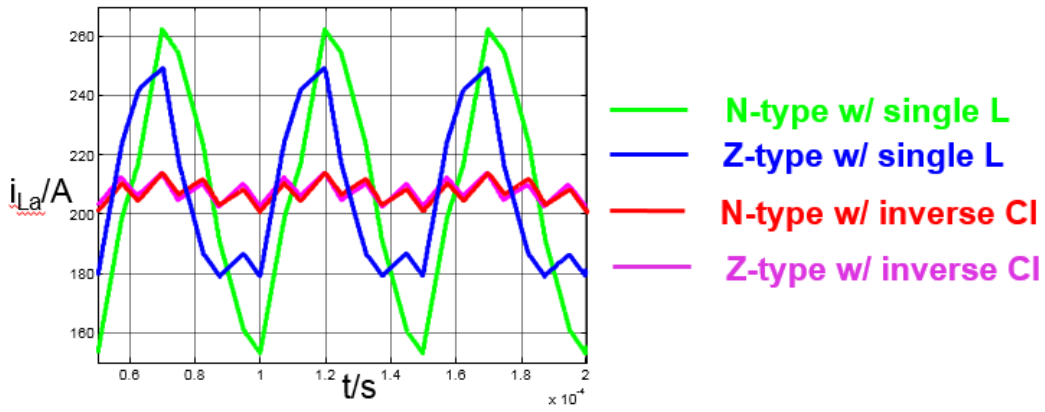

Figure 2.12 Inductor current ripple reduction with inverse coupling

The simulation result in Figure 2.12 verifies the effect of applying inverse coupled inductors, with duty cycle D=0.4. With inverse coupling, either N-type interleaving or Z-type interleaving can reduce the inductor current ripple dramatically compared with applying non-coupling inductors.

2.3 Common-mode Voltage Analysis of Different Interleaving Methods

Although both N-type and Z-type interleaving have the inductor current ripple reduction effect, there will be differences from other important aspects, including the common-mode voltage in terms of the common-mode noise issue of the converter. Figure 2.13 defines the common-mode voltage v_{GO} of the converter,

$$v_{GO} = \frac{v_{ao} + v_{bo} + v_{co} + v_{do}}{4} \tag{2.5}$$

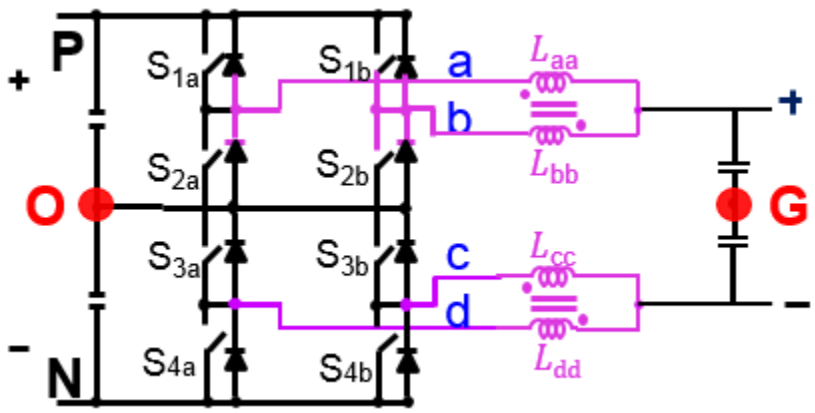

Figure 2.13 Common-mode voltage of the converter

As shown in the Figure 2.14 and Figure 2.15, the common-mode voltage of Z-type interleaving has the first peak at switching frequency in the spectrum, which is the same as the non-interleaving case. Also, the magnitude of the first peak is about the same as non-interleaving. In contrast, the first peak of N-type interleaving is at twice the frequency, with the magnitude reduced to 161dB. As a result, N-type interleaving is much better than the Z-type interleaving for the common-mode noise filter design.

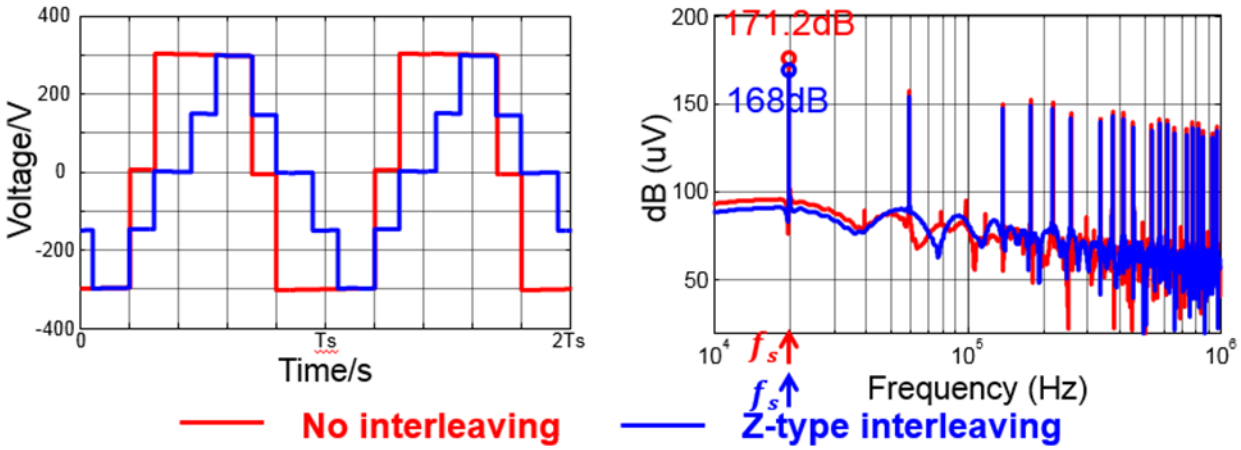

Figure 2.14 CM voltage comparison for Z-type interleaving

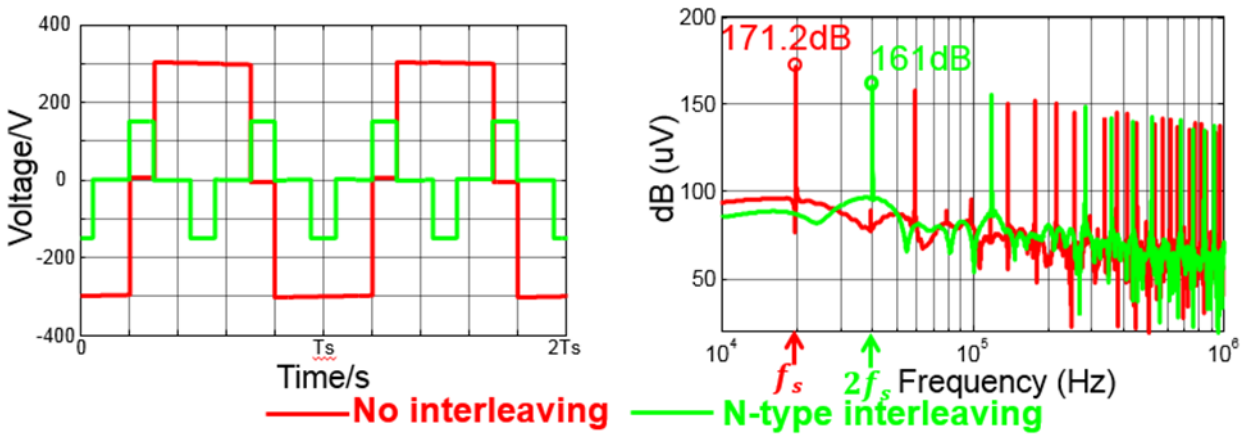

Figure 2.15 CM voltage comparison for N-type interleaving

2.4 Summary

In this chapter, different interleaving methods for the paralleled three-level DC/DC converter are analyzed and compared. To reduce the output current ripple, two types of interleaving methods were proposed, with the indispensable sacrifice in inductor current ripple. Using the equivalent circuit, the concept of circulating current between the phase legs caused by the interleaving is introduced, and inverse coupled inductors are applied to suppress the circulating current and reduce the inductor current ripple.

	Output current ripple	Inductor current ripple	CM voltage
No interleaving w/o coupled inductors	☹	☹	☹
N-type interleaving w/ coupled inductors	☺	☺	☺
Z-type interleaving w/ coupled inductors	☺	☺	☹

Figure 2.16 Summary on different interleaving methods

Three possible operating methods are listed in Figure 2.16, including non-interleaving with single inductors, N-type interleaving with inverse coupled inductors, and Z-type interleaving with inverse coupled inductors. The conventional non-interleaving serves as the benchmark, and both N-type and Z-type interleaving with inverse coupled inductors have much smaller output current ripple and inductor current ripple. For the benefit of the common-mode noise filter, N-type interleaving is more advantageous than the Z-type interleaving. In summary, N-type interleaving with inverse coupled inductors is the optimal configuration for the performance of two-phase three-level DC/DC converter.

Chapter 3 Modeling and Design of Inductor Inverse Coupling

Two coupled inductors are used in the three-level DC/DC converter to reduce the inductor current ripple, and this chapter will study in detail the effect of coupling for the steady-state operation of the converter. The coupling effect makes the inductors become non-linear, and different equivalent inductance shows up in one switching cycle. By using the concept of equivalent inductance, the coupled inductors can be decoupled in math and can easily be compared with the non-coupling inductor case. In this way, the relationship between coupling and both inductor current ripple and output current ripple will be built, and the benefit of coupling can be illustrated clearly. The coupled inductors can be designed based on the inductor current ripple and output current ripple requirements following the design procedure provided.

3.1 Review on the Concept of Non-linear Equivalent Inductance

The concept of non-linear equivalent inductance was first introduced by Pit-Leong Wong [31], analyzing the effect of coupled inductors to improve transient response and reduce steady-state ripple in the multi-phase interleaving buck VRM. Section 3.1 will give a brief introduction to the non-linear equivalent inductance in multi-phase buck. And the same analysis method using the equivalent inductance concept will be adopted in the following section for the case of two-phase three-level DC/DC converter with coupled inductors.

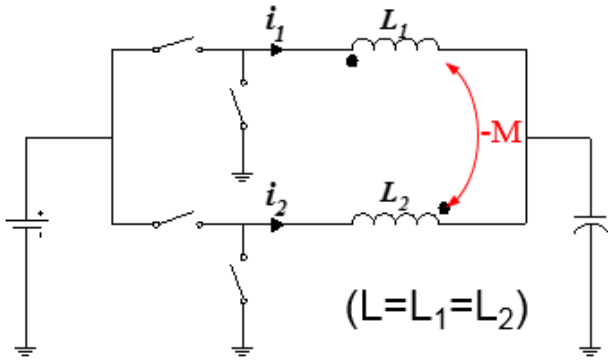

Figure 3.1 Interleaving bucks with coupled inductors

As shown in Figure 3.1, coupled inductors are used in interleaving bucks and the corresponding inductor voltage waveform is drawn in Figure 3.2. In one switching cycle, there are four different inductor voltage conditions.

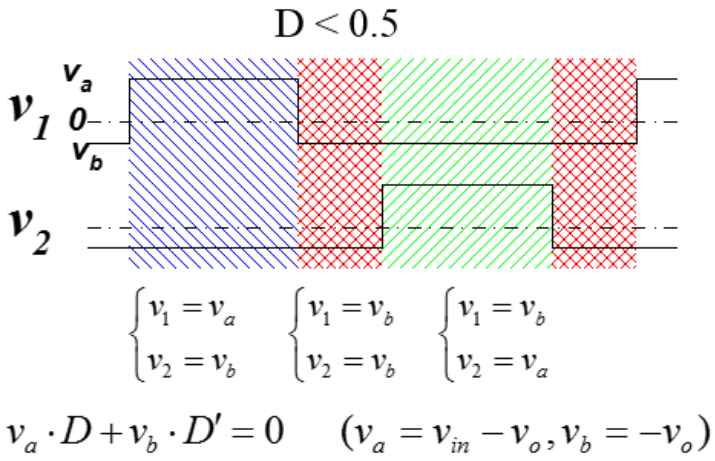

Figure 3.2 Inductor voltage waveform for interleaving buck

In addition, from Figure 3.3, the non-linearity of the inductors can be observed. To analyze the coupling effect for inductor current, Wong used the concept of equivalent inductance to mathematically decouple the coupled inductors. Overall, there are three different equivalent inductances in one switching cycle and can be defined and derived from the circuit analysis,

$$L_{eq1} = \frac{L - \frac{M^2}{L}}{1 - \frac{M}{L}\frac{D}{D'}} \tag{3.1}$$

$$L_{eq2} = L - M \tag{3.2}$$

$$L_{eq3} = \frac{L - \frac{M^2}{L}}{1 - \frac{M}{L}\frac{D'}{D}} \tag{3.3}$$

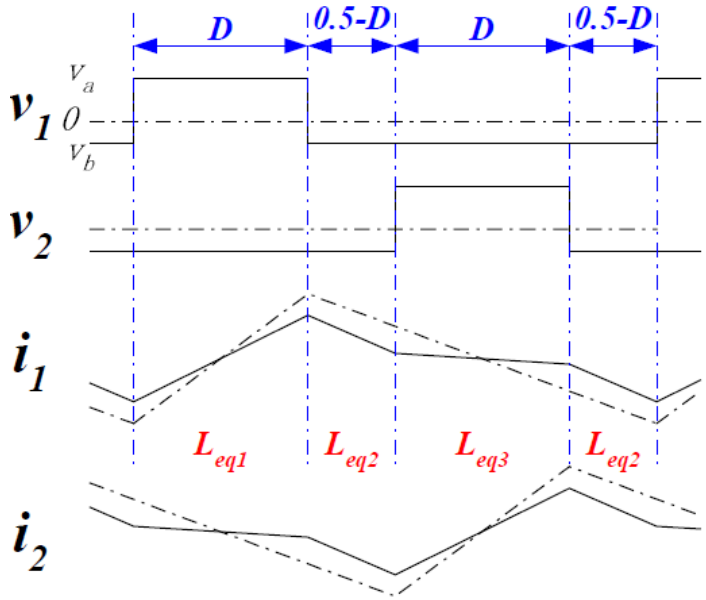

Figure 3.3 Inductor current waveform with coupled inductors

The case with duty cycle larger than 0.5 can be analyzed in a similar way.

By applying the concept of equivalent inductance, the coupled inductors are decoupled. Therefore, the inductor ripple and output current ripple can be derived easily with equivalent inductance by every time interval in one switching period. At the same time, the effect of coupling can be clarified by comparing with non-coupling inductor case. In Figure 3.3, inductor current

with coupled inductors is plotted in the solid line, and inductor current with non-coupling inductors is shown in the dashed line. Clearly, the first time interval determines the inductor current ripple,

$$\Delta i_{cp} = \frac{v_a D T_{sw}}{L_{eq1}} \tag{3.4}$$

With $L_{eq1}>L$, the inductor current ripple can be smaller by coupling. L_{eq1} is defined as steady-state equivalent inductance L_{ss} for it determines the steady-state inductor current ripple.

It could also be found that L_{eq2} determines the transient response of the converter. Therefore, L_{eq2} is defined as transient equivalent inductance L_{tr}.

From the equivalent inductance derivation from the inductor equation and waveform analysis above, one can conclude that the concept of equivalent inductance is a helpful tool to illustrate the benefit of coupled inductors in interleaving buck. Proper design of coupling can improve steady-state performance and transient response speed. Also, it should be pointed out that the concept of equivalent inductance is not purely mathematical, it also has strong physical meaning [31].

3.2 Equivalent Inductance for Coupled Inductors with N-type Interleaving

The concept of equivalent inductance can be extended to the two-phase three-level DC/DC converter with coupled inductors. Due to the N-type interleaving and three-level structure, there will be differences in the equivalent inductance derivation. By giving the equivalent inductance, the coupling effect on converter performance can then be discussed in the next section.

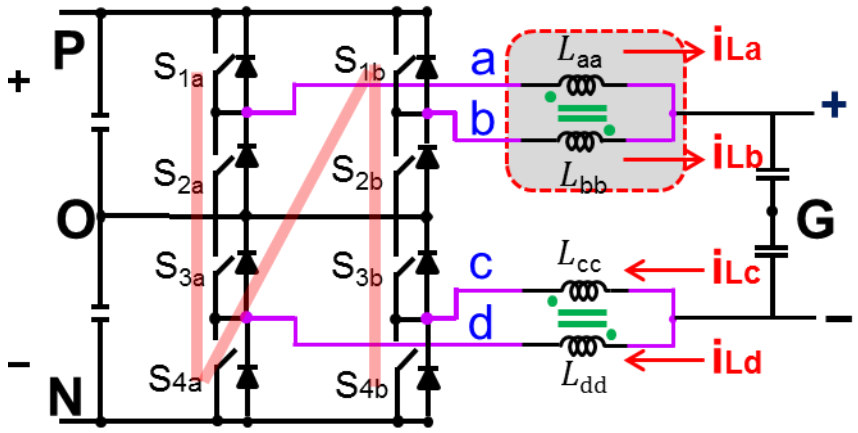

Figure 3.4 Three-level DC/DC converter with coupled inductors

There are two coupled inductors in the two-phase three-level DC/DC converter, as shown in Figure 3.4. Figure 3.5 gives the flux distribution for the coupled inductors on arm a and arm b. For the flux generated by winding of L_{aa}, part of flux goes through arm b and part goes through the center leg, namely Φ_{ba} and Φ_{lka}. The flux generated by winding of L_{bb} has a similar flux path, namely Φ_{ab} and Φ_{lkb}. Green lines represent the inverse coupled flux between two arms, and there is leakage flux, Φ_{lka} and Φ_{lkb}, flows through the center leg, as shown in the purple dashed lines.

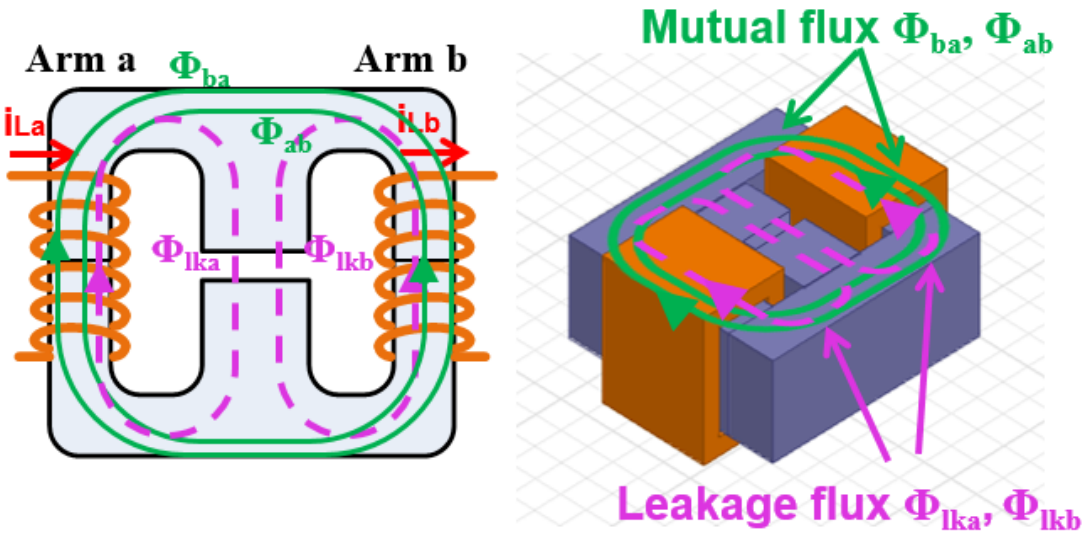

Figure 3.5 Flux analysis of coupled inductors

The two coupled inductors can be described by the mathematical model (3.5) and (3.6), where L_{aa}, L_{bb}, L_{cc} and L_{dd} are self-inductance of four arm inductors, M_{ab} is the mutual inductance between L_{aa} and L_{bb}, M_{cd} is the mutual inductance between L_{cc} and L_{dd}. By symmetry, one can assume that two coupled inductors can follow the same design principle, and only the coupled inductors on arm a and arm b will be discussed in this section. The analysis process and result for the coupled inductors on arm c and arm d will be comparable.

$$\begin{bmatrix} v_{La} \\ v_{Lb} \end{bmatrix} = \begin{bmatrix} L_{aa} & -M_{ab} \\ -M_{ab} & L_{aa} \end{bmatrix} \begin{bmatrix} \frac{di_{La}}{dt} \\ \frac{di_{Lb}}{dt} \end{bmatrix} \tag{3.5}$$

$$\begin{bmatrix} v_{Lc} \\ v_{Ld} \end{bmatrix} = \begin{bmatrix} L_{cc} & -M_{cd} \\ -M_{cd} & L_{dd} \end{bmatrix} \begin{bmatrix} \frac{di_{Lc}}{dt} \\ \frac{di_{Ld}}{dt} \end{bmatrix} \tag{3.6}$$

The inductor voltage and current waveforms for arm inductor L_{aa} and L_{bb} are shown in Figure 3.6, when duty cycle $0.25<D<0.5$ using as an example. Due to the characteristics of N-type interleaving, a switching cycle can be divided into eight time intervals, which is never observed before in the two-level interleaved buck converter with coupled inductors. To analyze this complex inductor current waveform, equivalent inductance concept is adopted here. From the slope of inductor current waveforms, there are five equivalent piece-wise linear inductances in one switching cycle. The equivalent inductance derivation for other duty cycle range shares the same analysis process, and the complete result for whole duty cycle range $0<D<1$ is summarized in Appendix I.

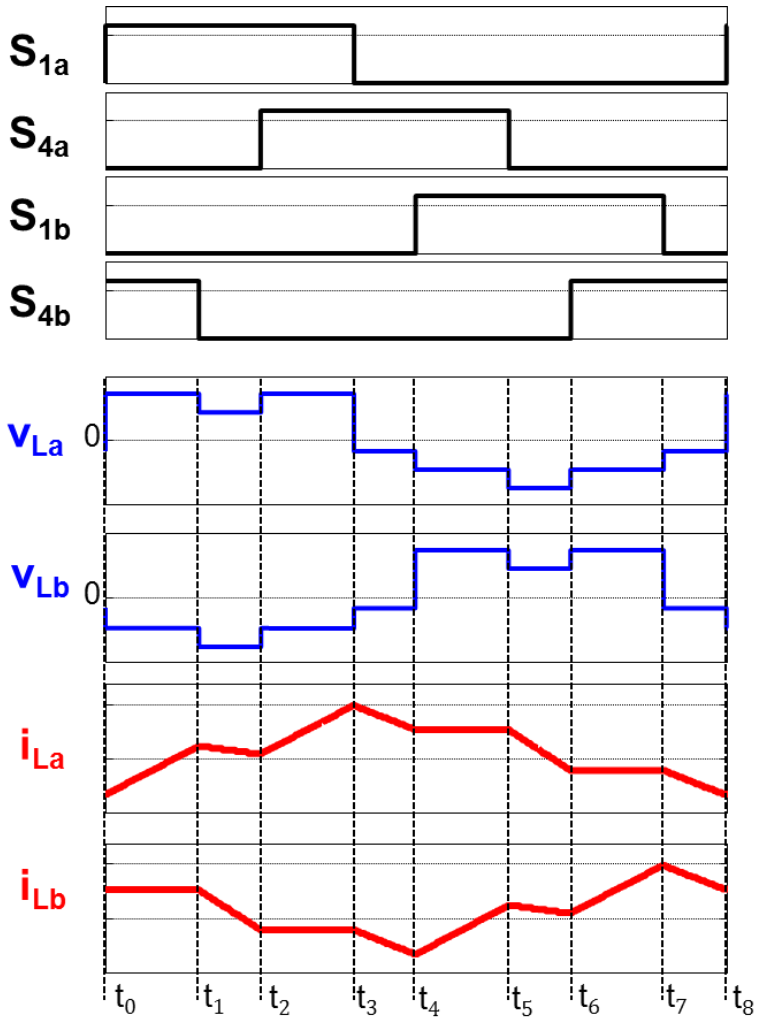

Figure 3.6 Inductor voltage and current waveforms for N-type interleaving

For the simplicity of analysis, the self-inductance of two inductors, L_{aa} and L_{bb}, are assumed to be identical, with

$$L = L_{aa} = L_{bb} \tag{3.7}$$

The mutual inductance M_{ab} is defined as,

$$M_{ab} = -\alpha L, (-1 < \alpha < 0) \tag{3.8}$$

As a result, the relationship of inductor voltage and current can be simplified by the 2x2 matrix below,

$$\begin{bmatrix} v_{La} \\ v_{Lb} \end{bmatrix} = \begin{bmatrix} L & -M_{ab} \\ -M_{ab} & L \end{bmatrix} \begin{bmatrix} \frac{di_{La}}{dt} \\ \frac{di_{Lb}}{dt} \end{bmatrix} \tag{3.9}$$

And it can be rewritten without assumption as,

$$\begin{bmatrix} v_{La} + \frac{M_{ab}}{L} v_{Lb} \\ v_{Lb} + \frac{M_{ab}}{L} v_{La} \end{bmatrix} = \begin{bmatrix} L - \frac{M_{ab}^{\ 2}}{L} & 0 \\ 0 & L - \frac{M_{ab}^{\ 2}}{L} \end{bmatrix} \begin{bmatrix} \frac{di_{La}}{dt} \\ \frac{di_{Lb}}{dt} \end{bmatrix} \tag{3.10}$$

Clearly, the right side of the equation is decoupled already. If the relationship between two inductor voltages v_{La} and v_{Lb} can be found, the coupled inductors can be decoupled mathematically.

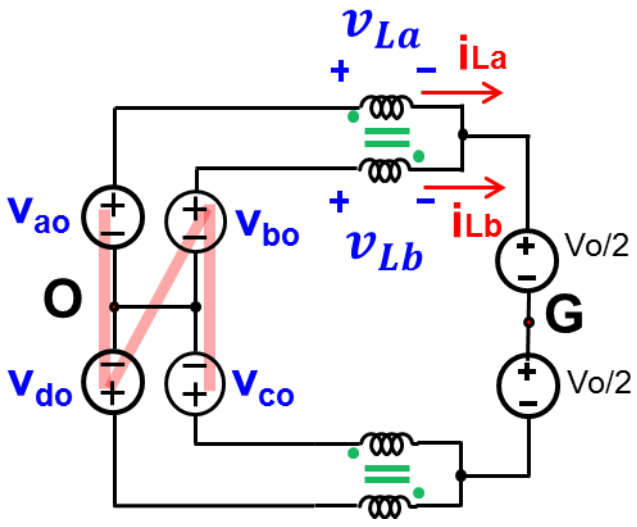

Figure 3.7 Equivalent circuit with coupled inductors

From the circuit diagram, or equivalent circuit of the converter with coupled inductors in Figure 3.7, the inductor voltage is,

$$\begin{cases} v_{La} = v_{ao} - \dfrac{V_o}{2} - v_{GO} \\ v_{Lb} = v_{bo} - \dfrac{V_o}{2} - v_{GO} \end{cases} \tag{3.11}$$

With v_{GO} is derived from the equivalent circuit and can be defined as,

$$v_{GO} = \frac{v_{ao} + v_{bo} + v_{co} + v_{do}}{4} \tag{3.12}$$

Using the first time interval t0-t1 in Figure 3.8 as an example to derive the equivalent inductance. For the there-level DC/DC converter, there exists,

$$DV_{in} = V_o \tag{3.13}$$

Where V_{in} is the input voltage, and V_o is the output voltage. Also,

$$v_{GO} = \frac{v_{ao} + v_{bo} + v_{co} + v_{do}}{4} = 0 \tag{3.14}$$

$$v_{La} = v_{ao} - \frac{V_o}{2} - v_{GO} = \frac{(1-D)V_{in}}{2} \tag{3.15}$$

$$v_{Lb} = v_{bo} - \frac{V_o}{2} - v_{GO} = -\frac{DV_{in}}{2} \tag{3.16}$$

The relationship for two inductor voltages can be found as,

$$v_{Lb} = -\frac{D}{1-D} v_{La} \tag{3.17}$$

With this relationship, (3.10) becomes,

$$\begin{bmatrix} v_{La} \\ v_{Lb} \end{bmatrix} = \begin{bmatrix} \dfrac{(L^2 - M_{ab}{}^2)}{L - \dfrac{D}{1-D} M_{ab}} & 0 \\ 0 & \dfrac{(L^2 - M_{ab}{}^2)}{L - \dfrac{1-D}{D} M_{ab}} \end{bmatrix} \begin{bmatrix} \dfrac{di_{La}}{dt} \\ \dfrac{di_{Lb}}{dt} \end{bmatrix} \tag{3.18}$$

By the mathematical process using inductor voltage relationship, now coupled inductors are decoupled in the inductor equation, and one can define the equivalent inductance in this time interval in terms of arm a,

$$L_{eq1} = \frac{(L^2 - M_{ab}{}^2)}{L - \dfrac{D}{1-D} M_{ab}} \tag{3.19}$$

For the equivalent inductance on arm b, it will be identical as arm a with only a difference of 180 degree phase shift due to the N-type interleaving.

Also notice that L_{eq1} in the three-level converter is the same as the L_{eq1} in two-level buck converter case in section 3.1. In time interval t2-t3, the two inductor voltages are identical as in time interval t0-t1, accordingly the equivalent inductance in this interval is still L_{eq1}.

Different inductor voltage combinations are shown with different color in Figure 3.8. For other time intervals, once the relationship of two inductor voltages are found, the corresponding equivalent inductance can be derived together with (3.18).

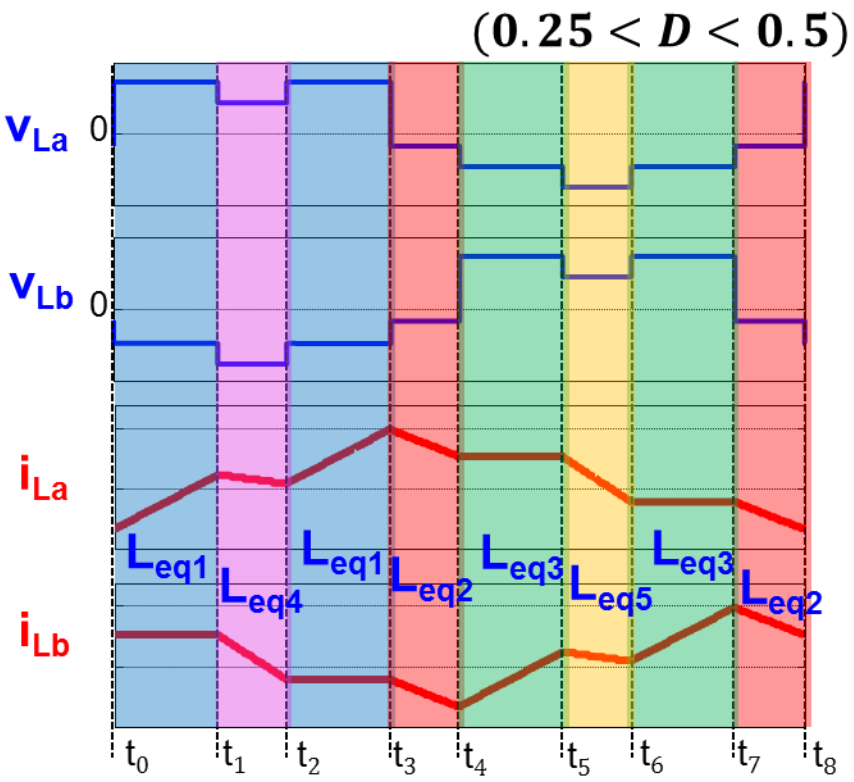

Figure 3.8 Five different equivalent inductance in three-level converter

For time interval t3-t4 and t7-t8 in the red shaded area in Figure 3.8,

$$v_{La} = \frac{(1-4D)V_{in}}{8} \tag{3.20}$$

$$v_{Lb} = \frac{(1-4D)V_{in}}{8} \tag{3.21}$$

$$L_{eq2} = L - M_{ab} \tag{3.22}$$

For time interval t4-t5 and t6-t7 in the green shaded area in Figure 3.8,

$$v_{La} = \frac{-DV_{in}}{2} \tag{3.23}$$

$$v_{Lb} = \frac{(1-D)V_{in}}{2} \tag{3.24}$$

$$L_{eq3} = \frac{(L^2 - M_{ab}{}^2)}{L - \frac{1-D}{D} M_{ab}} \tag{3.25}$$

For time interval t1-t2 in the pink shaded area in Figure 3.8,

$$v_{La} = \frac{(3-4D)V_{in}}{8} \tag{3.26}$$

$$v_{Lb} = -\frac{(1+4D)V_{in}}{8} \tag{3.27}$$

$$L_{eq4} = \frac{(L^2 - M_{ab}{}^2)}{L - \frac{(1+4D)}{(3-4D)} M_{ab}} \tag{3.28}$$

For the last remaining time interval t5-t6 in the yellow shaded area in Figure 3.8,

$$v_{La} = -\frac{(1+4D)V_{in}}{8} \tag{3.29}$$

$$v_{Lb} = \frac{(3-4D)V_{in}}{8} \tag{3.30}$$

$$L_{eq5} = \frac{(L^2 - M_{ab}{}^2)}{L - \frac{(3-4D)}{(1+4D)} M_{ab}} \tag{3.31}$$

Totally, there are five different inductor voltage combinations. As a result, five different equivalent inductances exist within one switching period.

Among the five equivalent inductances, L_{eq1}, L_{eq2} and L_{eq3} showed up in section 3.1 for the interleaving buck converter case, and L_{eq4}, L_{eq5} are two new equivalent inductances that uniquely exist in the three-level interleaving with coupled inductors case.

3.3 Coupling Effect on Inductor Current Ripple and Output Current Ripple

Figure 3.9 provides the waveform of inductor current with coupled inductors, as shown in the red solid lines. And the inductor current with non-coupling inductors for the three-level DC/DC converter in the dashed lines is set as the benchmark. Comparing with the inductor current waveform in interleaving buck converter, now inductor current ripple is not determined solely by one equivalent inductance in the three-level case. Instead, the first three time intervals determine the inductor current ripple together.

$$\Delta i_{nc} = \frac{\left\langle v_{La} \right\rangle_{T1} + \left\langle v_{La} \right\rangle_{T2} + \left\langle v_{La} \right\rangle_{T3}}{L} \tag{3.32}$$

$$\Delta i_{cp} = \frac{\left\langle v_{La} \right\rangle_{T1}}{L_{eq1}} + \frac{\left\langle v_{La} \right\rangle_{T2}}{L_{eq4}} + \frac{\left\langle v_{La} \right\rangle_{T3}}{L_{eq1}} \tag{3.33}$$

Where Δi_{nc} is inductor current ripple with non-coupling inductors and Δi_{cp} is for the coupled inductors case.

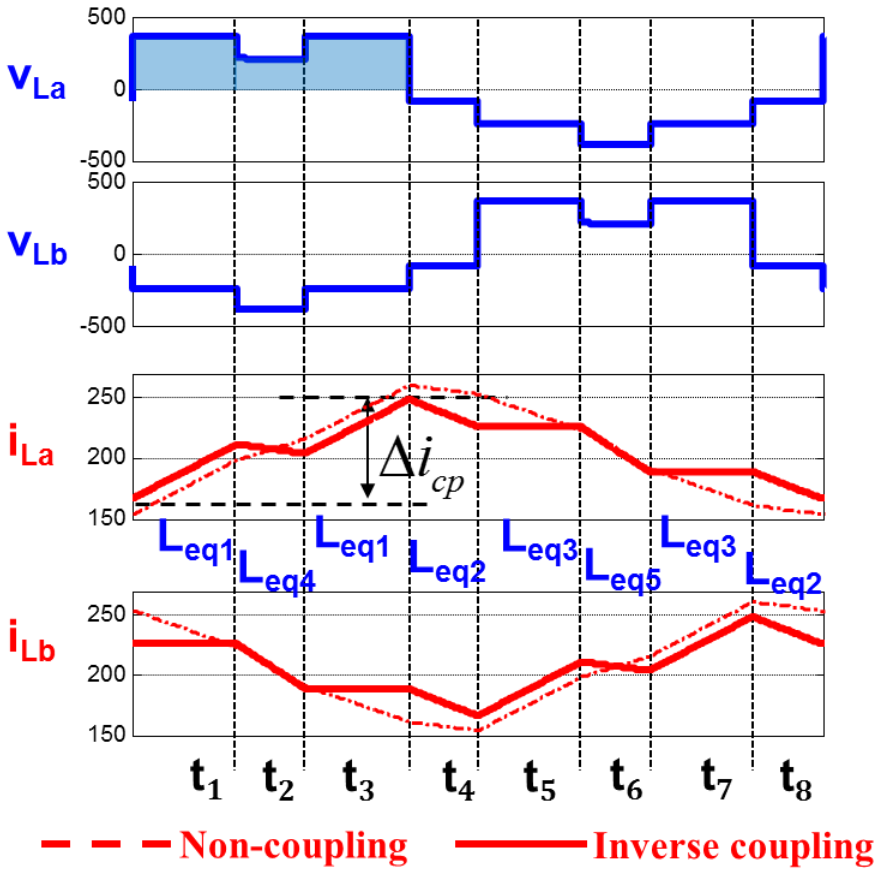

Figure 3.9 Inductor current waveform with coupled inductors in three-level DC/DC converter, 0.25<D<0.5

Considering the case 0.25<D<0.5, due to the special characteristics of inductor current ripple determination, it is hard to compare the inductor current ripple between the coupled inductors case and the non-coupling case by comparing equivalent inductance with non-coupling inductance L. To solve this problem, the steady-state equivalent inductance in the three-level DC/DC converter is defined as,

$$L_{ss} = \frac{\langle v_{La} \rangle_{T1} + \langle v_{La} \rangle_{T2} + \langle v_{La} \rangle_{T3}}{\Delta i_{cp}} = \frac{\langle v_{La} \rangle_{T1} + \langle v_{La} \rangle_{T2} + \langle v_{La} \rangle_{T3}}{\frac{\langle v_{La} \rangle_{T1}}{L_{eq1}} + \frac{\langle v_{La} \rangle_{T2}}{L_{eq4}} + \frac{\langle v_{La} \rangle_{T3}}{L_{eq1}}} \tag{3.34}$$

With simple mathematical derivation, (3.34) becomes,

$$L_{ss} = \frac{(-8D^2 + 10D - 1)(L^2 - M_{ab}{}^2)}{(-8D^2 + 10D - 1)L - (8D^2 - 2D + 1)M_{ab}} \tag{3.35}$$

And now L_{ss} can be compared with non-coupling inductance L to find the inductor current ripple reduction effect with coupled inductors.

Under the condition that,

$$\frac{M_{ab}}{L} < \frac{8D^2 - 2D + 1}{-8D^2 + 10D - 1} \tag{3.36}$$

Steady-state equivalent inductance L_{ss} will be larger than the non-coupling inductance L. And the inductor current ripple can be reduced with coupled inductors with proper coupling coefficient.

Besides inductor current ripple, output current ripple is another important design specifications need to be considered. As shown in Figure 3.10, the output current waveform i_o is the summation of two inductor currents, i_{La} and i_{Lb}. In the time interval t3-t4, the output current ripple is derived as the summation of two inductor current ripples,

$$\Delta i_o = \frac{\langle v_{La} \rangle_{T4}}{L_{eq2}} + \frac{\langle v_{Lb} \rangle_{T4}}{L_{eq2}} \tag{3.37}$$

Clearly, equivalent inductance L_{eq2} determines the output current ripple. And the same conclusion can be drawn for all other duty cycle cases.

Another way to find out the output current ripple determination is to add the two equations in (3.9) together, and,

$$v_{La} + v_{Lb} = (L - M_{ab}) \frac{d(i_{La} + i_{Lb})}{dt} = L_{eq2} \frac{di_o}{dt} \tag{3.38}$$

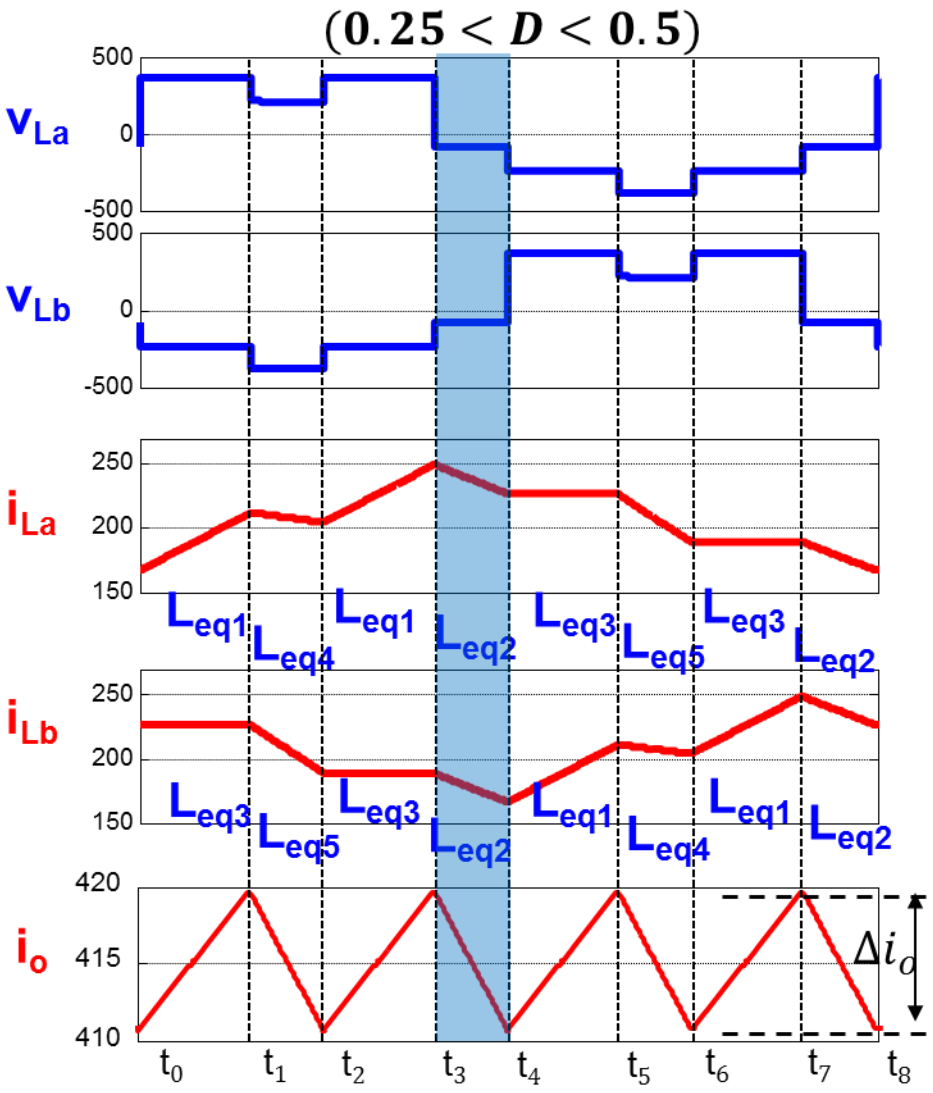

Figure 3.10 Output current waveform with coupled inductors in three-level DC/DC converter

Since voltage on inductors are decided by the operation condition of the converter, one can conclude that L_{eq2} determines the output current waveform. Noted that,

$$L_{eq2} = L - M_{ab} = L_{lk} \tag{3.39}$$

And L_{eq2}, or the leakage inductance L_{lk} in fact determines the output current ripple.

Up to this point, the relationship between the equivalent inductance and current ripple with coupled inductors is found. However, to better illustrate the benefit of applying coupled inductors,

converter with non-coupling inductor case should be adopted as the benchmark. To have a fair comparison, the same output current ripple is set as the condition for comparison. Under this scenario, L_{eq2} in coupled inductors case should be equal to non-coupling inductance,

$$L_{nc} = L_{eq2} \tag{3.40}$$

Where L_{nc} is the non-coupling inductance.

Under the condition (3.40), the ratio of inductor current ripples between coupling and non-coupling case is,

$$\frac{\Delta i_{cp}}{\Delta i_{nc}} = \frac{L_{nc}}{L_{ss}} = \frac{(-8D^2+10D-1)+(8D^2-2D+1)\alpha}{(-8D^2+10D-1)(1-\alpha)}, 0.25 < D \le 0.5 \tag{3.41}$$

With duty cycle ranges from 0.25 to 0.5. Other duty cycle cases can be defined with same comparison method.

$$\frac{\Delta i_{cp}}{\Delta i_{nc}} = \frac{L_{nc}}{L_{ss}} = \frac{(-4D+3)+(4D+1)\alpha}{(4D-3)(\alpha-1)}, 0 < D \le 0.25 \tag{3.42}$$

$$\frac{\Delta i_{cp}}{\Delta i_{nc}} = \frac{L_{nc}}{L_{ss}} = \frac{(-8D^2+6D+1)+(8D^2-14D+7)\alpha}{(-8D^2+6D+1)(1-\alpha)}, 0.5 < D \le 0.75 \tag{3.43}$$

$$\frac{\Delta i_{cp}}{\Delta i_{nc}} = \frac{L_{nc}}{L_{ss}} = \frac{(4D-1)+(-4D+5)\alpha}{(4D-1)(1-\alpha)}, 0.75 < D \le 1 \tag{3.44}$$

Based on (3.41)-(3.44), the inductor current ripple reduction effect with different coupling coefficient and duty cycle can be demonstrated clearly in Figure 3.11.

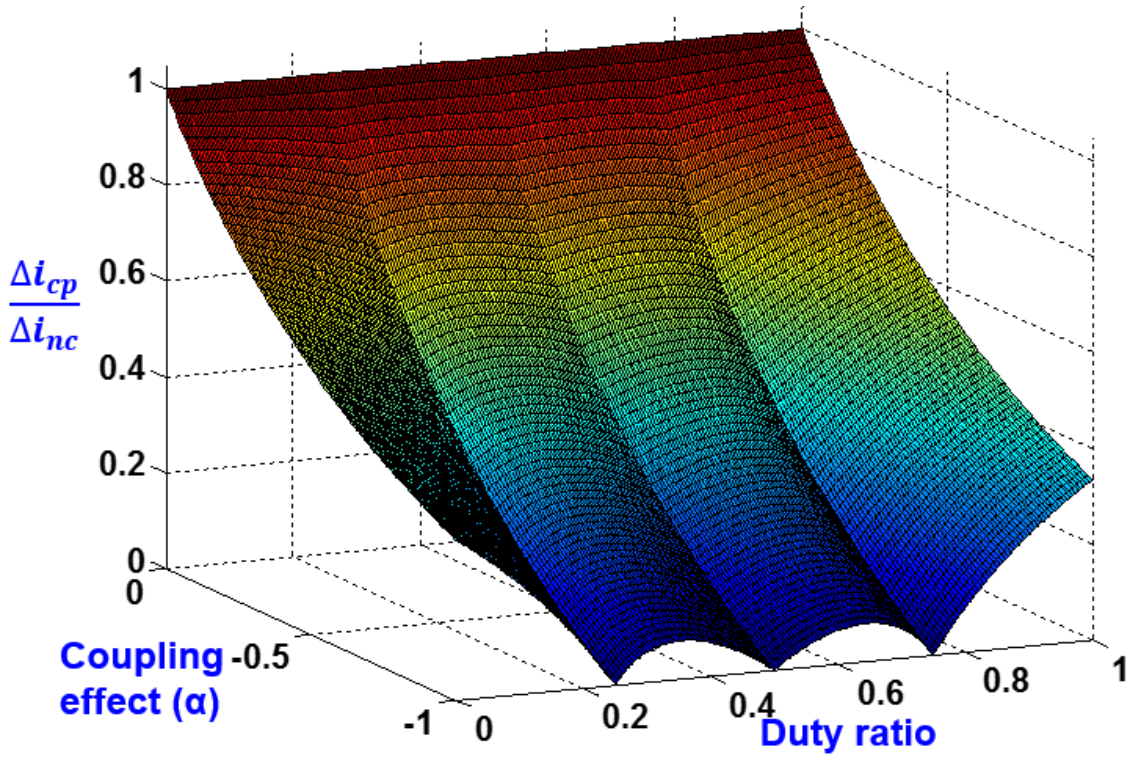

Figure 3.11 Inductor current ripple reduction with changing coupling coefficient and duty ratio

At any duty cycle, the inductor current ripple reduction effect will be stronger as the coupling effect of coupled inductors increases. And it should be noted that the comparison is based on keeping same L_{eq2} as L_{nc} to guarantee a same output current ripple. Strong coupling is preferred for inductor current ripple reduction while keeping same L_{eq2}.

In order to see the effect of duty cycle on inductor current ripple reduction, the 3-D plot in Figure 3.11 can be rotated into Figure 3.12. From the figure, when the coupling coefficient is fixed, there are three maximum reduction effect points at D=0.25, D=0.5 and D=0.75. In other words, given a coupled inductors design, it has the minimum inductor current ripple when operating at D=0.25, D=0.5 and D=0.75.

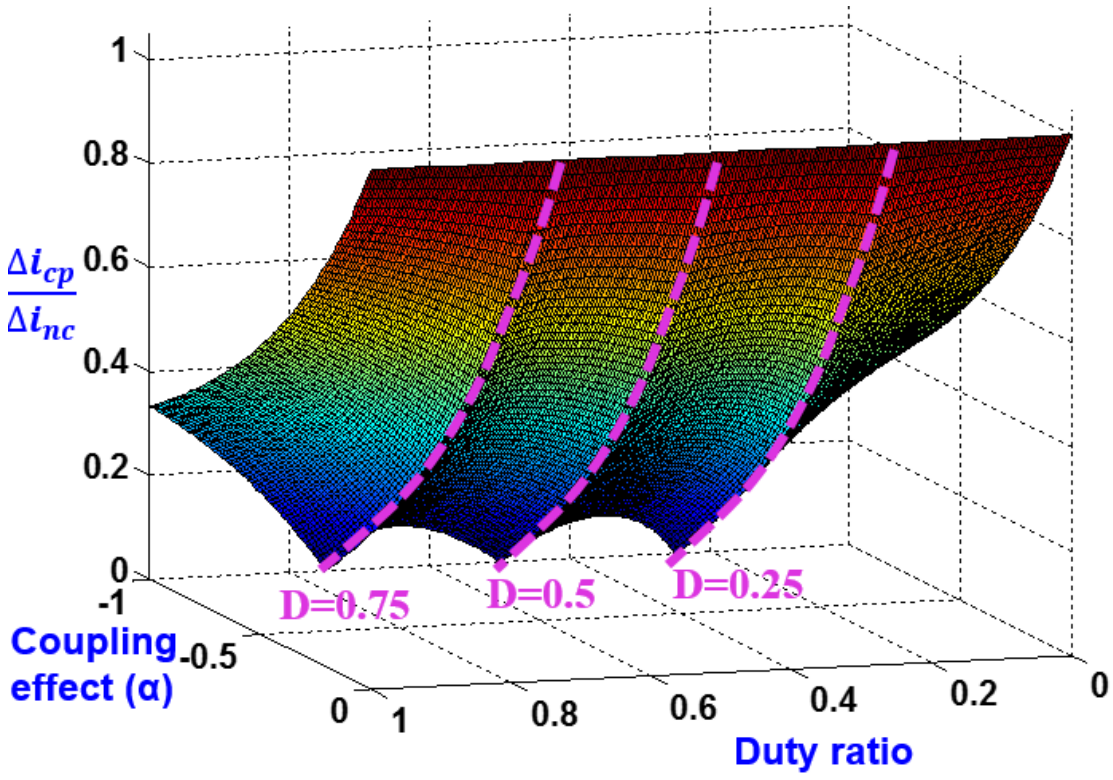

Figure 3.12 Inductor current ripple reduction with changing coupling coefficient and duty ratio, from different view

3.4 Coupling Design based on Current Ripple Requirement

For the inverse coupled inductors, two parameters in the (3.9) should be designed based on the current ripple requirement, the mutual inductance M_{ab} and the leakage inductance L_{lk}. The self-inductance equals to $L=M_{ab}+L_{lk}$.

In section 3.3, it can be concluded that equivalent inductance L_{eq2} will determine the output current ripple of three-level DC/DC converter with coupled inductors, and multiple equivalent inductances will affect the inductor current ripple. By calculating the relationship between equivalent inductance and the current ripple,

$$\Delta i_o = \begin{cases} \dfrac{V_{dc}\cdot(1-4D)}{4L_{eq2}}\cdot DT & D<0.25 \\ \dfrac{V_{dc}\cdot(4D-1)}{8L_{eq2}}\cdot(1-2D)T & 0.25\le D<0.5 \\ \dfrac{V_{dc}\cdot(3-4D)}{8L_{eq2}}\cdot(2D-1)T & 0.5\le D<0.75 \\ \dfrac{V_{dc}\cdot(4D-3)}{4L_{eq2}}\cdot(1-D)T & 0.75\le D<1 \end{cases} \tag{3.45}$$

$$\Delta i_{La} = \begin{cases} \dfrac{V_{dc}(1-4D)}{8L_{lk}}DT+\dfrac{V_{dc}D}{4(2M_{ab}+L_{lk})}T & D<0.25 \\ \dfrac{V_{dc}(4D-1)}{16L_{lk}}(1-2D)T+\dfrac{V_{dc}D}{4(2M_{ab}+L_{lk})}T & 0.25\le D<0.5 \\ \dfrac{V_{dc}(3-4D)}{16L_{lk}}(2D-1)T+\dfrac{V_{dc}(1-D)}{4(2M_{ab}+L_{lk})}T & 0.5\le D<0.75 \\ \dfrac{V_{dc}(4D-3)}{8L_{lk}}(1-D)T+\dfrac{V_{dc}(1-D)}{4(2M_{ab}+L_{lk})}T & 0.75\le D \end{cases} \tag{3.46}$$

Clearly, only L_{eq2} (=L_{lk}) will affect the output current ripple, while both M_{ab} and L_{lk} will affect inductor current ripple. As a result, the design process can be summarized as two steps. First, the leakage inductance L_{lk} should be designed based on the output current ripple requirement. With L_{lk} determined, the mutual inductance M_{ab} then will be designed based on the inductor current ripple requirement.

As the first step, L_{eq2} should be designed based on the output current ripple. With different L_{eq2} value, the output current ripple varies in the whole duty cycle range from 0 to 1, as shown in Figure 3.13. Input voltage V_{dc}=1200V, switching frequency f_{sw}=20kHz. As the value of L_{eq2}

increases, the output current ripple will drop accordingly. Since duty cycle D is not pre-determined, one should design under the worst case scenario at this step, and the peak output current ripple is calculated under different L_{eq2}. Here, when L_{eq2}=30μH, the peak output current ripple is 31A. When L_{eq2} increases to 60μH or 100μH, the peak ripple drops to 16A and 9A.

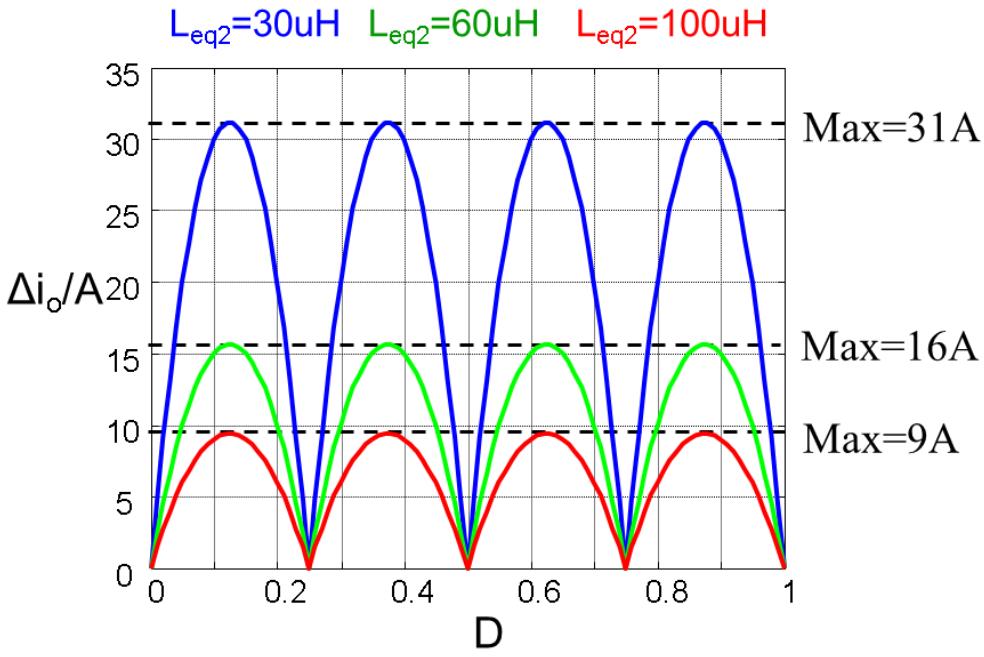

Figure 3.13 Output current ripple with different L_{eq2}

The three L_{eq2} cases mentioned above can be plotted as three dots in Figure 3.14. By sweeping continuously on L_{eq2} value, the curve for maximum output current ripple under different L_{eq2} value can be drawn. As expected, the maximum output current ripple will continue to decrease as L_{eq2} increases. Given a design target for 16A output current ripple, the L_{eq2}, or the leakage inductance L_{lk}, is designed to be 60μH at the corner of this curve.

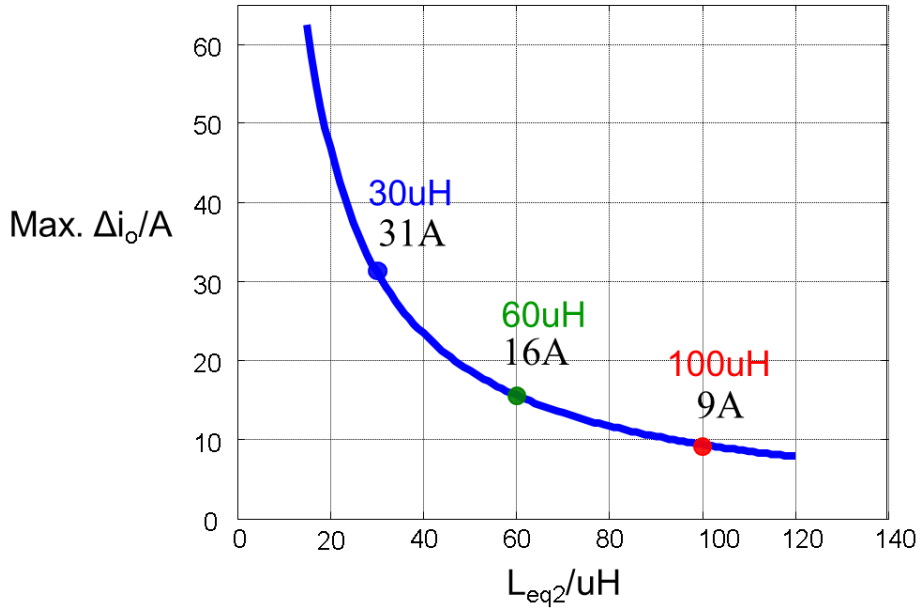

Figure 3.14 Design L_{eq2} based on output current ripple

In the second step, the mutual inductance M_{ab} will be designed based on inductor current ripple. With L_{lk}=60μH, the inductor current ripple is calculated with different mutual inductance. With M_{ab}=200μH, 500μH and 800μH, the peak inductor current ripple is calculated as 21A, 13A, and 11A, respectively in Figure 3.15.

By sweeping the maximum inductor current ripple with different M_{ab} value, Figure 3.16 is drawn. As M_{ab} increases, the maximum inductor current ripple drops, while the benefit will continue to diminish. Again, M_{ab} value should be designed on the corner of the curve to have the best trade-off. Given the inductor current ripple requirement as 13A, the mutual inductance M_{ab} is designed as 500μH.

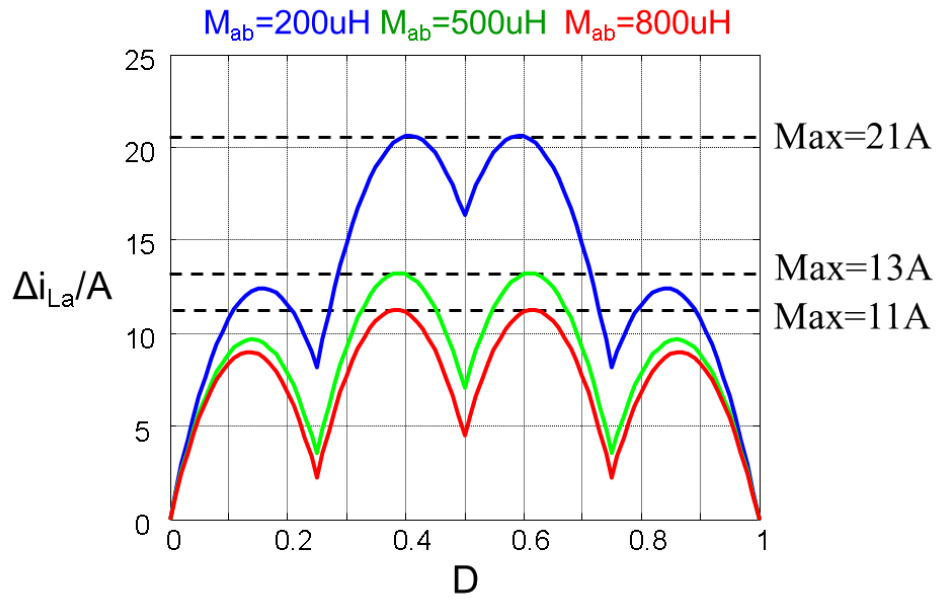

Figure 3.15 Inductor current ripple with different M_{ab}

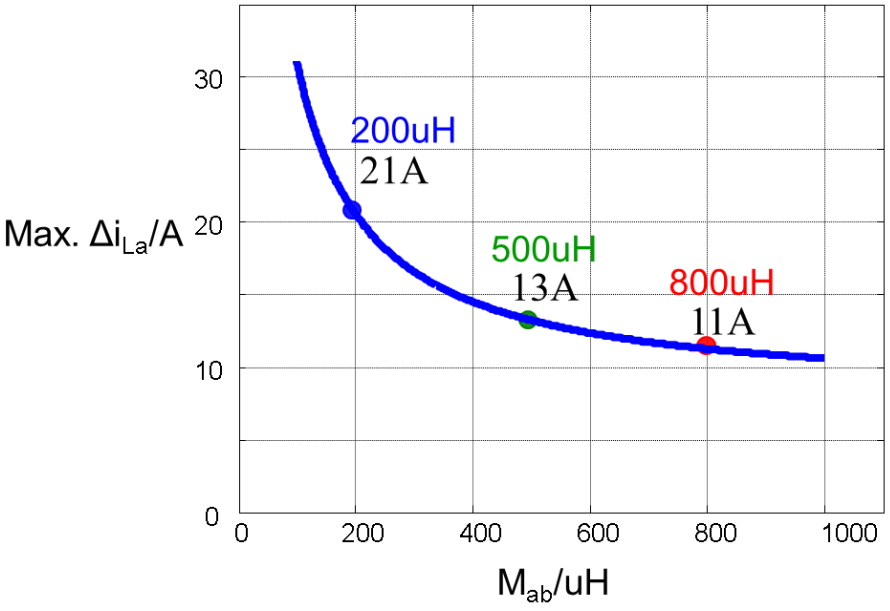

Figure 3.16 Design M_{ab} based on inductor current ripple

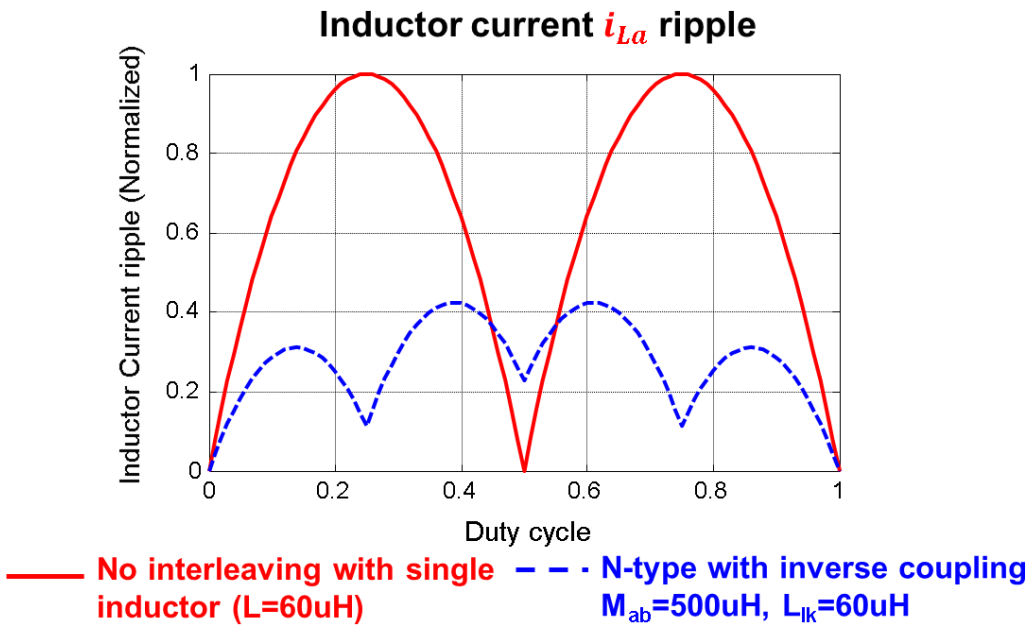

Figure 3.17 Inductor current ripple comparison

With the two steps above, mutual inductance M_{ab} is design as 500μH and leakage inductance L_{lk} is designed as 60μH for the inverse coupled inductors. Under this condition, the effect of inductor current ripple reduction is compared to the case of non-interleaving with single inductors (L=60μH) in Figure 3.17. For most of the duty cycle ranges, the inductor current ripple is largely reduced.

3.5 Magnetic Circuit Analysis

From the analysis from the previous section, it is important to have strong coupling for the coupled inductors for inductor current ripple reduction. And this section will discuss the method to provide strong coupling for proper air gap design. In the magnetic circuit shown in Figure 3.18, the reluctance of the magnetic path is represented by the resistor and the winding is represented by the magnetomotive force (MMF) source, which has similar characteristics of voltage source in

electric circuits. Assuming that the reluctance of the air gap is much larger than the reluctance of the core, only air gap reluctance is considered in the magnetic circuit [32].

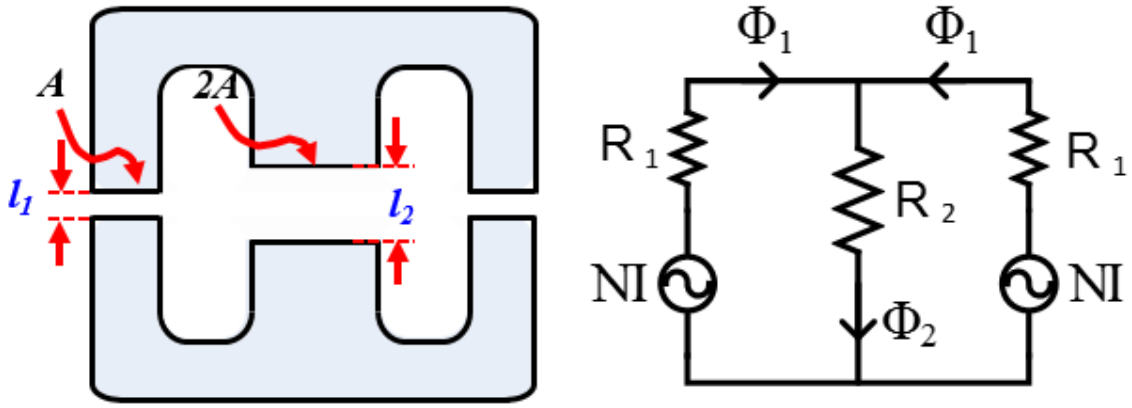

Figure 3.18 Magnetic circuit of coupled inductors

For the case where the cross section area for outer leg is A and 2A for the center leg, the corresponding reluctance are,

$$R_1 = \frac{l_1}{\mu_o A} \tag{3.47}$$

$$R_2 = \frac{l_2}{2\mu_o A} \tag{3.48}$$

Where l_1 is the length of air gap in outer legs, l_2 is the length of air gap in center leg.

As mentioned in the previous section, since $L_{eq2}=L-M_{ab}=L_{lk}$ determines the output current ripple, one can keep the leakage inductance constant and then design proper air gap to achieve strong coupling. From the magnetic circuit,

$$L_{eq2} = L_{lk} = \frac{N^2}{2R_2 + R_1} = \frac{N^2 \mu_0 A}{l_1 + l_2} \tag{3.49}$$

So to keep leakage inductance constant, the summation of l_1 and l_2 should be constant. Also, the coupling coefficient is derived as,

$$M_{ab} = \frac{N^2 R_2}{R_1(R_1 + 2R_2)} \tag{3.50}$$

$$\alpha = -\frac{M_{ab}}{M_{ab} + L_{lk}} = -\frac{R_2}{R_1 + R_2} = -\frac{l_2}{2l_1 + l_2} \tag{3.51}$$

(3.51) is plotted in Figure 3.19, with the condition that l_1+l_2=constant to guarantee a constant leakage inductance.

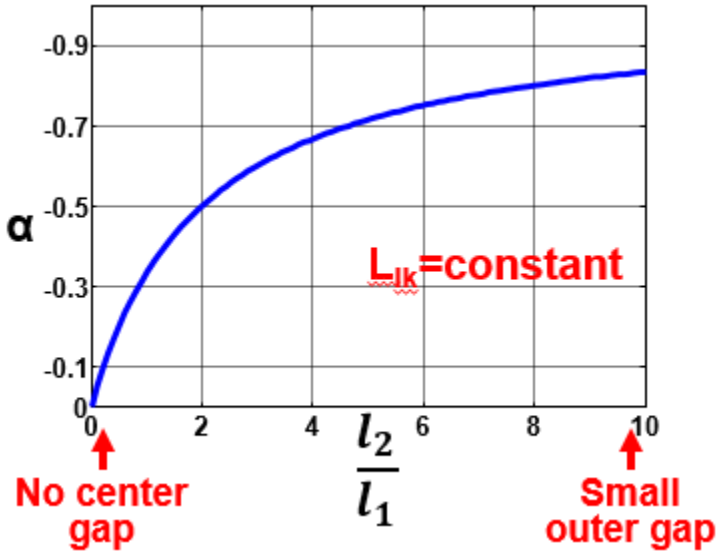

Figure 3.19 Impact of air gap on coupling coefficient

As the ratio between l_2 and l_1 increases, the coupling effect will become stronger. When l_2 is equal to zero, or no air gap exists in the center leg, all the flux generated by the windings will go through the low reluctance center leg, and no coupling effect exists for the inductors. It should be noted that with a larger ratio between l_2 and l_1, the speed of coupling increase will drop continuously because of the constant leakage inductance. To reduce the inductor current ripple

while keeping output current ripple controlled, strong coupling is preferred by increasing the center air gap or reducing the outer air gap, while keeping the summed length of two air gaps constant.

3.6 Summary

This chapter is aiming at using the equivalent inductance concept to analyze the effect of coupled inductors in the steady-state performance of three-level DC/DC converter, and to provide guidance for coupling design.

With the equivalent inductance analysis for interleaving buck as a reference, the same method is applied to derive the equivalent inductance in three-level DC/DC converter. The connection between equivalent inductance and both inductor current ripple and output current ripple is built. For inductor current ripple, it is not determined by one equivalent inductance, and a new steady-state equivalent inductance is derived for its determination. For output current ripple, it is decided by the L_{eq2}, or the leakage inductance L_{lk} of the coupled inductors.

To design the coupled inductors, a two-step procedure is provided based on the current ripple requirements. The leakage inductance L_{lk} is designed based on the maximum output current ripple requirement, and then mutual inductance M_{ab} will be designed based on the maximum inductor current ripple requirement.

To have a fair comparison between coupling and non-coupling inductors, the same output current ripple is assumed and L_{eq2} of coupled inductors is equal to the non-coupling inductance L_{nc}. Under this condition, it is discovered that strong coupling is desired for inductor current ripple reduction. And by analyzing the magnetic circuit, the strong coupling can be designed by controlling the air gaps in the magnetic core, and both small inductor current ripple and output current ripple can be achieved.

Chapter 4 Magnetic Integration for Coupled Inductors

Coupled inductors are required for interleaving three-level DC/DC converter to have small inductor current ripple and output current ripple, as stated in chapter 3. The coupling can be designed based on the current ripple requirement with equivalent inductance analysis. In this chapter, a new type of integrated coupled inductors [33] is introduced to further reduce the size of the magnetics and improve the power density of the converter. Two types of coupling effects, both negative coupling to suppress the circulating current and positive coupling to increase output filter inductance, exist in the integrated coupled inductors. The coupling effect on the current ripple reduction will be discussed based on the equivalent inductance analysis, the same method as is applied in chapter 3. With equivalent inductance defined, the relationship between current ripple and coupling effect can be found, and design procedure for coupling will be given. A prototype of integrated coupled inductors is built with nano-crystalline material, and is verified and tested with the three-level DC/DC converter hardware.

4.1 Introduction on Concept of Integrated Coupled Inductors

Coupled inductors in three-level DC/DC converter is crucial to improve steady-steady performance with interleaving. Due the requirement of the converter, two coupled inductors are required. L_{aa} and L_{bb} are inverse coupled, and L_{cc} and L_{dd} are inverse coupled, as shown in the Figure 3.4. The core structure is shown in the Figure 4.1, and two sets of E-E core are needed.

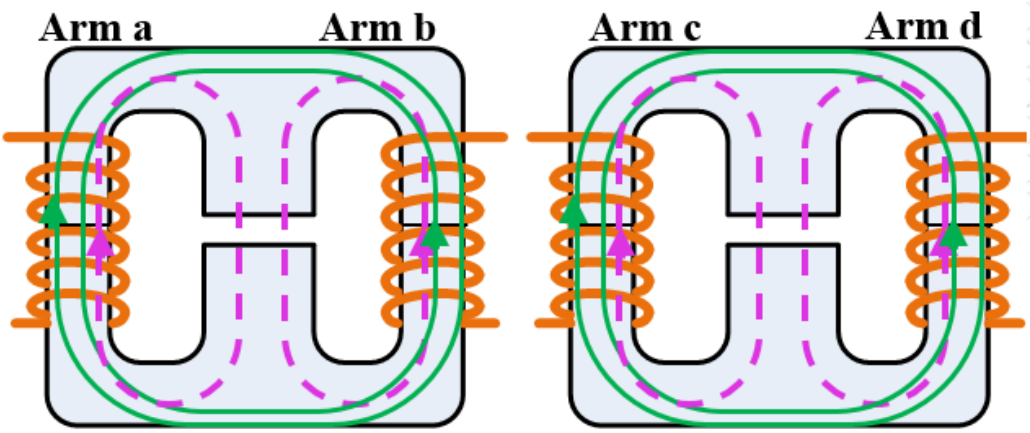

Figure 4.1 Core structure of two coupled inductors case

As analyzed in chapter 3, strong negative coupling exists within the core to reduce the inductor current ripple, as shown in the solid green line in Figure 4.1. The dashed purple line represents the leakage flux through the center leg of the E-E core, and the leakage inductance determines the output current ripple.

As a matter of fact, two coupled inductors share the same structure and function, and the design can be duplicated. As a result, they can be integrated to reduce the size of the magnetic structure, and the integration process is explained from Figure 4.2 to Figure 4.5.

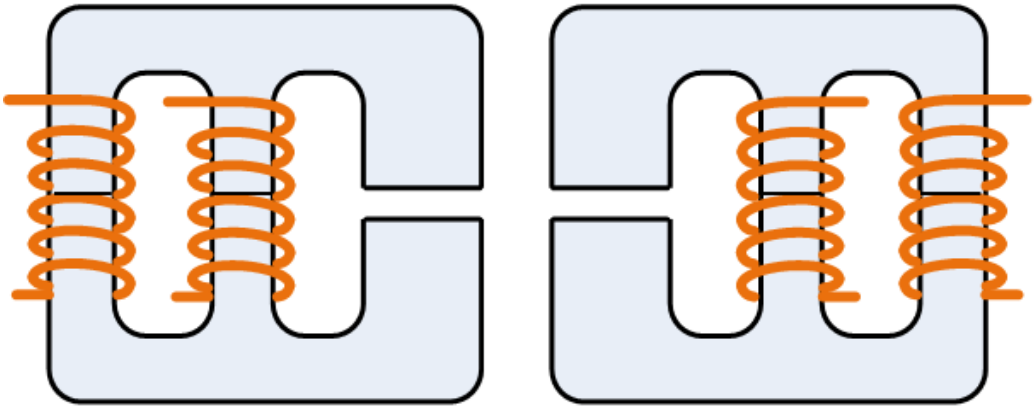

Figure 4.2 Integration process I

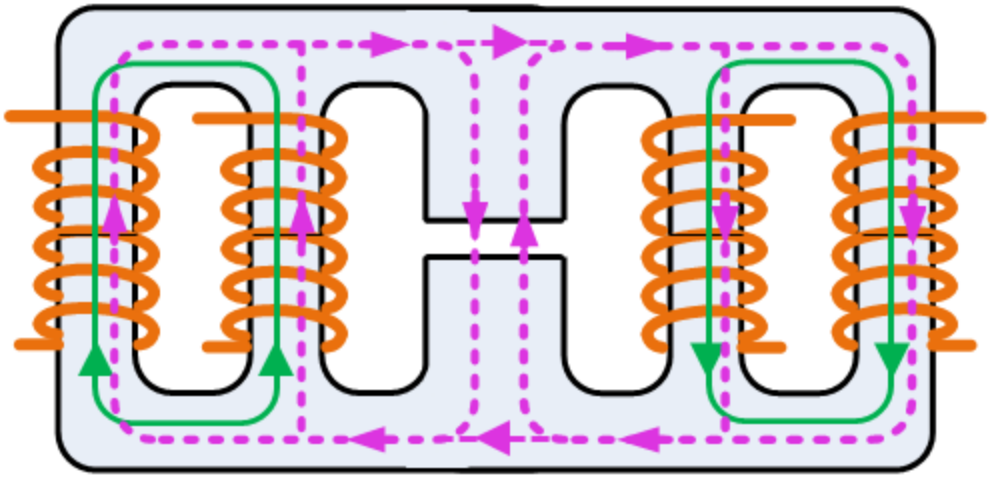

Figure 4.3 Integration process II

As shown in Figure 4.1, the center leg provides the path for leakage flux. It can be moved to the outer side, as shown in Figure 4.2, and this new structure will not affect the coupling effect. Since two coupled inductors are required for the converter, the two center legs can be moved to the outer side and combined as one, as shown in the Figure 4.3 as the second step of integration. Under this condition, the leakage flux from winding a & b, and the leakage flux generated by winding c & d, will share the same path in the new center leg. At the same time, it should be noted that the leakage flux represented by the purple dashed line is positively coupled through the low reluctance path of core magnetic material. As a result, it is easy to form the idea of removing the center leg and letting all previous leakage flux positively couple together, as shown in Figure 4.4.

Now two types of coupling exist in the integrated coupled inductors, including negative coupling represented by the solid green line to reduce the circulating current in arm a-b or c-d, and the positive coupling represented by the dashed purple line to increase the output inductance. The inductor equation now becomes a 4x4 matrix,

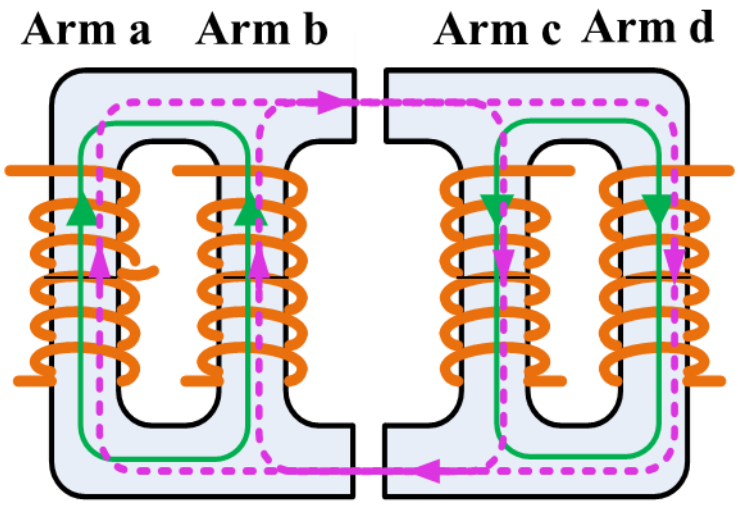

Figure 4.4 Integration process III

$$\begin{bmatrix} v_{La} \\ v_{Lb} \\ v_{Lc} \\ v_{Ld} \end{bmatrix} = \begin{bmatrix} L_{aa} & -M_{ab} & M_{ac} & M_{ad} \\ -M_{ab} & L_{bb} & M_{bc} & M_{bd} \\ M_{ac} & M_{bc} & L_{cc} & -M_{cd} \\ M_{ad} & M_{bd} & -M_{cd} & L_{dd} \end{bmatrix} \begin{bmatrix} \frac{di_{La}}{dt} \\ \frac{di_{Lb}}{dt} \\ \frac{di_{Lc}}{dt} \\ \frac{di_{Ld}}{dt} \end{bmatrix} \tag{4.1}$$

And the negative terms $-M_{ab}$, $-M_{cd}$ represent the negative coupling between winding a and b, and between winding c and d. The positive terms M_{ac}, M_{ad}, M_{bc}, M_{bd} represent the positive coupling between the corresponding windings.

In real implementation of the integrated coupled inductors, two C-C cores are used for providing negative coupled flux, as shown in the exploded 3-D view of Figure 4.5. Because of the volume of winding, two blocks of magnetic material with low permeability are put between two C-C cores to minimize the gap between the C-C cores. And the coupling can still be described in (4.1).

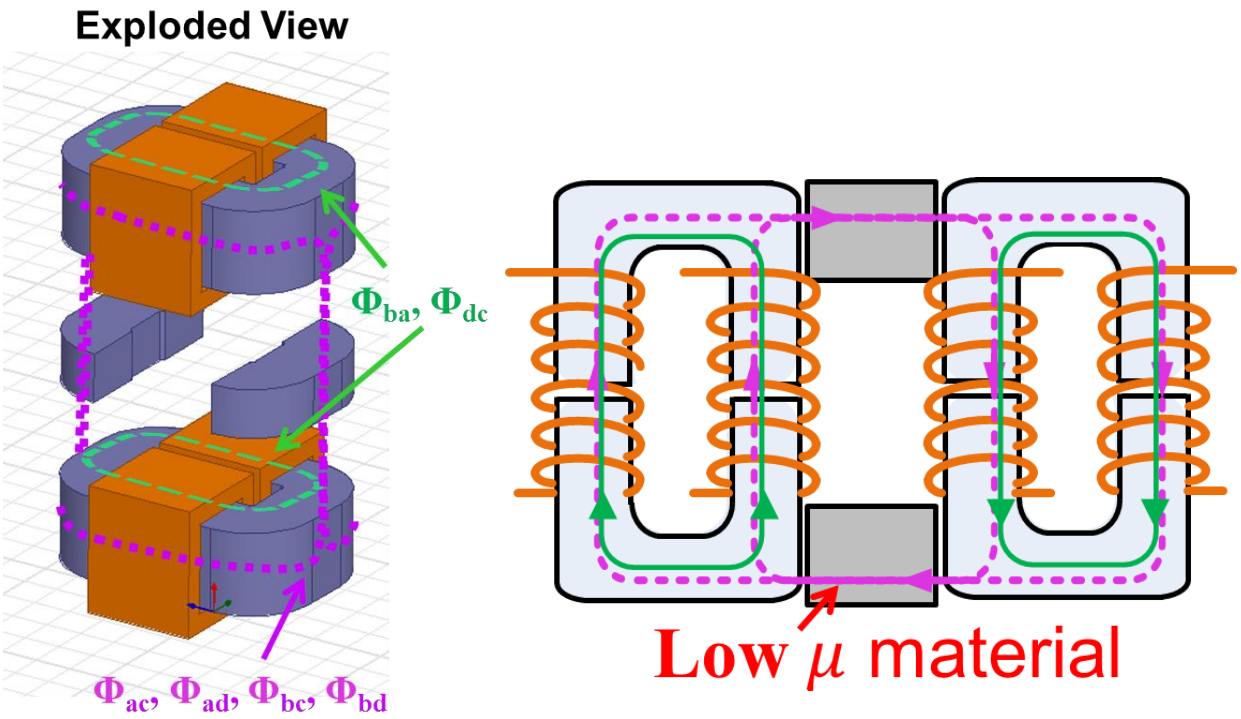

Figure 4.5 Integrated coupled inductors and its exploded 3-D view

For the simplicity of the problem, two assumptions are made before further analysis in the next section. First, all the previous leakage flux shown in the dashed purple line are coupled and there is no residue leakage flux to the air. In other words,

$$\begin{cases} L_{aa} = M_{ab} + M_{ac} + M_{ad} \\ L_{bb} = M_{ab} + M_{bc} + M_{bd} \\ L_{cc} = M_{cd} + M_{ac} + M_{bc} \\ L_{dd} = M_{cd} + M_{ad} + M_{bd} \end{cases} \tag{4.2}$$

Second, considering the 3-D diagram of integrated coupled inductors in Figure 4.5, it is a symmetrical structure,

$$\begin{cases} M_{ab} = M_{cd} = M_x \\ M_{ac} = M_{ad} = M_{bc} = M_{bd} = M_y \\ L_{aa} = L_{bb} = L_{cc} = L_{dd} = L \end{cases} \tag{4.3}$$

With the two assumptions above, the inductor equation can be simplified as,

$$\begin{bmatrix} v_{La} \\ v_{Lb} \\ v_{Lc} \\ v_{Ld} \end{bmatrix} = \begin{bmatrix} L & -M_x & M_y & M_y \\ -M_x & L & M_y & M_y \\ M_y & M_y & L & -M_x \\ M_y & M_y & -M_x & L \end{bmatrix} \begin{bmatrix} \frac{di_{La}}{dt} \\ \frac{di_{Lb}}{dt} \\ \frac{di_{Lc}}{dt} \\ \frac{di_{Ld}}{dt} \end{bmatrix} \tag{4.4}$$

With only two independent variables, the negatively-coupled mutual inductance is M_x and the positively-coupled mutual inductance is M_y. Self-inductance $L=M_x+M_y+M_y$.

4.2 Equivalent Inductance for Integrated Coupled Inductors

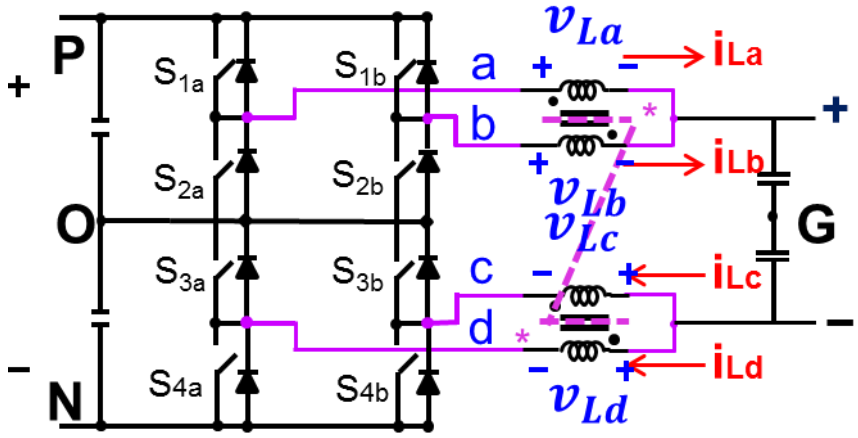

Figure 4.6 Three-level DC/DC converter with integrated coupled inductors

With four arm inductors all coupled together, the coupling analysis is much more complex. Similar to the two coupled inductors case in Chapter 3, there are eight different inductor voltage combinations in one switching cycle, and strong non-linearity effect of the inductor is shown in Figure 4.7. Considering the complex coupling structure, equivalent inductance is again applied for the analysis.

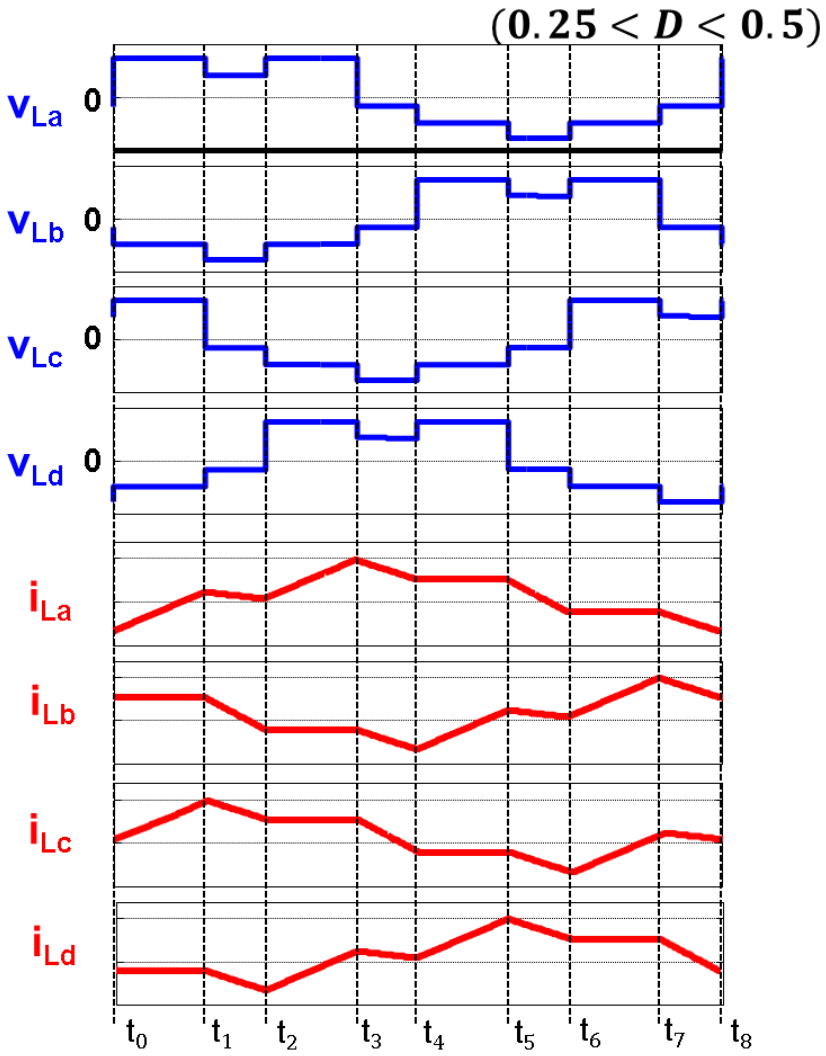

Figure 4.7 Inductor voltage and current waveform with integrated coupled inductors

The equivalent inductance with integrated coupled inductors can be derived in the same procedure as analyzed in chapter 3, although the coupling condition is more complex as shown in

(4.4). If the relationship between the four inductor voltages can be found, the four arm inductors can be mathematically decoupled from (4.4). It should be noted that analysis is still based on the N-type interleaving condition.

To find the inductor voltage relationship, the equivalent circuit of the converter is drawn first in Figure 4.8.

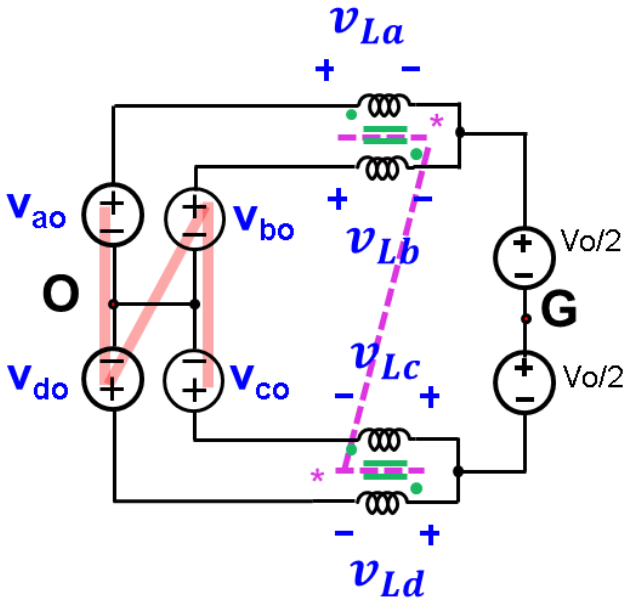

Figure 4.8 Equivalent circuit of the converter with integrated coupled inductors

(4.4) can be reorganized to (4.5) without assumptions that,

$$\begin{bmatrix} L^2 v_{La} - M_x^2 v_{Lb} - (2M_y^2 + LM_x)(v_{La} - v_{Lb}) - M_y(L + M_x)(v_{Lc} + v_{Ld}) \\ L^2 v_b - M_x^2 v_{La} - (2M_y^2 + LM_x)(v_{Lb} - v_{La}) - M_y(L + M_x)(v_{Lc} + v_{Ld}) \\ L^2 v_c - M_x^2 v_{Ld} - (2M_y^2 + LM_x)(v_{Lc} - v_{Ld}) - M_y(L + M_x)(v_{La} + v_{Lb}) \\ L^2 v_d - M_x^2 v_{Lc} - (2M_y^2 + LM_x)(v_{Ld} - v_{Lc}) - M_y(L + M_x)(v_{La} + v_{Lb}) \end{bmatrix} = \begin{bmatrix} (L + M_x)(L^2 - 2LM_x + M_x^2 - 4M_y^2) & 0 & 0 & 0 \\ 0 & (L + M_x)(L^2 - 2LM_x + M_x^2 - 4M_y^2) & 0 & 0 \\ 0 & 0 & (L + M_x)(L^2 - 2LM_x + M_x^2 - 4M_y^2) & 0 \\ 0 & 0 & 0 & (L + M_x)(L^2 - 2LM_x + M_x^2 - 4M_y^2) \end{bmatrix} \begin{bmatrix} \frac{di_{La}}{dt} \\ \frac{di_{Lb}}{dt} \\ \frac{di_{Lc}}{dt} \\ \frac{di_{Ld}}{dt} \end{bmatrix}$$

(4.5)

If the relationship between the four inductor voltages v_{La}, v_{Lb}, v_{Lc} and v_{Ld} in the left part of (4.5) can be found, the four inductors can be mathematically decoupled.

By Kirchhoff's voltage law, the inductor voltage is first derived as,

$$\begin{cases} v_{La} = v_{ao} - \dfrac{V_o}{2} - v_{GO} \\ v_{Lb} = v_{bo} - \dfrac{V_o}{2} - v_{GO} \\ v_{Lc} = -v_{co} - \dfrac{V_o}{2} + v_{GO} \\ v_{Ld} = -v_{do} - \dfrac{V_o}{2} + v_{GO} \end{cases} \tag{4.6}$$

With v_{GO} defined in (3.12).

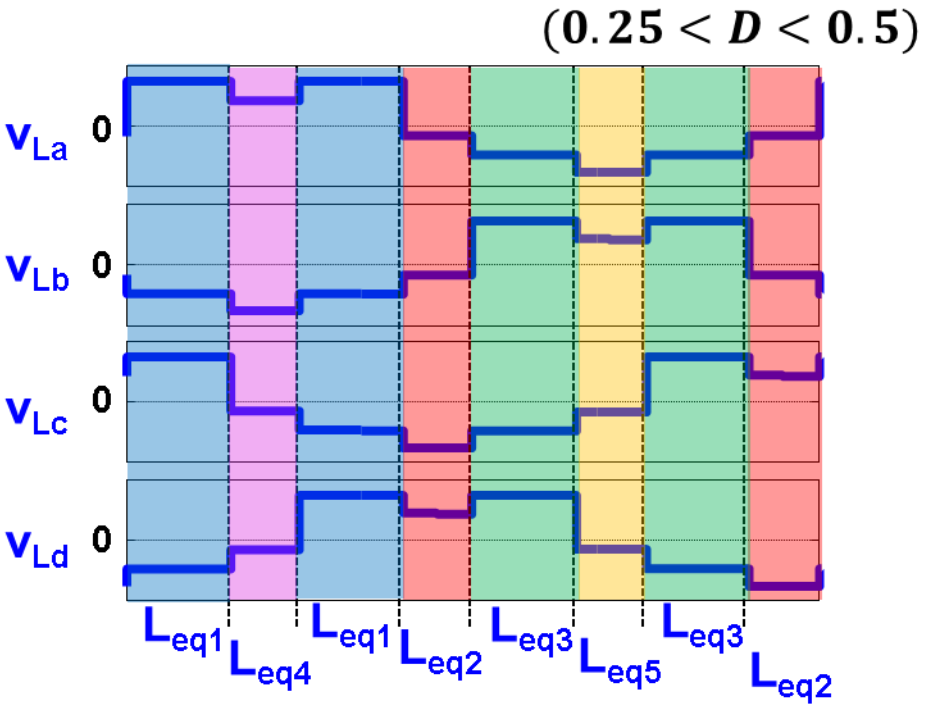

Figure 4.9 Inductor voltage in three-level converter

Figure 4.9 gives the inductor voltage within one switching cycle when duty ratio 0.25<D<0.5 with N-type interleaving. Based on these inductor voltage waveforms, equivalent inductance can be derived. For other duty cycle conditions, there are also eight different time intervals, and the analysis method is similar.

The first time interval in Figure 4.9 is used as an example to demonstrate the process of deriving equivalent inductance. From both circuit and waveform, one can easily find that,

$$\begin{cases} v_{La} = \dfrac{V_{in} - DV_{in}}{2} \\ v_{Lb} = \dfrac{-DV_{in}}{2} \\ v_{Lc} = \dfrac{V_{in} - DV_{in}}{2} \\ v_{Ld} = \dfrac{-DV_{in}}{2} \\ v_{GO} = \dfrac{v_{ao} + v_{bo} + v_{co} + v_{do}}{4} = 0 \end{cases} \tag{4.7}$$

By take (4.7) into (4.5), one can decouple the matrix of inductor equation (4.5), and the relationship for inductor voltage and current of each arm can be directly connected. (4.5) becomes,

$$\begin{bmatrix} v_{La} \\ v_{Lb} \\ v_{Lc} \\ v_{Ld} \end{bmatrix} = \begin{bmatrix} \frac{(1-D)(L+M_x)(L-M_x+2M_y)}{L(1-D)-M_xD+M_y} & 0 & 0 & 0 \\ 0 & \frac{D(L+M_x)(L-M_x+2M_y)}{LD-M_x(1-D)+M_y} & 0 & 0 \\ 0 & 0 & \frac{(1-D)(L+M_x)(L-M_x+2M_y)}{L(1-D)-M_xD+M_y} & 0 \\ 0 & 0 & 0 & \frac{D(L+M_x)(L-M_x+2M_y)}{LD-M_x(1-D)+M_y} \end{bmatrix} \begin{bmatrix} \frac{di_{La}}{dt} \\ \frac{di_{Lb}}{dt} \\ \frac{di_{Lc}}{dt} \\ \frac{di_{Ld}}{dt} \end{bmatrix} \tag{4.8}$$

And

$$v_{La} = \frac{(1-D)(L+M_x)(L-M_x+2M_y)}{L(1-D)-M_xD+M_y}\frac{di_{La}}{dt} \tag{4.9}$$

And now the equivalent inductance is defined as,

$$L_{eq1} = \frac{(1-D)(L+M_x)(L-M_x+2M_y)}{L(1-D)-M_xD+M_y} \tag{4.10}$$

Note the equivalent inductance is defined based on arm a. For the equivalent inductance on arm b, c and d, the only difference would be a 90 degree phase shift due to the N-type interleaving. Because of the positive-coupling of the integrated coupled inductors, the equivalent inductance is quite different compared to the two separated coupled inductors case, which is analyzed in chapter 3.

By going over the eight time intervals within one switching cycle one by one, there are five different equivalent inductances within one switching cycle, as shown in the shaded area of different color in Figure 4.9.

$$\begin{cases} L_{eq1} = \dfrac{(1-D)(L+M_x)(L-M_x+2M_y)}{L(1-D)-M_xD+M_y} \\ L_{eq2} = L-M_x+2M_y \\ L_{eq3} = \dfrac{D(L+M_x)(L-M_x+2M_y)}{LD-M_x(1-D)+M_y} \\ L_{eq4} = \dfrac{(3-4D)(L+M_x)(L-M_x+2M_y)}{L(3-4D)-M_x(4D+1)+M_y} \\ L_{eq5} = \dfrac{(1+4D)(L+M_x)(L-M_x+2M_y)}{L(1+4D)-M_x(3-4D)+M_y} \end{cases} \tag{4.11}$$

Note Leq2 has a direct physical meaning, since,

$$L_{eq2} = L - M_x + 2M_y = 4M_y \tag{4.12}$$

L_{eq2} is not affected by M_x and it is only determined by the positive coupling mutual inductance M_y.

4.3 Coupling Effect on Inductor Current Ripple and Output Current Ripple

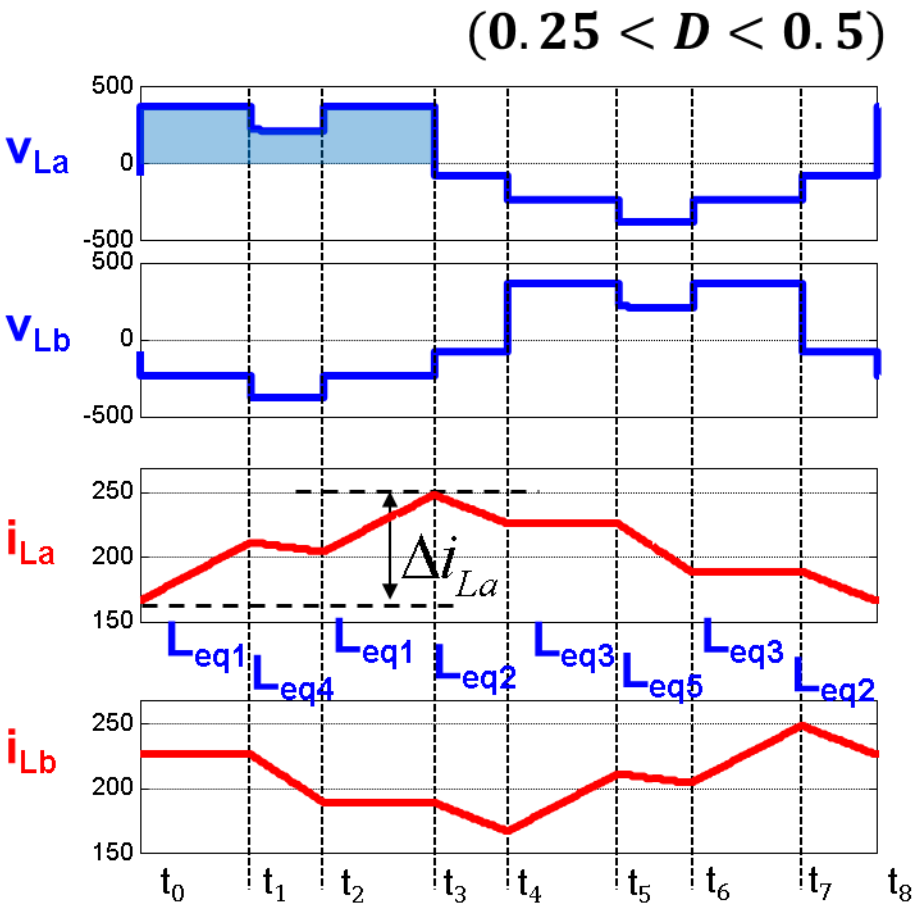

Figure 4.10 Inductor current waveform with integrated coupled inductors

Inductor current waveform with integrated coupled inductors is shown in Figure 4.10, and inductor current ripple with integrated coupled inductors are derived as,

$$\Delta i_{La} = \frac{\langle v_{La} \rangle_{T1}}{L_{eq1}} + \frac{\langle v_{La} \rangle_{T2}}{L_{eq4}} + \frac{\langle v_{La} \rangle_{T3}}{L_{eq1}} \tag{4.13}$$

Similar to the two coupled inductors case in chapter 3, inductor current ripple with integrated coupled inductors is also determined by the first three time intervals. To have a fair comparison with the two coupled inductors case, the steady-state equivalent inductance determining the inductor current ripple is defined,

$$L_{ss} = \frac{\langle v_{La} \rangle_{T1} + \langle v_{La} \rangle_{T2} + \langle v_{La} \rangle_{T3}}{\Delta i_{La}} = \frac{\langle v_{La} \rangle_{T1} + \langle v_{La} \rangle_{T2} + \langle v_{La} \rangle_{T3}}{\frac{\langle v_{La} \rangle_{T1}}{L_{eq1}} + \frac{\langle v_{La} \rangle_{T2}}{L_{eq4}} + \frac{\langle v_{La} \rangle_{T3}}{L_{eq1}}} \tag{4.14}$$

With simple mathematical derivation, (4.14) becomes,

$$L_{ss} = \frac{(-8D^2 + 10D - 1)(L + M_x)(L - M_x + 2M_y)}{(-8D^2 + 10D - 1)L - (8D^2 - 2D + 1)M_x + 8DM_y} \tag{4.15}$$

For the output current ripple, the relationship with equivalent inductance can be observed from the current waveform directly in Figure 4.11. In the time interval t3-t4, both inductor current ripples i_{La} and i_{Lb} are determined by L_{eq2}, and the overall output current ripple is also solely determined by L_{eq2}, or $4M_y$. The same conclusion can be drawn for other duty cycle ranges.

$$\Delta i_o = \frac{\langle v_{La} \rangle_{T4}}{L_{eq2}} + \frac{\langle v_{Lb} \rangle_{T4}}{L_{eq2}} \tag{4.16}$$

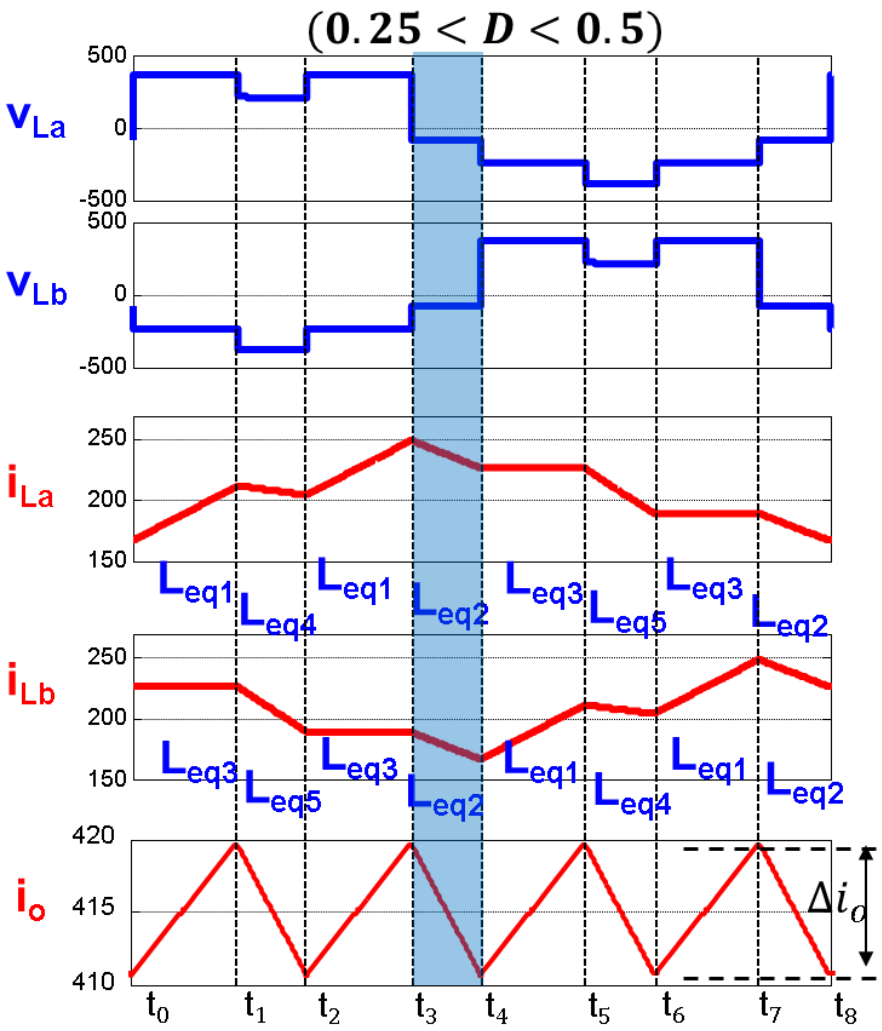

Figure 4.11 Output current ripple determination with integrated coupled inductors

Another way to analyze output current ripple is using (4.4). The four inductor equations in (4.4) can be added together, and

$$\begin{aligned} & v_{La} + v_{Lb} + v_{Lc} + v_{Ld} \\ & = (L - M_x + 2M_y)\frac{d(i_{La} + i_{Lb} + i_{Lc} + i_{Ld})}{dt} \\ & = L_{eq2}\frac{d2i_o}{dt} \end{aligned} \tag{4.17}$$

With the inductor voltages determined by the operation condition of the converter, the output current waveform is totally determined by L_{eq2}.

For a fair comparison between the integrated coupled inductors case and the two coupled inductors case, output current ripple is assumed to be identical. In other words, L_{eq2} for both cases should be equal. Under this condition, one can compare the two cases in terms of inductor current ripple reduction effect.

For duty ratio 0.25<D<0.5 case,

$$\frac{\Delta i_{La}(integrated\ CI\ case)}{\Delta i_{La}(two\ CI\ case)} = \frac{(2+\frac{M_x}{M_y})[(8D^2-6D+1)\frac{M_x}{M_y}+(8D^2-14D+1)]}{(1+\frac{M_x}{M_y})[(8D^2-6D+1)\frac{M_x}{M_y}+(16D^2-20D+2)]} \quad (4.18)$$

Based on (4.18), Figure 4.12 is drawn to compare the inductor current reduction effect in terms of the ratio between M_x and M_y, which represent negative coupling and positive coupling, respectively. The duty ratio is selected as 0.5 as an example.

When the ratio of M_x and M_y is low, the inductor current ripple with integrated coupled inductors is much higher than the two coupled inductors case. It is not preferable although integration can reduce the size of magnetic components. As the ratio becomes larger, the difference of inductor current ripple reduction effect diminishes. As a result, a large ratio between M_x and M_y is preferred, such that the two cases will have similar inductor current ripple reduction effects, while the integrated case has the advantage of higher power density due to the integrated magnetic core. The result is valid within the whole duty cycle range, as shown in Figure 4.13.

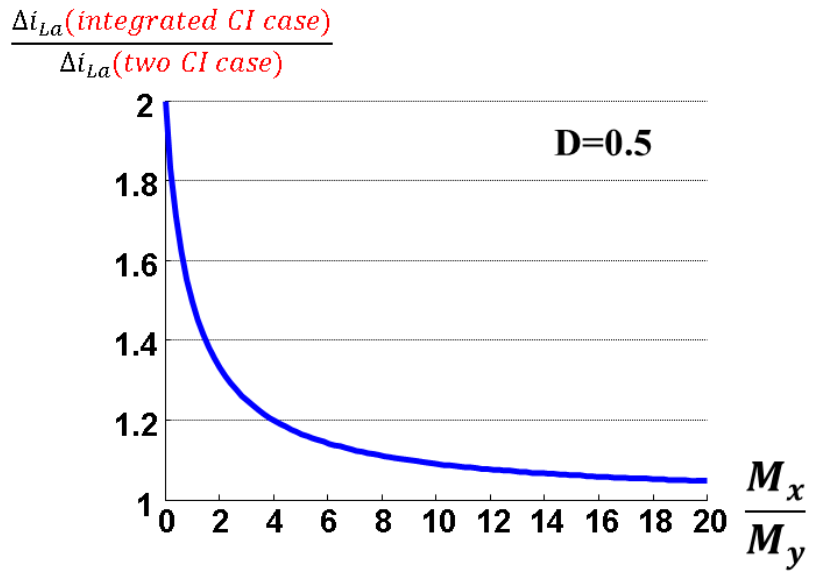

Figure 4.12 Inductor current ripple comparison

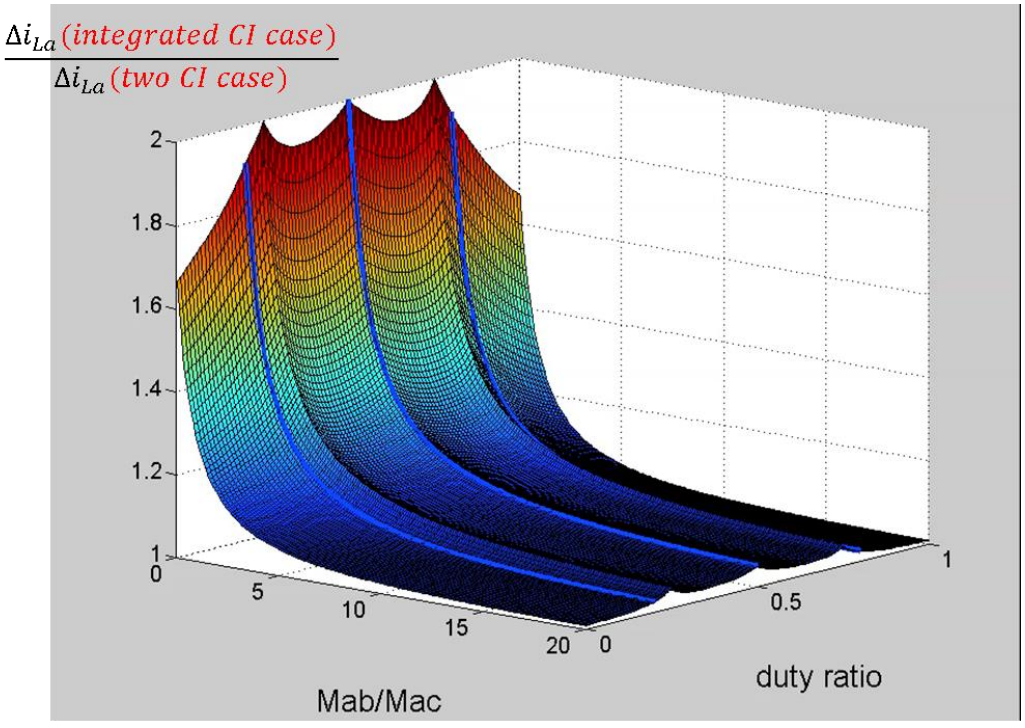

Figure 4.13 Inductor current ripple comparison within whole duty cycle range

4.4 Coupling Design based on Current Ripple Requirement

As discussed in section 4.1, two types of coupling effects exist in integrated coupled inductors and should be properly designed. Mutual inductance M_x represents the negative coupling effect to suppress the circulating current, and mutual inductance M_y represents the positive coupling effect to reduce the output current ripple. And the self-inductance $L=M_x+2M_y$.

The coupling of integrated coupled inductors should be designed based on the performance requirement of the converter. Through the equivalent inductance analysis, the inductor current ripple and output current ripple equation is,

$$\Delta i_o = \begin{cases} \dfrac{V_{dc}\cdot(1-4D)}{4L_{eq2}}\cdot DT & D<0.25 \\ \dfrac{V_{dc}\cdot(4D-1)}{8L_{eq2}}\cdot(1-2D)T & 0.25\le D<0.5 \\ \dfrac{V_{dc}\cdot(3-4D)}{8L_{eq2}}\cdot(2D-1)T & 0.5\le D<0.75 \\ \dfrac{V_{dc}\cdot(4D-3)}{4L_{eq2}}\cdot(1-D)T & 0.75\le D<1 \end{cases} \tag{4.19}$$

$$\Delta i_{La} = \begin{cases} \dfrac{V_{dc}(1-4D)}{32M_y}DT+\dfrac{V_{dc}D}{4(2M_x+2M_y)}T & D<0.25 \\ \dfrac{V_{dc}(4D-1)}{64M_y}(1-2D)T+\dfrac{V_{dc}D}{4(2M_x+2M_y)}T & 0.25\le D<0.5 \\ \dfrac{V_{dc}(3-4D)}{64M_y}(2D-1)T+\dfrac{V_{dc}(1-D)}{4(2M_x+2M_y)}T & 0.5\le D<0.75 \\ \dfrac{V_{dc}(4D-3)}{32M_y}(1-D)T+\dfrac{V_{dc}(1-D)}{4(2M_x+2M_y)}T & 0.75\le D \end{cases} \tag{4.20}$$

The design process includes two steps. Since the L_{eq2} determines the output current ripple and equals to $4M_y$, the mutual inductance M_y can be designed directly with the output current

ripple requirement. With M_y determined, mutual inductance M_x will be designed based on the inductor current ripple requirement. Input voltage V_{dc}=1200V, switching frequency f_{sw}=1/T=20 kHz, power rating P=200kW.

In the first step, L_{eq2} is designed based on the output current ripple, which is the same process as the two coupled inductors case in section 3.4. The only difference is that now $L_{eq2}=4M_y$. From Figure 4.14, the maximum output current ripple can be calculated by sweeping different L_{eq2} value, and Figure 4.15 can be drawn accordingly. If the required maximum output current ripple is given, for example 16A, the designed L_{eq2} will be 60μH. In other words, the designed mutual inductance M_y should be larger than 15μH to guarantee the maximum output current ripple to be less than 16A.

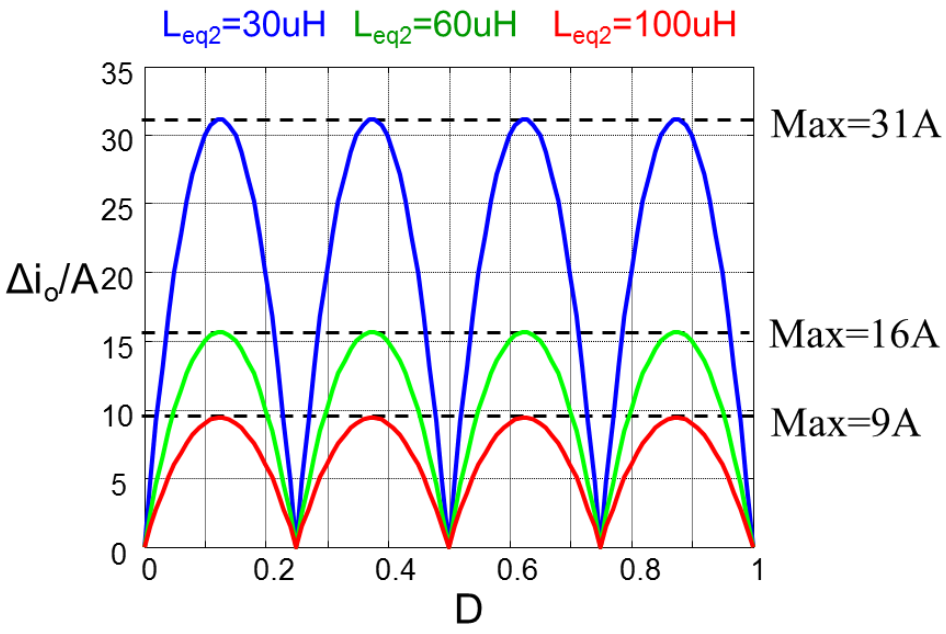

Figure 4.14 Output current ripple with different L_{eq2}

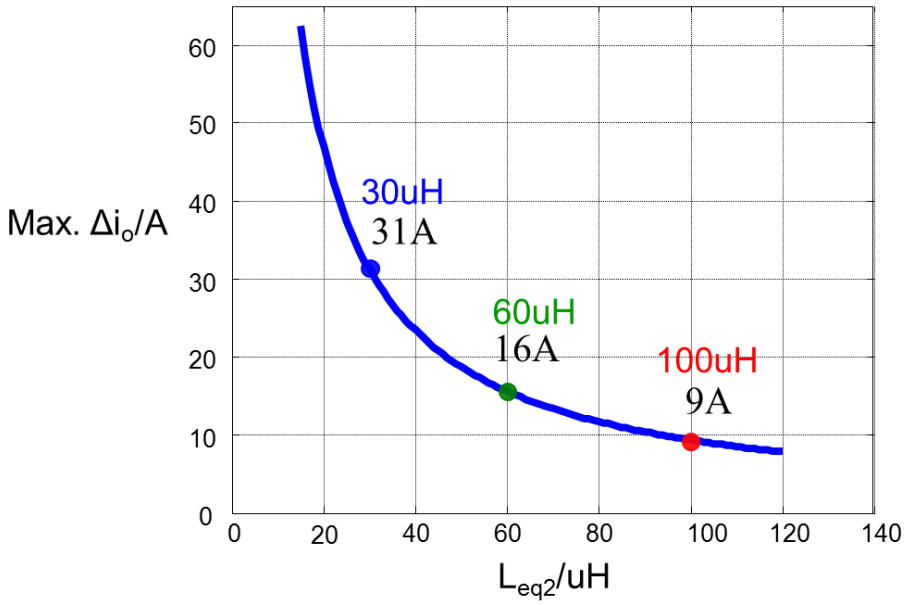

Figure 4.15 Design L_{eq2} based on output current ripple

With M_y value determined, mutual inductance M_x could be designed based on the inductor current ripple requirement.

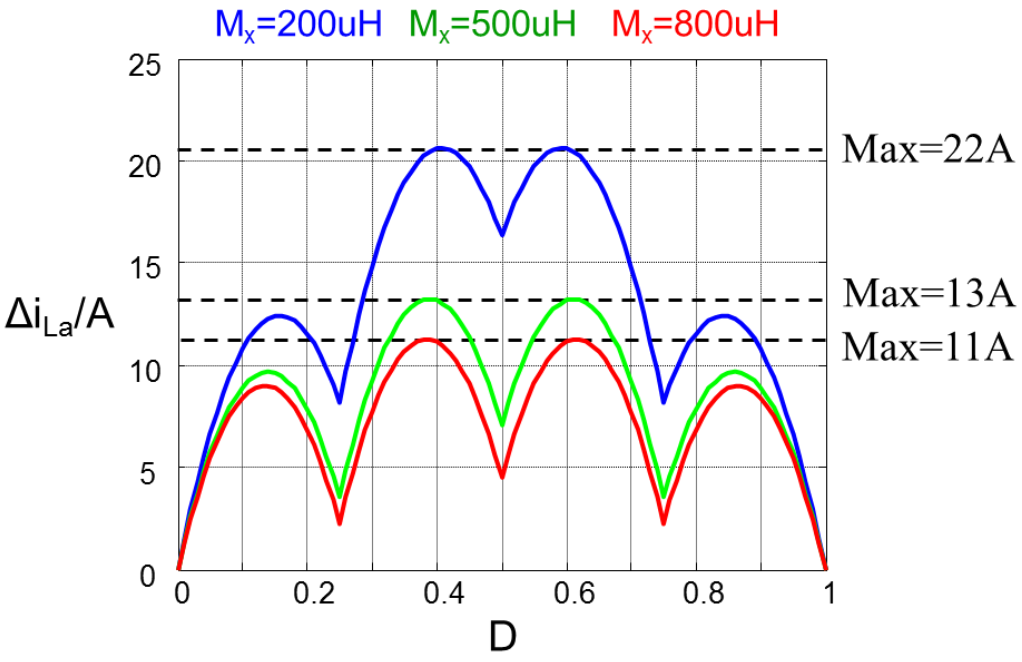

Figure 4.16 Inductor current ripple with different M_x

With M_y=15μH, the inductor current ripple can be plotted using (4.20) in Figure 4.16. By sweeping the maximum inductor current ripple with different M_x values, Figure 4.17 is drawn. M_x is designed at the corner of the curve for 500μH to guarantee the maximum inductor current ripple of 13A.

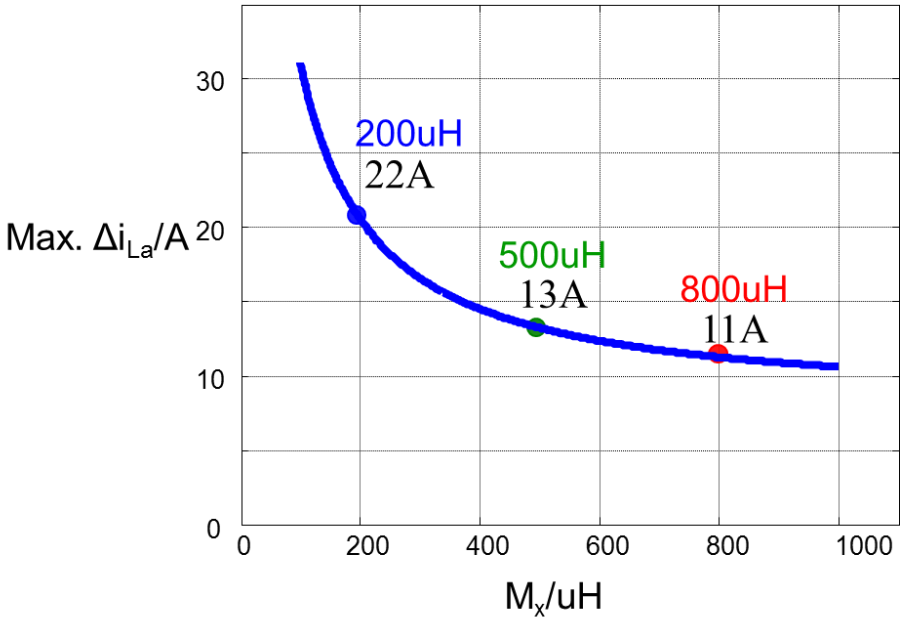

Figure 4.17 Design M_x based on inductor current ripple

Followed by the two steps above, M_x=500μH, M_y=15μH is designed for the 16A output current ripple and 13A inductor current ripple.

Simulation is used the check the analysis result. The integrated coupled inductors indicated in the shaded area of Figure 4.18 is simulated using six ideal transformers. Figure 4.18 gives the converter circuit, and the parameters are input voltage V_{in}=1200V, output voltage V_o=480, duty ratio D=0.4, switching frequency f_{sw}=20kHz, and power rating P=200kW. As shown in Figure 4.19, the different coupling effects among the four arms a, b c and d are represented by ideal transformers, with the magnetizing inductance equal to the mutual inductance designed.

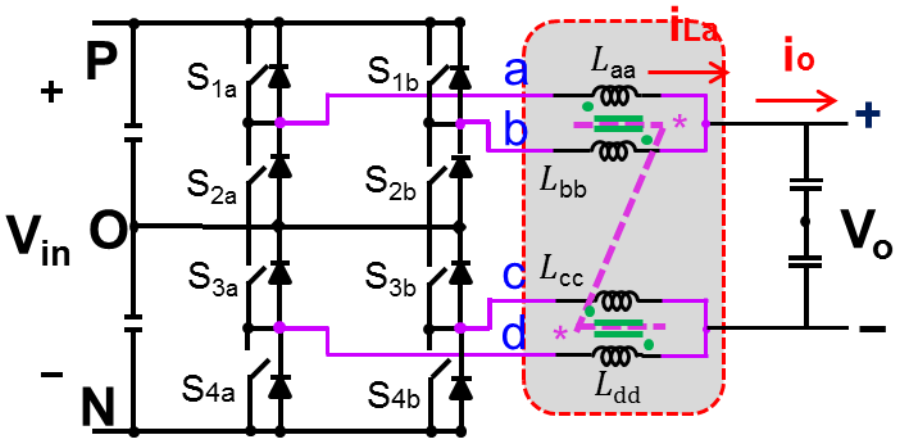

Figure 4.18 Three-level DC/DC Converter with integrated coupled inductors

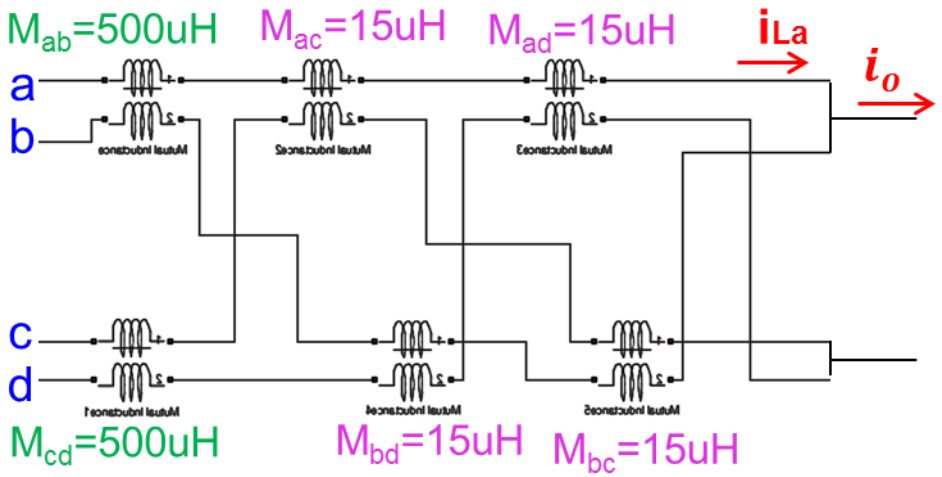

Figure 4.19 Simulation circuit model for integrated coupled inductors

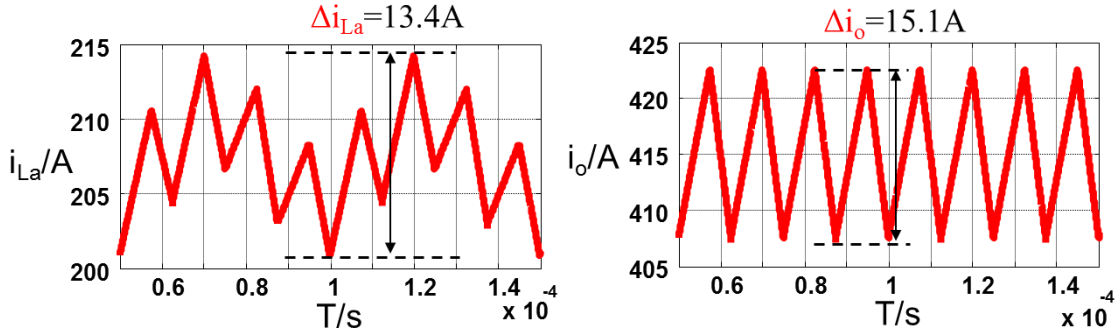

Figure 4.20 Simulation waveform of inductor current and output current

In the simulation result of Figure 4.20, both inductor current ripple and output current ripple are within the design target, which is Δi_{La}=13A, Δi_o=15A.

4.5 Magnetic Circuit Analysis

Considering the three-dimensional structure of the integrated coupled inductors, the proper air gap should be used to guarantee the required positive coupling and negative coupling. By Figure 4.21, the air gap of the C-C core is defined as l_1 and the air gap between the center block and C-C core is defined as l_2. The relative permeability of the center block is μ_r. In this case the cross-section area of C-C core is A and for center block is 2A.

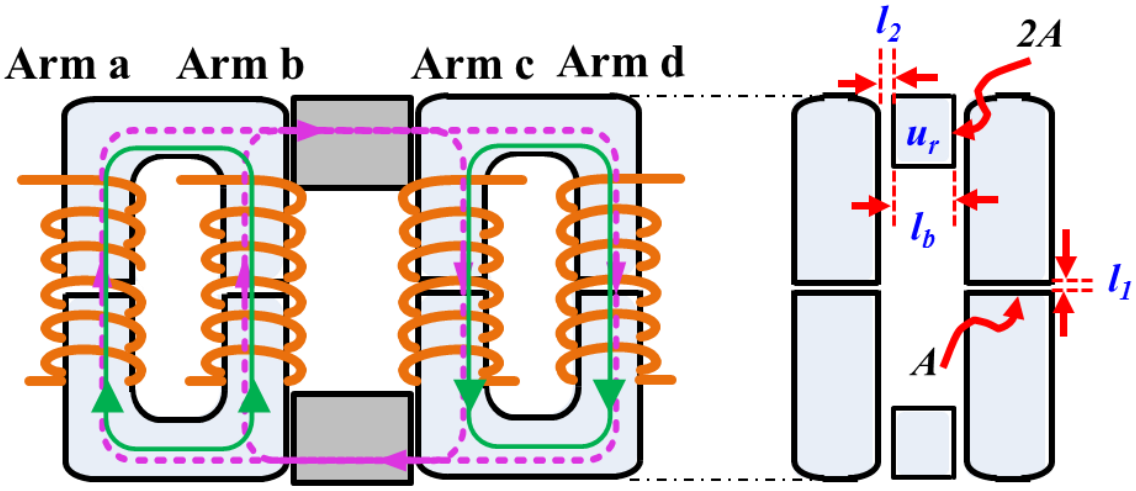

Figure 4.21 Geometry of integrated coupled inductors

Based on Figure 4.21, the magnetic circuit is shown as below, with

$$R_1 = \frac{l_1}{\mu_0 A} \tag{4.21}$$

$$R_2 = \frac{2l_2}{2\mu_0 A} + \frac{l_b}{2\mu_0 \mu_r A} \tag{4.22}$$

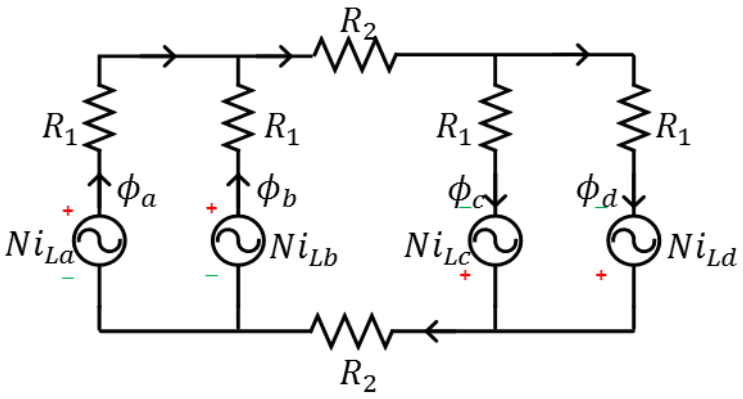

Figure 4.22 Magnetic circuit of integrated coupled inductors

Where R_1 is the reluctance of air gap l_1 and R_2 is the reluctance of air gap l_2 together with the center block. It should be noted that high permeability material is used for the C-C core and its reluctance is assumed to be neglected in the analysis.

From the magnetic circuit, the negative coupled mutual inductance M_x and positive coupled mutual inductance M_y can be derived,

$$M_x = \frac{N^2(4R_2 + R_1)}{8R_1R_2 + 4R_1^2} \tag{4.23}$$

$$M_y = \frac{N^2}{4R_1 + 8R_2} \tag{4.24}$$

And the ratio representing two coupling effects is,

$$\frac{M_x}{M_y} = \frac{4R_2 + R_1}{R_1} = \frac{4l_2 + \frac{2l_b}{\mu_r} + l_1}{l_1} \tag{4.25}$$

As stated in the previous section, the high ratio of M_x and M_y is preferred, such that the integrated coupled inductors case will have comparable performance with the two coupled inductors case,

while the volume of the inductor can be reduced. A high ratio can be guaranteed by either increasing l_1, decreasing l_2, or using the center block with high reluctance. As a result, to provide a high ratio and also to reduce the air gap l_2, a material with low permeability should be used for the center block.

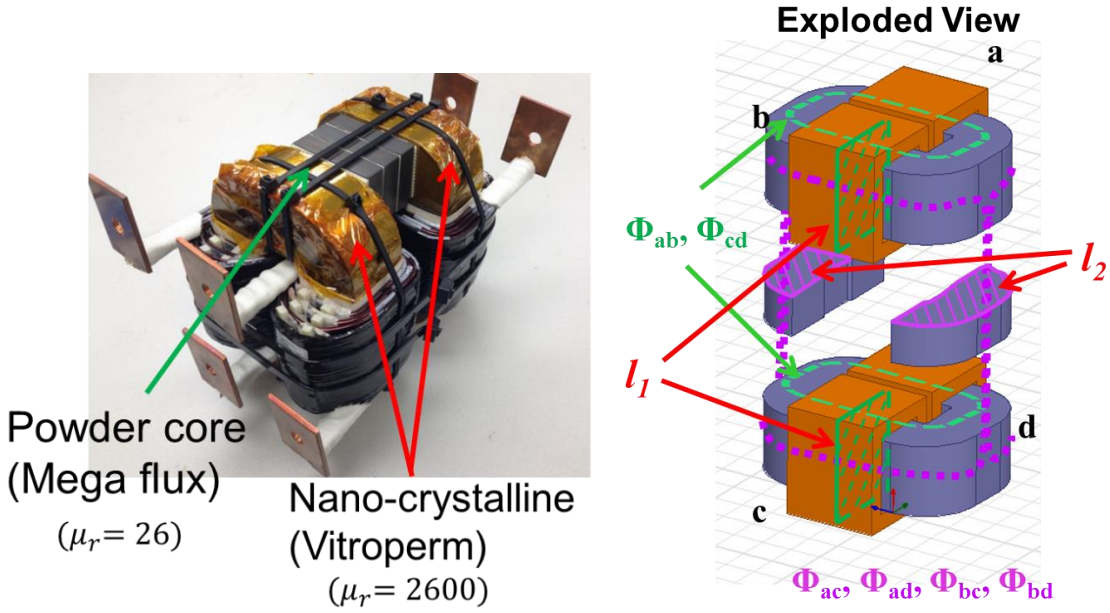

Figure 4.23 Fabricated integrated coupled inductors

In real implementation, with the mutual inductance value determined, nano-crystalline material is used for the C-C core, and the low permeability power core is applied as the center block [34]. With the material determined, the required air gap for l_1 and l_2 is then designed as l_1=0.4mm, l_2=1.4mm.

4.6 Inductor Test and Verification

With the integrated coupled inductors designed, the dimension of the magnetic component is decided, and the inductor size reduction of integrated coupled inductors can be compared and evaluated with the non-coupling inductor case and the two coupled inductors case. It should be

noted that the three scenarios are compared with the same inductor current ripple and output current ripple conditions.

The first scenario is non-interleaving three-level DC/DC converter with non-coupling inductors, and four single inductors are required for the converter. The second scenario is N-type interleaving with two separate coupled inductors, and the last scenario is N-type interleaving with integrated coupled inductors. Figure 4.24 gives the converter circuit and corresponding 3-D inductor structure. With integrated structure, the volume for magnetics is 3.95L, which is only half of the inductor size in non-coupling inductor case [34]. Therefore, the integration of magnetics brings benefits of increased power density and better ripple performance.

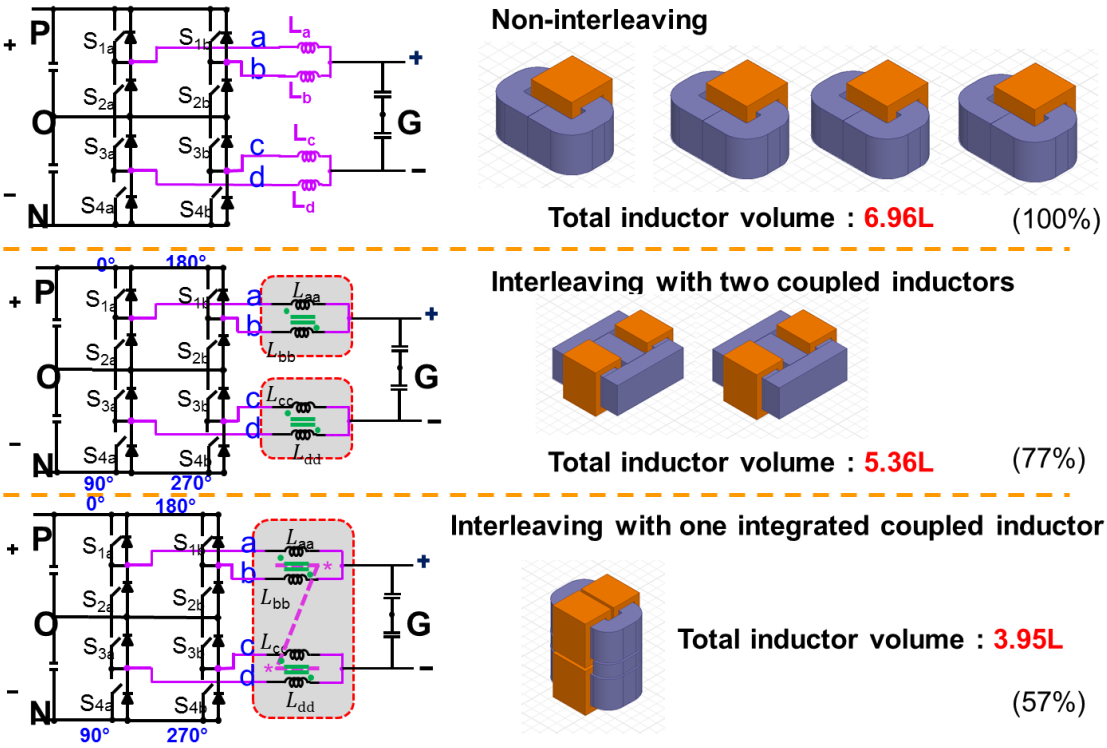

Figure 4.24 Inductor size comparison

With the fabricated integrated coupled inductors, it is crucial to have the inductor tested and verified first to see if it can fulfill the mutual inductance requirements, as mentioned in the previous section.

The verification process includes two parts: the test of negative coupling mutual inductance M_{ab} & M_{cd}, and the test of positive coupling mutual inductance M_{ac}, M_{ad}, M_{bc} & M_{bd}. As the inductor is assumed to be a symmetrical structure, here $M_x=M_{ab}=M_{cd}$ and $M_y=M_{ac}=M_{ad}=M_{bc}=M_{bd}$ will be set as variables for the test. Also, the self-inductance can be calculated using (4.2) if needed. Figure 4.25 gives the structure of the integrated coupled inductors with eight terminals. a_1, b_1, c_1, d_1 represent four terminals connecting to the phase legs side, while a_2, b_2, c_2, d_2 represent four terminals connecting to the output side.

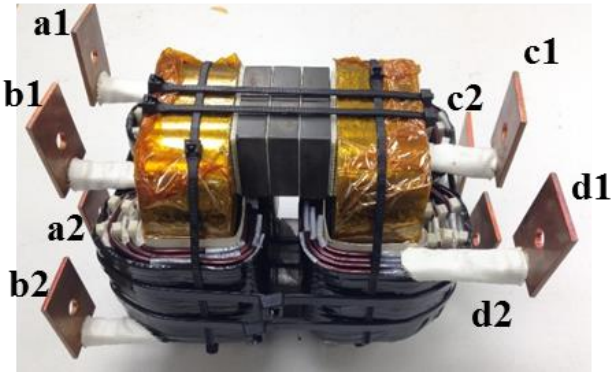

Figure 4.25 Fabricated integrated coupled inductors for test

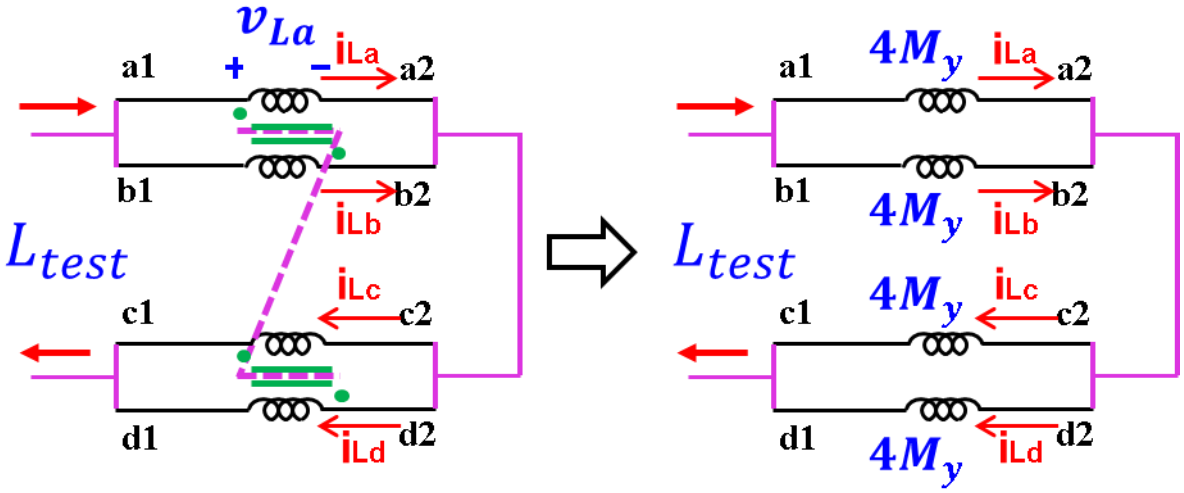

Figure 4.26 Test circuit for M_y

To test the mutual inductance M_y, the inductor is configured in the left-side circuit in Figure 4.26. Arm a and b are connected in parallel, and then connecting with arm c & d paralleled in series. Under this condition,

$$i_{La} = i_{Lb} = i_{Lc} = i_{Ld} \tag{4.26}$$

$$v_{La} = L\frac{di_{La}}{dt} - M_x\frac{di_{Lb}}{dt} + M_y\frac{di_{Lc}}{dt} + M_y\frac{di_{Ld}}{dt} \tag{4.27}$$

Put (4.26) into (4.27),

$$v_{La} = (L - M_x + M_y + M_y)\frac{di_{La}}{dt} = 4M_y\frac{di_{La}}{dt} \tag{4.28}$$

Now integrated coupled inductors are decoupled and the same conclusion can be drawn for the other three arms b, c & d. As a result, the right-side circuit in Figure 4.26 is derived for the representation of decoupled inductors. For all four arms a, b, c & d, the inductance is just $4M_y$. And the tested inductance L_{test} is,

$$L_{test} = 4M_y \tag{4.29}$$

Figure 4.27 and Figure 4.28 give the tested inductance L_{test} result from impedance analyzer and single pulse test, respectively. From both test methods, the measured inductance is about 60μH, or the mutual inductance M_y is 15μH, which is the design target to meet the current ripple requirement. Also note the saturation current is over 800A.

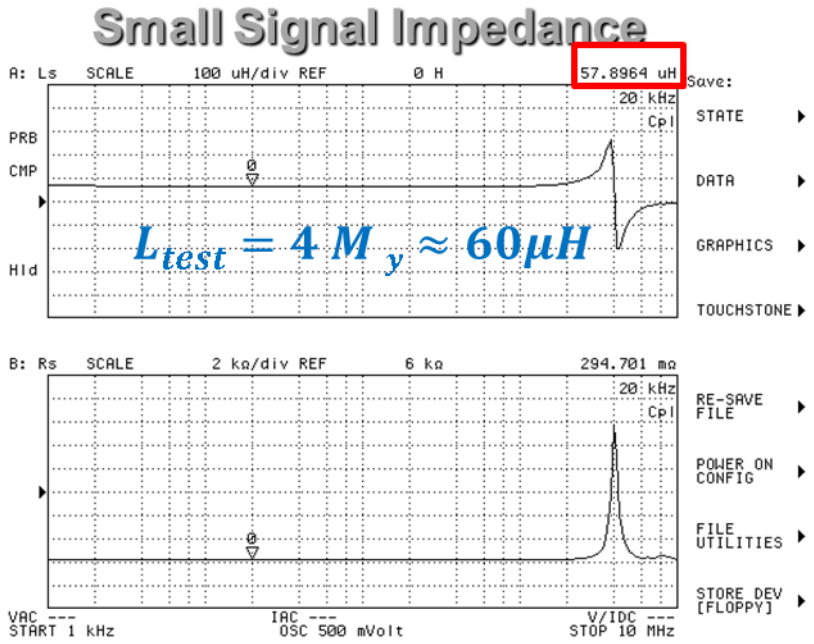

Figure 4.27 Test result for M_y with impedance analyzer

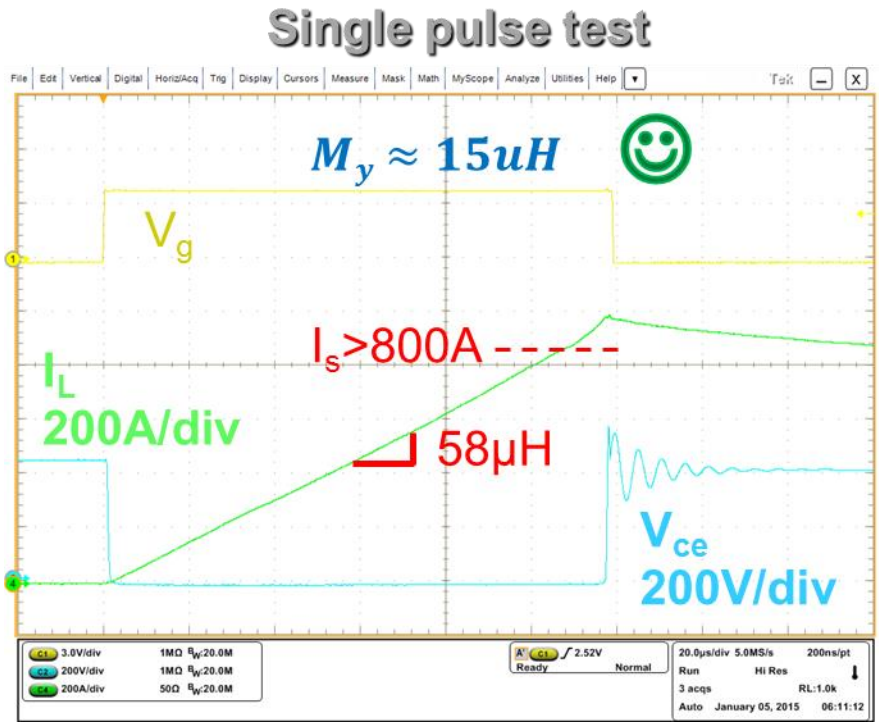

Figure 4.28 Test result for M_y with single pulse test

As the second test step, the mutual inductance M_x needs verification, and its test circuit is shown in the left part of Figure 4.29. Arm a and arm b are connected in series, with arm c and d left open.

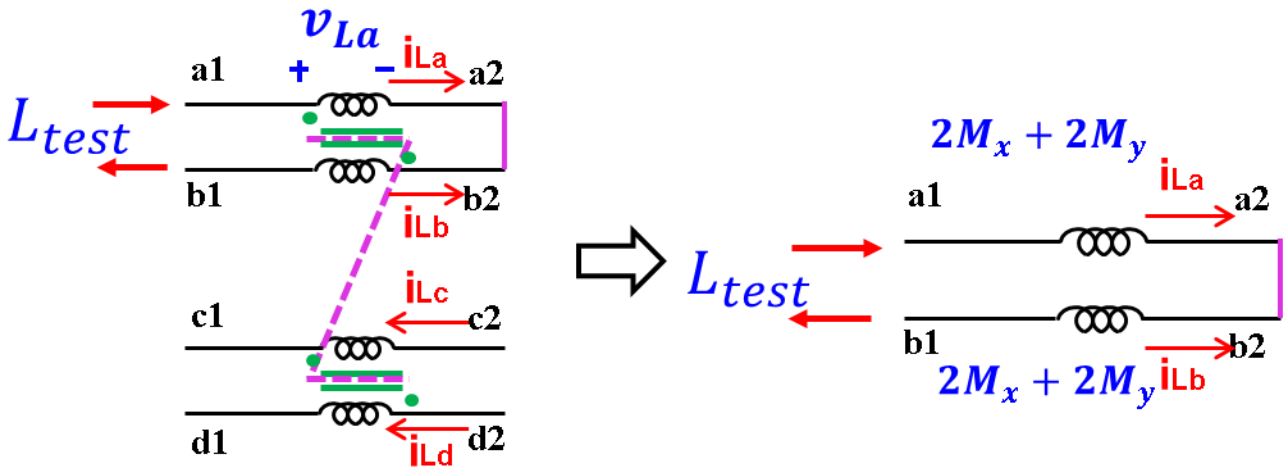

Figure 4.29 Test circuit for M_x

Under this condition,

$$i_{La} = -i_{Lb}, \quad i_{Lc} = -i_{Ld} = 0 \tag{4.30}$$

By taking (4.30) into (4.27),

$$v_{La} = (L + M_x)\frac{di_{La}}{dt} = (2M_x + 2M_y)\frac{di_{La}}{dt} \tag{4.31}$$

The relationship of inductor voltage and current is built for arm a, and the conclusion for arm b is exactly the same. As a result, under this circuit configuration, the tested inductance is just two inductor series connected with the inductance value of $2M_x+2M_y$, as shown in the right part of Figure 4.29.

$$L_{test} = 4M_x + 4M_y \tag{4.32}$$

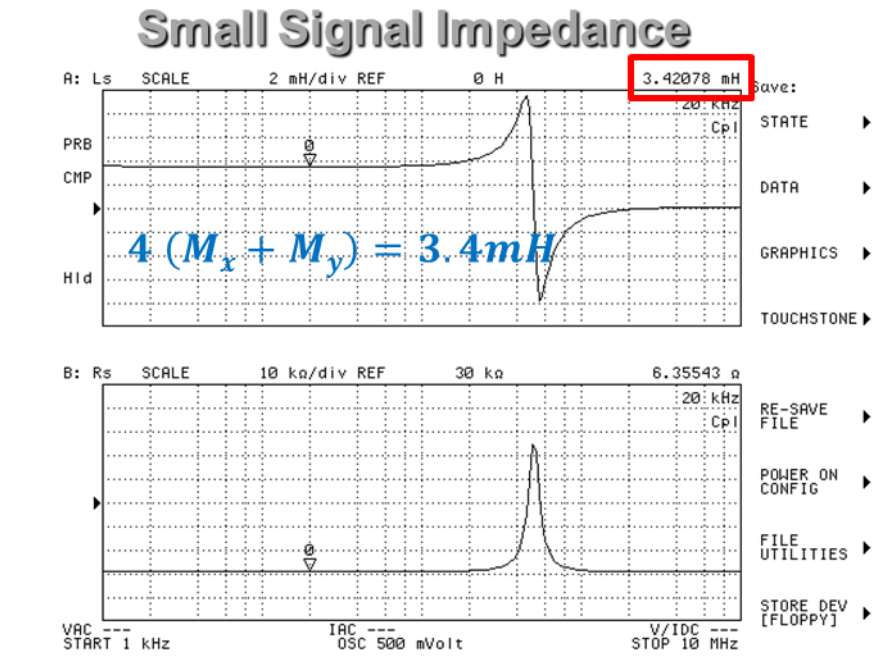

Figure 4.30 Test result for M_x with impedance analyzer

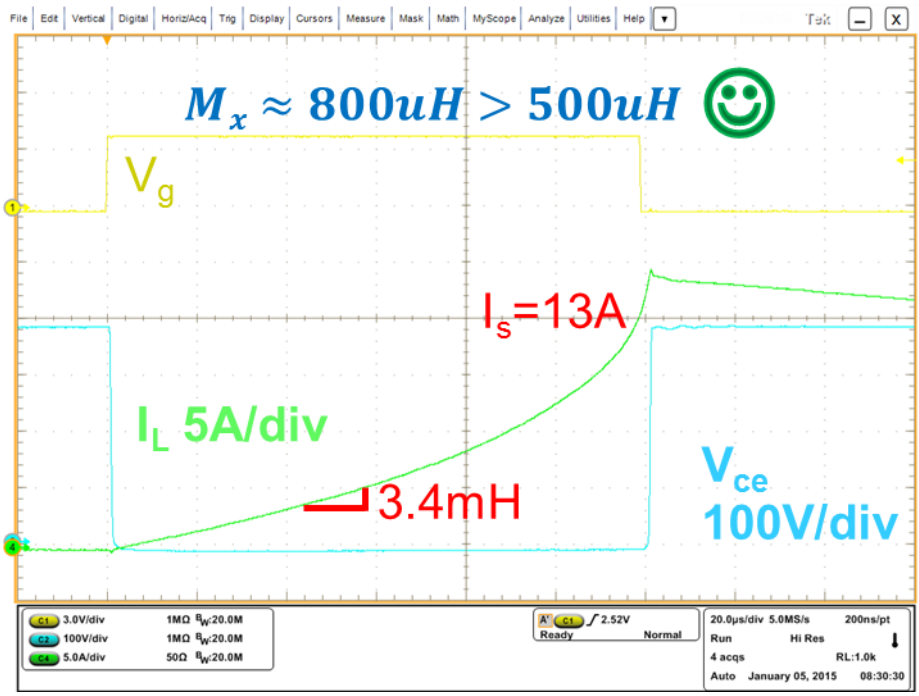

Figure 4.31 Test result for M_x with single pulse test

With M_y known from the first step of the test, the mutual inductance M_x can be calculated, which is around 800μH. Considering the current ripple requirement, 800μH is high enough for inductor current ripple reduction.

With the above two steps, both mutual inductance M_x and M_y are verified to meet the inductor current ripple and output current ripple reduction requirements.

4.7 Controller Design and Experiment Result of the Converter

For the three-level DC/DC converter with integrated coupled inductors, the proper controller should be designed first based on the small-signal model before the hardware experiment.

For the paralleled phase legs, the small-signal model is derived by inserting three-terminal switch model. As shown in Figure 4.32, there are four three-terminal switches, and each of them can be replaced with the small-signal model for three-terminal switch in Figure 4.33. It should be noted that two assumptions are made for modeling. 1). all the parasitic is neglected. 2). the converter works under balanced neutral-point voltage and inductor current sharing condition,

$$V_{po} = V_{on} = \frac{V_{dc}}{2} \tag{4.33}$$

$$I_{La} = I_{Lb} = I_{Lc} = I_{Ld} = \frac{I_o}{2} \tag{4.34}$$

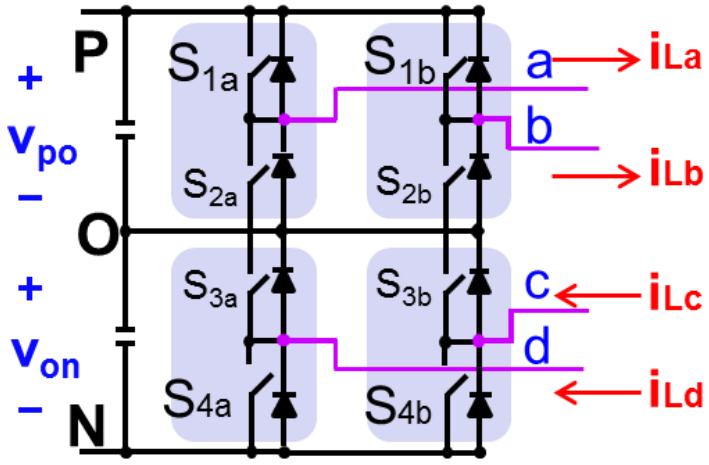

Figure 4.32 Paralleled phase legs

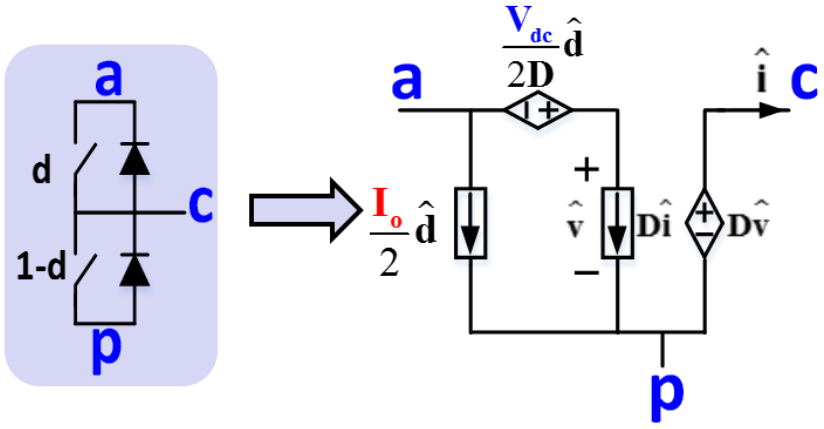

Figure 4.33 Small-signal model for three-terminal switch

By applying KVL and KCL, the complete small-signal model of the converter can be much simplified, as is shown in Figure 4.34. Considering that all parameters in the integrated coupled inductors are symmetrical as shown in (4.4), the open-loop control-to-output transfer function can be derived as,

$$\frac{\hat{i}_o}{d} = \frac{V_{dc}}{R_O} \frac{1+\frac{s}{s_z}}{1+\frac{s}{w_0 Q}+\frac{s^2}{w_0^{\,2}}} \tag{4.35}$$

$$\omega_0 = \frac{1}{\sqrt{L_{eq} C_O}} \qquad Q = R_O \sqrt{\frac{C_O}{L_{eq}}} \qquad s_z = \frac{1}{C_O R_O} \tag{4.36}$$

$$L_{eq} = 4M_y \tag{4.37}$$

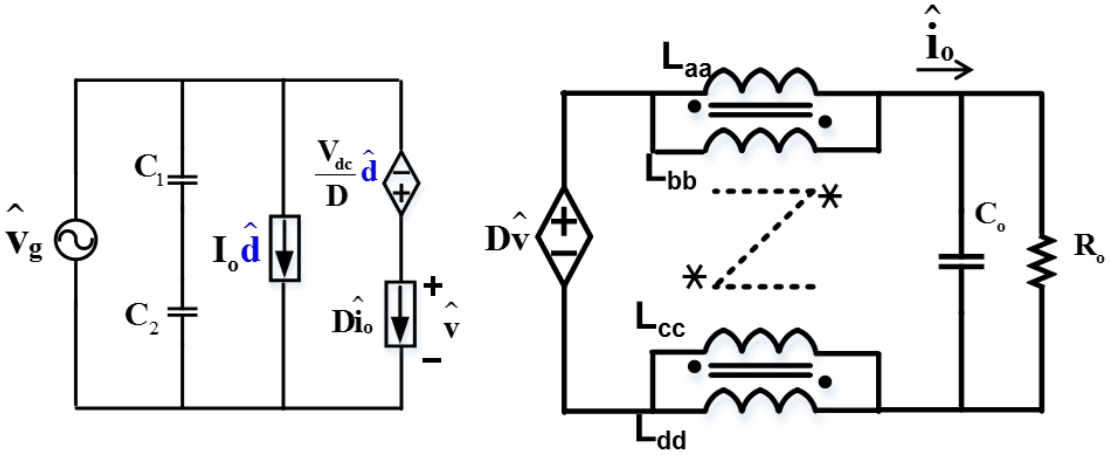

Figure 4.34 Complete small-signal model of the converter

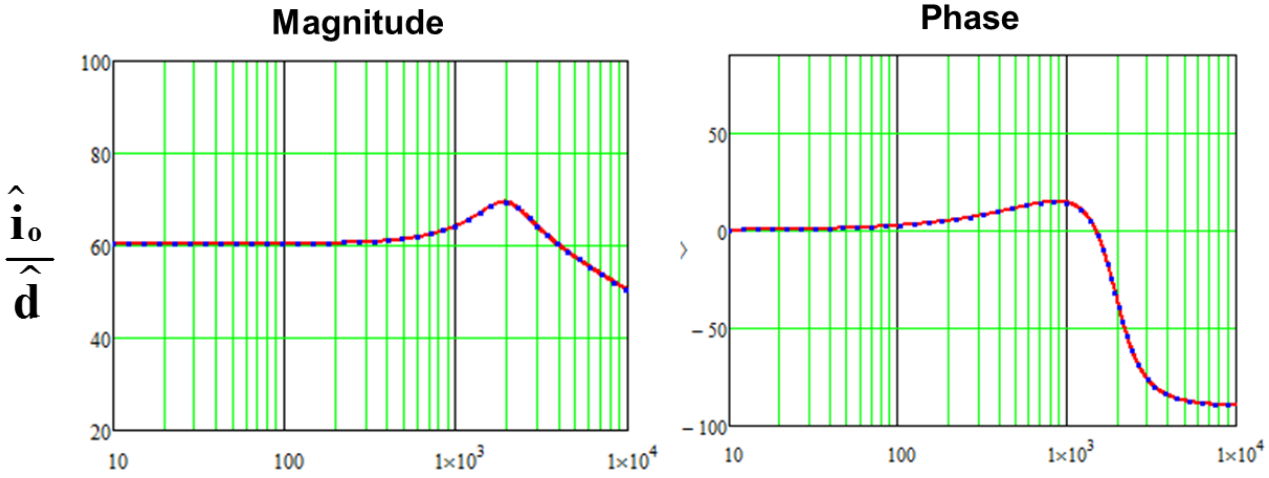

Figure 4.35 Open-loop control-to-output current transfer function

The derived small-signal model is verified in the bode plot Figure 4.35. The solid red line represents the modeling derivation result, while the dash blue line represents the SIMPLIS simulation result. The converter parameters are, input voltage V_{in}=1200V, duty ratio D=0.4,

switching frequency f_{sw}=20kHz, equivalent output inductance L_{eq}=60μH, and output capacitor Co=100μF. Clearly, the result from two curves matches with each other up to half of the switching frequency.

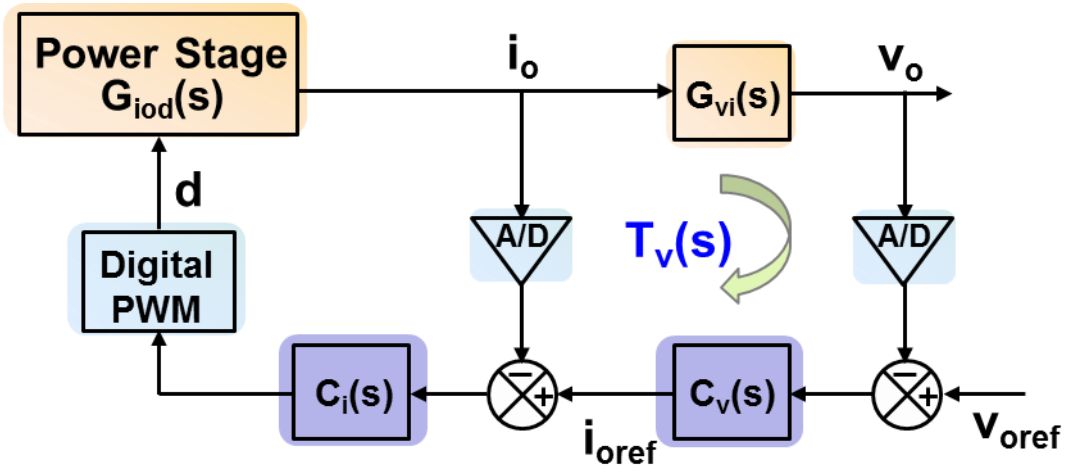

Figure 4.36 Control loop diagram

For the three-level DC/DC converter for renewable energy systems, both output current and voltage loop should be built based on application requirements. In the control loop diagram in Figure 4.36, both inner current loop and outer voltage loop are considered. For inner current loop, type-III compensator is adopted, with designed bandwidth BW=500Hz, phase margin PM=70degree, and gain margin GM=8dB. For outer voltage loop, only an integrator is required for compensation, with designed BW=100Hz, PM=74degree and GM=18dB. The corresponding bode plot of designed loop gain are shown in Figure 4.37 and Figure 4.38, respectively. 1.5Tsw digital delay is considered in the control loop design caused by digital PWM delay and computational delay in the DSP.

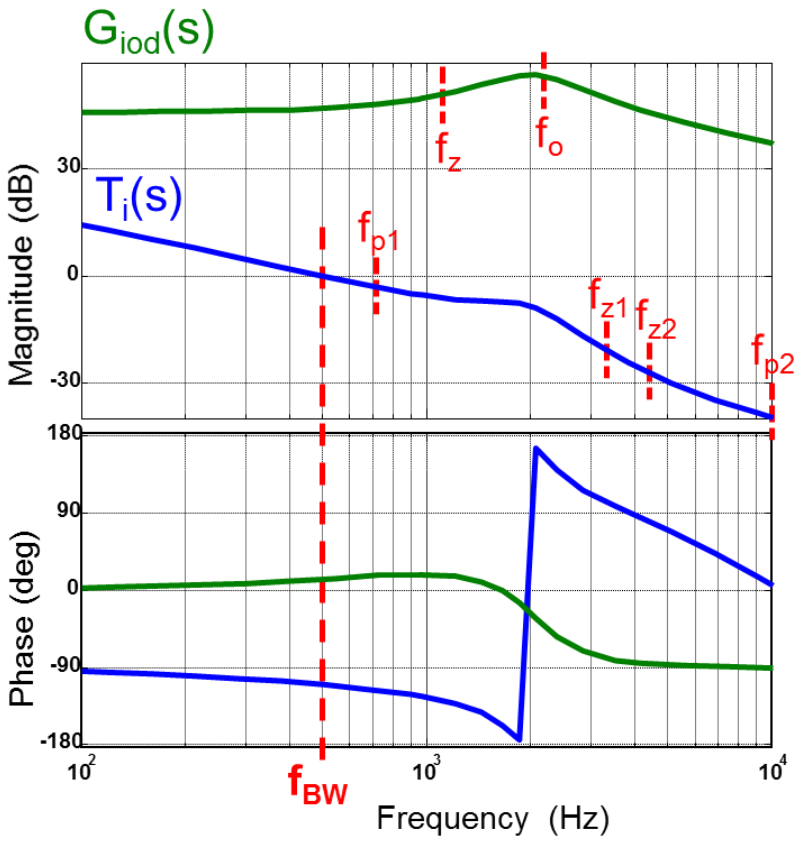

Figure 4.37 Inner current loop gain bode plot

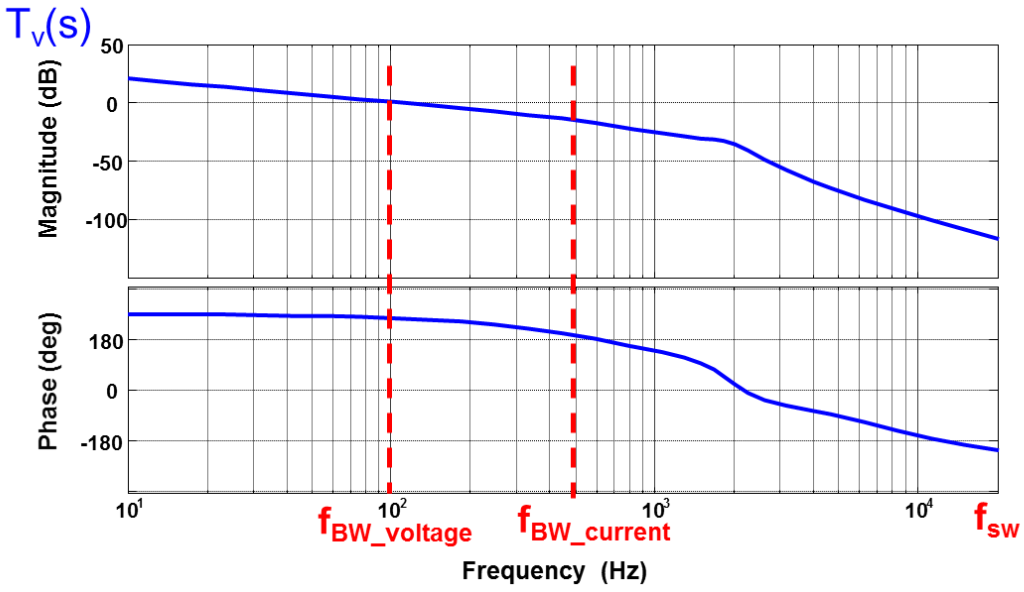

Figure 4.38 Outer voltage loop gain bode plot

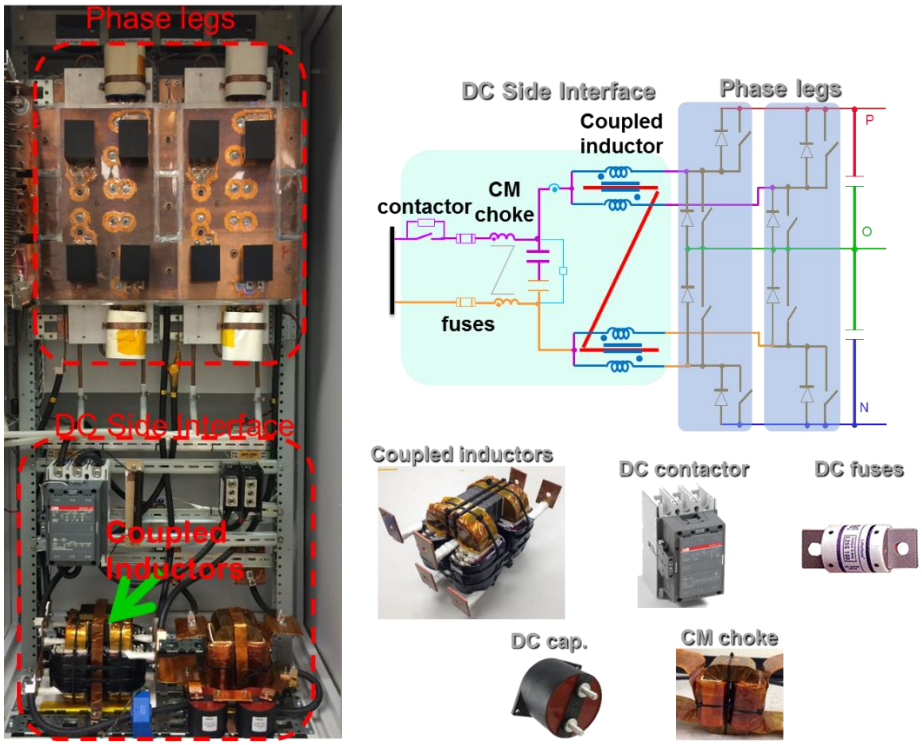

Figure 4.39 Hardware overview for three-level DC/DC Converter

The integrated coupled inductors are tested with three-level DC/DC converter hardware, as shown in Figure 4.39. The two phase legs constitute the two three-level buck converter, using 1200V/400A IGBT modules from Semikron. N-type interleaving is applied to reduce the output current ripple. DC contactor and DC fuses are also applied for protection. The experimental setup is shown in Figure 4.40.

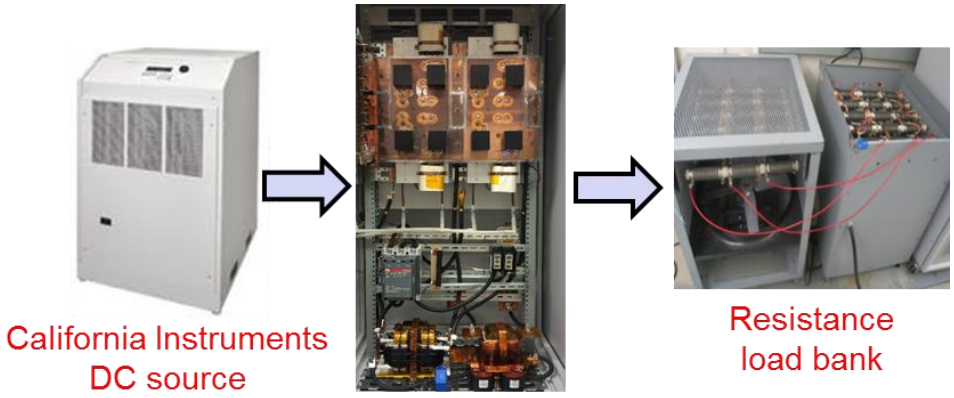

Figure 4.40 Experimental setup

The step response in Figure 4.41 and Figure 4.42 is tested at scaled down power rating (1/5). Figure 4.41 shows the result with only current loop closed, and Figure 4.42 gives the result with both inner current loop and outer voltage loop closed. The input voltage is V_{in}=240V and load resistance is R_o=1.2Ω. Output current steps from 50A to 84A (power steps from 3kW to 8kW), while the output voltage steps from 71V to 100V (power steps from4kW to 8kW). Clearly there is no obvious peaking and the transient response is stable.

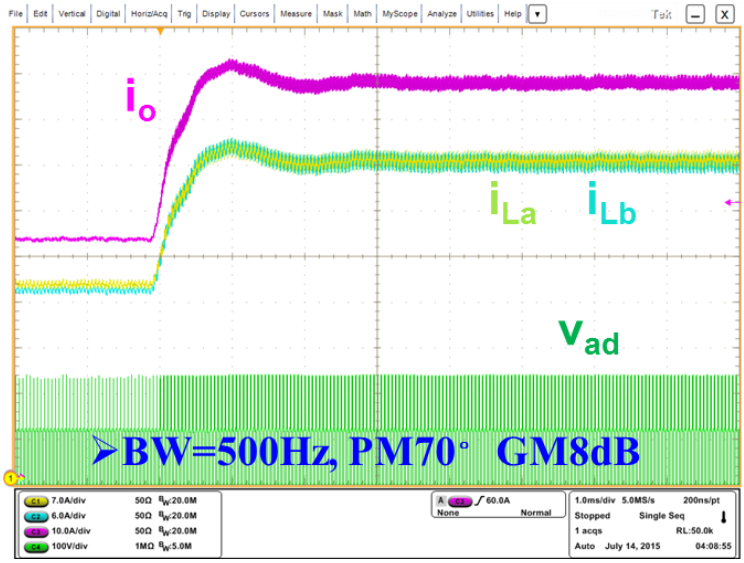

Figure 4.41 Current loop control step response

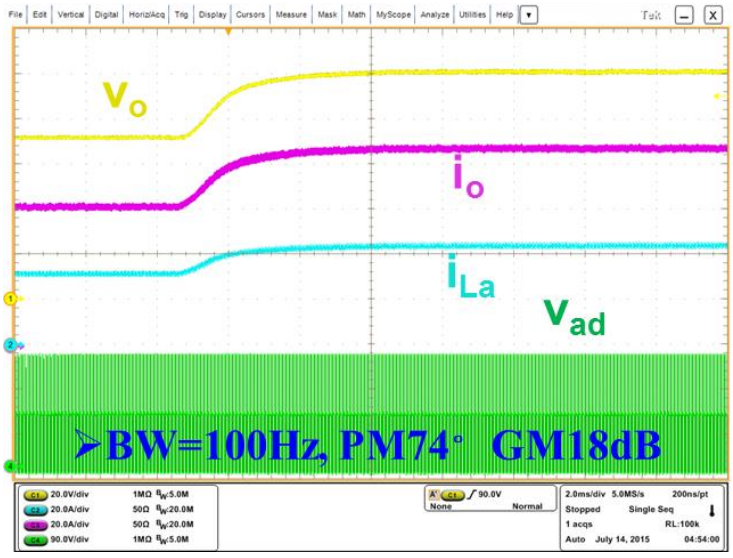

Figure 4.42 Voltage loop control step response

The simulation result in Figure 4.43 is used to compare the inductor current waveform with the hardware test result. For the test result in Figure 4.44, the operation condition is the input voltage V_{in}=1000V, output voltage V_o=600V, duty ratio D=0.6, output voltage I_o=27A, power rating P=16kW, and switching frequency f_{sw}=20kHz.

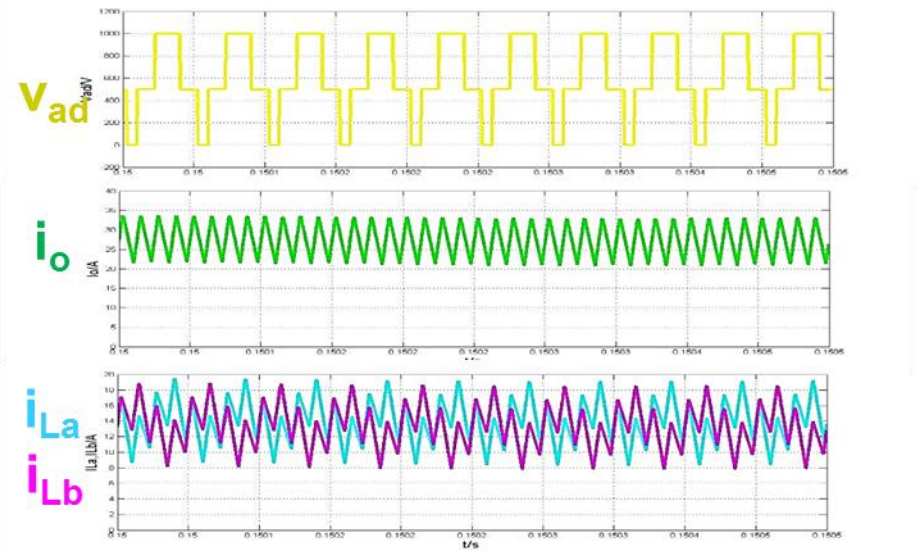

Figure 4.43 Simulation waveform of three-level DC/DC converter with integrated coupled inductors

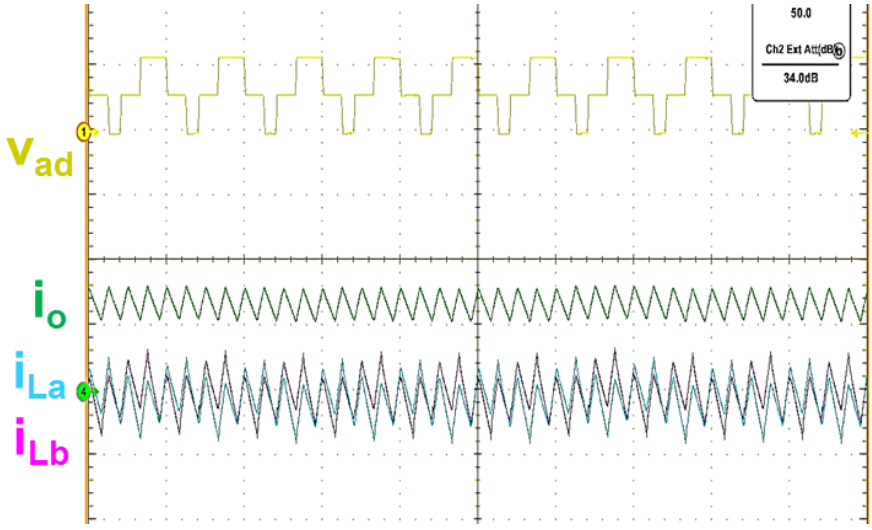

Figure 4.44 Hardware test result waveform of three-level DC/DC converter with integrated coupled inductors

Clearly, the test waveform matches with the simulation result. The phase leg output voltage v_{ad} is a three-level waveform and the inductor current i_{La} and i_{Lb} has a zig-zag shape due to the non-linear inductance within one switching cycle.

4.8 Summary

By using the equivalent inductance analysis method, this chapter provides a systematical way to design the integrated coupled inductors fulfilling the current ripple requirements.

Since two coupled inductors are required for paralleled three-level DC/DC converter, a novel integrated coupled inductors structure is adopted to reduce the size of the magnetic components. Instead of the conventional negatively coupled inductors, now the leakage flux are positively coupled together and there are two types of coupling effects in the integrated coupled inductors. The negative coupling effect is aimed at reducing the circulating current between two phase legs, while the positive coupling effect is aimed at increasing the output inductance and reduce the output current ripple.

Similar to the conventional coupled inductors, the integrated coupled inductors case has the characteristics of non-linear inductance within one switching cycle. Based on the equivalent inductance analysis, the relationship between the current ripple and equivalent inductance is built, and it provides a clear method to determine the negative and positive coupled mutual inductance desired for inductor current ripple and output current ripple reduction targets. A prototype of integrated coupled inductors is built with nano-crystalling C-C core and powder block core, with air gaps finely designed to meet the inductance value requirements.

Comparing the solution with the two coupled inductors case for three-level DC/DC converter, the integrated coupled inductors case has the benefit of greatly increased power density.

Under the identical current ripple performance condition, the case with integrated coupled inductors can reduce the size of the magnetics by almost fifty percent.

A paralleled three-level DC/DC converter platform is built and the fabricated integrated coupled inductors are tested in hardware experiment to verify its function within the converter.

Chapter 5 Conclusion and Future Work

5.1 Conclusion

The multi-phase three-level DC/DC converter with integrated coupled inductors is demonstrated and analyzed in this paper to elaborate its benefit as a high-power, high-voltage converter for renewable energy applications including the battery storage system, PV farm and electric vehicle charge station. Together with a three-phase three-level AC/DC inverter stage, the two-stage three-level power conversion system has the benefit of high power density, high efficiency with modularized structure and bi-directional power flow.

In this paper, a two-phase three-level structure is adopted to fulfill the high power rating requirement for DC/DC stage. Compared with the conventional non-interleaving case, interleaving for the two phase legs has the ripple cancelling effect, and output current ripple of the converter can be reduced. From the analysis in Chapter 2, N-type interleaving is more advantageous than non-interleaving and Z-type interleaving methods in terms of current ripple and common-mode noise. To solve the issue of huge circulating current between two phase legs caused by interleaving, usually negative coupled inductors are applied together with the interleaving method to suppress circulating current and maintain good ripple performance.

Due the negative coupling, the inductor becomes a non-linear one within one switching cycle, and equivalent inductance can be defined with different inductor voltage combinations. Through the inductor current and output waveform analysis, the relationship between the equivalent inductance and current ripple can be built, and coupling can be designed based on the inductor current ripple and output current ripple targets. With the same output current ripple, the

strong negative coupling effect is preferred to reduce the inductor current ripple when comparing with the non-coupling inductor case.

Since two coupled inductors are needed for the two-phase three-level DC/DC converter, the integrated coupled inductors can be adopted to replace the two coupled inductors, thus further increasing the power density of the converter. Besides the negative coupling effect to suppress the circulating current between phase legs, the leak flux now are positively coupled together between the four arm inductors. And again by the equivalent inductance analysis, the relationship between the coupling effect and maximum current ripple is clarified, and the two types of coupling effects within the integrated coupled inductors can be directly designed based on the current ripple requirements.

An integrated coupled inductors prototype is designed and assembled with given converter operation conditions and current ripple requirements. From both the inductance value measurement and the converter experiment, the function of integrated coupled inductors is verified in terms of inductor current ripple and output current ripple reduction. Comparing the non-interleaving, non-coupling solution for two-phase three-level DC/DC converter, N-type interleaving with integrated coupled inductors can reduce the volume of the magnetic component by almost fifty percent, given the same current ripple performance requirements.

5.2 Future Work

This work demonstrates a solution for high-power, high-voltage DC/DC conversion using multi-phase three-level DC/DC converter with interleaving method and integrated coupled inductors. To further extend the depth for this research area, the following topics can be continued:

1). Study the design of integrated coupled inductors with different magnetic materials to optimize its power density, performance and efficiency.

2). Expand the concept of integrated magnetics to three-phase three-level interleaved DC/DC converter. A systematical magnetic design method using equivalent inductance analysis can be developed for three-phase interleaving, or even for four-phase interleaving DC/DC conversion.

3). Study the control strategy for the three-level power conversion system, including both the DC/AC inversion stage and the DC/DC conversion stage, and the possible issues for the interaction of the two stages in control.

References

[1] Yu Du, Xiaohu Zhou, Sanzhong Bai, Srdjan Lukic and Alex Huang, “Review of non-isolated bi-directional DC/DC converters for plug-in hybrid electric vehicle charge station application at municipal parking decks”, Applied Power Electronics Conference and Exposition (APEC), 2010 Twenty-Fifth Annual IEEE

[2] Kevork Haddad, “Three Level DC/DC Converters as Efficient Interface in Two Stage PV Power Systems”, Energytech, 2012 IEEE

[3] A. Lachichi, “DC/DC Converters for High Power Application: A Survey”, Electric Power and Energy Conversion Systems (EPECS), 2013 3rd International Conference on

[4] M. Hirakawa, Y. Watanabe, M. Nagano, K. Andoh, S. Nakatomi, S. Hashino, Honda R&D Co., Ltd, “High Power DC/DC Converter using Extreme Close-Coupled Inductors aimed for Eletric Vehicles”, IPEC 2010

[5] Kansuke Fuji, Peter Koellensperger, Rik W. De Doncker, “Characterization and Comparison of High Blocking Voltage IGBTs and IEGTs under Hard- and Soft-Switching Conditions”, Power Electronics Specialists Conference, 2006. PESC '06. 37th IEEE

[6] Akira Nabae, Isao Takahashi, Hirofumi Akagi, “A New Neutral-Point-Clamped PWM Inverter”, IEEE Transactions on Industry Applications, 1981

[7] J. Renes Pinheiro and Ivo Barbi, “The three-level ZVS PWM converter-a new concept in high voltage DC-to-DC conversion”, Industrial Electronics, Control, Instrumentation, and Automation, 1992. Power Electronics and Motion Control., Proceedings of the 1992 International Conference on

[8] Hideyuki Okui and Hisaichi Irie, “New NPC multi-level four-quadrant DC/DC converter controlled by the integrated-voltage-control method”, Power Conversion Conference - Nagaoka 1997., Proceedings of the (Volume:2)

[9] T.A. Meynard, H. Foch, “Multi-level conversion: high voltage choppers and voltage-source inverters”, Power Electronics Specialists Conference, 1992. PESC '92 Record., 23rd Annual IEEE

[10] Ke Jin, Mengxiong Yang and Xinbo Ruan, “Three-Level Bi-Directional Converter — A Novel DC/DC Converter Suitable for Fuel Cell Power System”, Power Electronics Specialists Conference, 2006. PESC '06. 37th IEEE

[11] Zhang, M.T., et al. “Single-phase three-level boost power factor correction converter”. in Applied Power Electronics Conference and Exposition, 1995. APEC '95. Conference Proceedings 1995., Tenth Annual. 1995. Dallas, TX.

[12] Petar J. Grbovic, et al. “A Bidirectional Three-Level DC–DC Converter for the Ultracapacitor Applications”, Industrial Electronics, IEEE Transactions on (Volume:57 , Issue: 10), 2010

[13] Fang Zheng Peng, “A Generalized Multilevel Inverter Topology with Self Voltage Balancing”, Industry Applications, IEEE Transactions on (Volume:37 , Issue: 2)

[14] Xinbo Ruan, Bin Li, and Qianhong Chen, “Three-level converters-a new approach for high voltage and high power DC-to-DC conversion”, Power Electronics Specialists Conference, 2002. pesc 02. 2002 IEEE 33rd Annual (Volume:2)

[15] Xinbo Ruan, Bin Li, Qianhong Chen, Siew-Chong Tan, Chi K. Tse, “Fundamental Considerations of Three-Level DC/DC Converters: Topologies, Analyses, and Control”, Circuits and Systems I: Regular Papers, IEEE Transactions on (Volume:55 , Issue: 11)

[16] Fan Zhang, Fang Z. Peng and Zhaoming Qian, “Study of Multilevel Converters in DC/DC Applications”, Power Electronics Specialists Conference, 2004. PESC 04. 2004 IEEE 35th Annual (Volume:2)

[17] Leopoldo G. Franquelo, Jose I. Leon, Samir Kouro and Marcelo Perez, “Multilevel Converteres: Present and Future”, tutorial on IECON 2012

[18] Sergio Busquets-Monge, Salvador Alepuz, Josep Bordonau, “A Bidirectional Multilevel Boost–Buck DC–DC Converter”, Power Electronics, IEEE Transactions on (Volume:26 , Issue: 8)

[19] Fang Z. Peng, Fan Zhang and Zhaoming Qian, “A Novel Compact DC/DC Converter for 42 V Systems”, Power Electronics Specialist Conference, 2003. PESC '03. 2003 IEEE 34th Annual (Volume:1)

[20] Wei Qian, Honnyong Cha, Fang Zheng Peng and Leon M. Tolbert, “55-kW Variable 3X DC/DC Converter for Plug-in Hybrid Electric Vehicles”, Power Electronics, IEEE Transactions on (Volume:27 , Issue: 4)

[21] Liyu Yang, Tiefu Zhao, Jun Wang and Alex Q. Huang, ”Design and Analysis of a 270kW Five-level DC/DC Converter for Solid State Transformer Using 10kV SiC Power Devices”, Power Electronics Specialists Conference, 2007. PESC 2007. IEEE

[22] Levy F. Costa, Samir A. Mussa and Ivo Barbi, “Multilevel buck DC/DC converter for high voltage application”, Industry Applications (INDUSCON), 2012 10th IEEE/IAS International Conference on

[23] Levy F. Costa, Samir A. Mussa and Ivo Barbi, “Multilevel boost DC/DC converter derived from basic double-boost converter”, Power Electronics and Applications (EPE), 2013 15th European Conference on

[24] Levy F. Costa, Samir A. Mussa and Ivo Barbi, “Steady-state analysis of a 5-level bidirectional buck+boost DC/DC converter”, Industrial Electronics Society, IECON 2013 - 39th Annual Conference of the IEEE

[25] Levy F. Costa, Samir A. Mussa and Ivo Barbi, “Multilevel Buck/Boost-type DC/DC Converter for High Power and High Voltage Application”, Industry Applications, IEEE Transactions on (Volume:PP , Issue: 99)

[26] David Reusch, Fred C. Lee, Ming Xu, “Three Level Buck Converter with Control and Soft Startup”, Energy Conversion Congress and Exposition, 2009. ECCE 2009. IEEE

[27] Yang Jiao, Sizhao Lu, Fred C. Lee, “Switching Performance Optimization of a High Power High Frequency Three-Level Active Neutral Point Clamped Phase Leg”, Power Electronics, IEEE Transactions on (Volume:29 , Issue: 7), 2014

[28] Robert M. Cuzner, Ashish R. Bendre, Peter J. Faill, Boris Semenov, “Implementation of a Non-isolated Three Level DC/DC Converter Suitable for High Power Systems”, Industry Applications Conference, 2007. 42nd IAS Annual Meeting. Conference Record of the 2007 IEEE

[29] Antonio Coccia, Franscisco Canales, “3-level interleaved boost converter assembly”, European patent, EP 2244367 A1, 2010

[30] Sizhao Lu, Mingkai Mu, Yang Jiao and Fred C. Lee, Zhengming Zhao, “Coupled Inductors in Interleaved Multiphase Three-Level DC–DC Converter for High-Power Applications”, IEEE Transactions on Power Electronics (Volume: 31, Issue: 1, Jan. 2016)

[31] Pit-leong Wong, Peng Xu, P. Yang, Fred C. Lee, “Performance improvements of interleaving VRMs with coupling inductors”, IEEE Transactions on Power Electronics (Volume: 16, Issue: 4, Jul 2001)

[32] Jinghai Zhou, “High Frequency, High Current Density Voltage Regulators”, dissertation, CPES, Virginia Tech, 2005

[33] Mingkai Mu, Fred C. Lee, Yang Jiao, Sizhao Lu, “Analysis and design of coupled inductor for interleaved multiphase three-level DC-DC converters”, Applied Power Electronics Conference and Exposition (APEC), 2015 IEEE

[34] Mingkai Mu, Fred C. Lee, “Comparison and selection of magnetic materials for coupled inductor used in interleaved three-level multi-phase DC-DC converters”, Energy Conversion Congress and Exposition (ECCE), 2015 IEEE

Appendix A

Appendix A gives the equivalent inductance derivation result within the whole duty ratio range for two-phase interleaved three-level DC/DC converter with coupled inductors in Chapter 3.

For 0<D<0.25, three different equivalent inductances L_{eq2}, L_{eq4}, L_{eq5} appear.

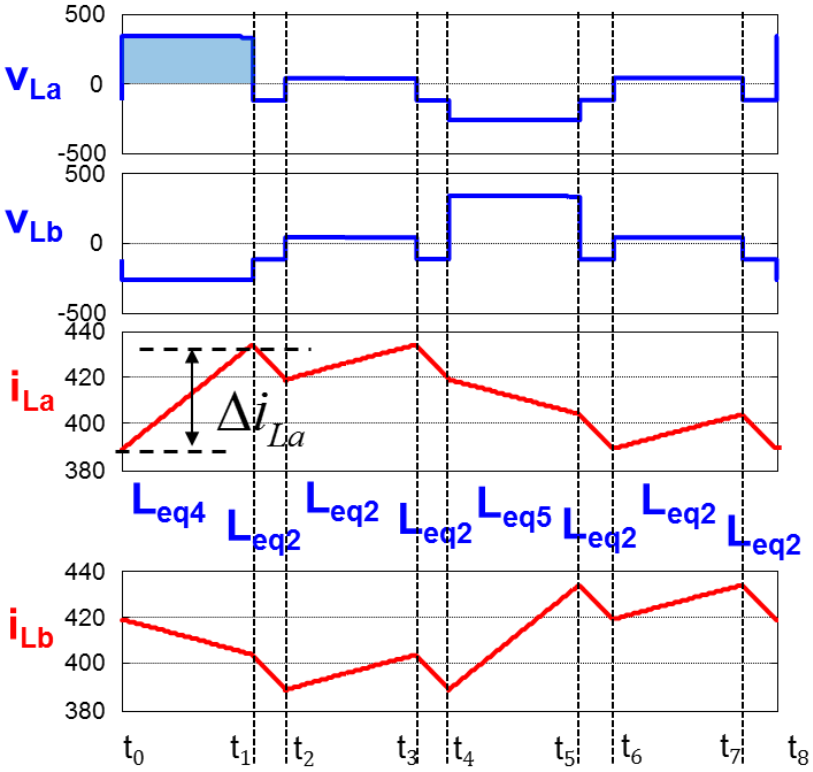

Figure A.1 Inductor current waveform with coupled inductors, 0<D<0.25

$$L_{eq2} = L - M_{ab}$$

$$L_{eq4} = \frac{(L^2 - M_{ab}{}^2)}{L - \frac{(1+4D)}{(3-4D)} M_{ab}}$$

$$L_{eq5} = \frac{(L^2 - M_{ab}{}^2)}{L - \frac{(3-4D)}{(1+4D)} M_{ab}}$$

The inductor current ripple is determined in the first time interval t_0-t_1, and only L_{eq4} determines the ripple value.

$$\Delta i_{La} = \frac{\langle v_{La} \rangle_{T1}}{L_{eq4}}$$

For 0.25<D<0.5, five different equivalent inductances L_{eq1}, L_{eq2}, L_{eq3}, L_{eq4}, L_{eq5} appear.

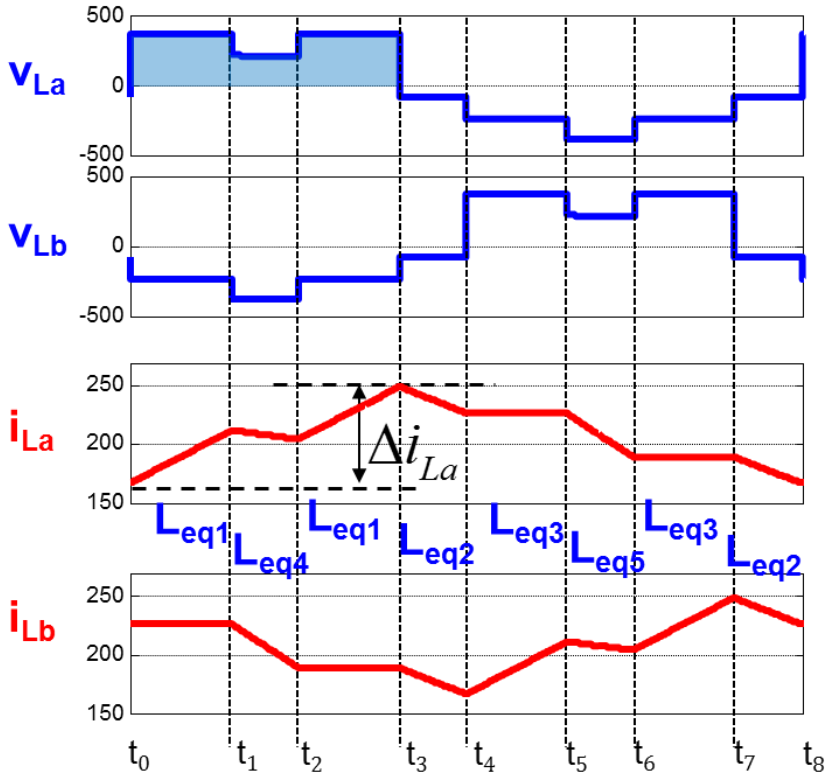

Figure A.2 Inductor current waveform with coupled inductors, 0.25<D<0.5

$$L_{eq1} = \frac{(L^2 - M_{ab}{}^2)}{L - \frac{D}{1-D} M_{ab}}$$

$$L_{eq3} = \frac{(L^2 - M_{ab}{}^2)}{L - \frac{1-D}{D} M_{ab}}$$

The inductor current ripple is determined in the first three time intervals t_0-t_3 together, and L_{eq1} and L_{eq4} determine the ripple value.

$$\Delta i_{La} = \frac{\langle v_{La} \rangle_{T1}}{L_{eq1}} + \frac{\langle v_{La} \rangle_{T2}}{L_{eq4}} + \frac{\langle v_{La} \rangle_{T3}}{L_{eq1}}$$

For 0.5<D<0.75, five different equivalent inductances L_{eq1}, L_{eq2}, L_{eq3}, L_{eq6}, L_{eq7} appear.

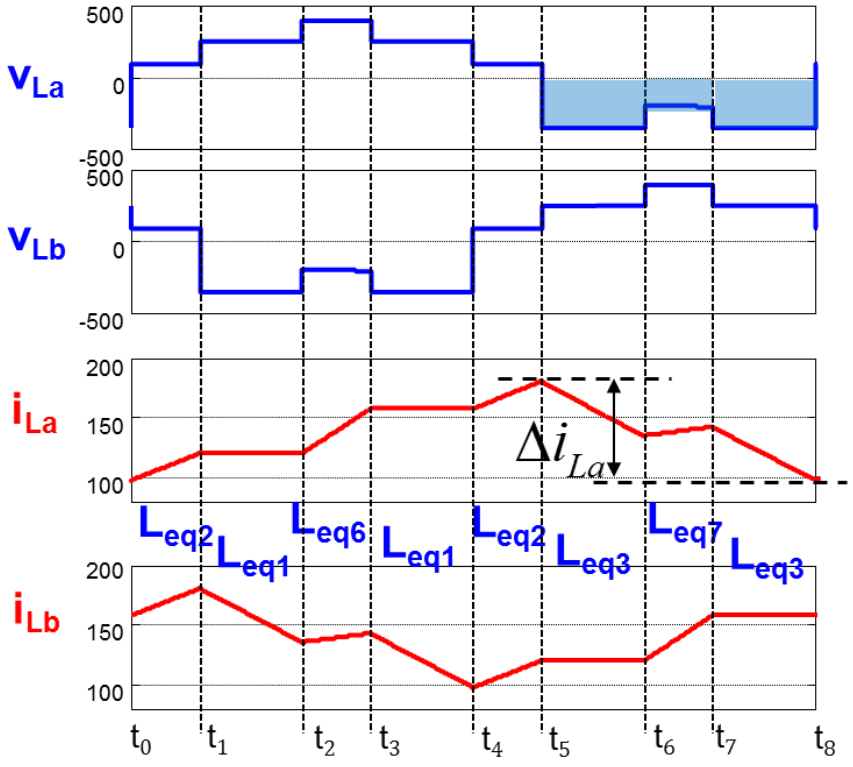

Figure A.3 Inductor current waveform with coupled inductors, 0.5<D<0.75

$$L_{eq6} = \frac{(L^2 - M_{ab}{}^2)}{L - \frac{(4D-1)}{(5-4D)} M_{ab}}$$

$$L_{eq7} = \frac{(L^2 - M_{ab}{}^2)}{L - \frac{(5-4D)}{(4D-1)} M_{ab}}$$

The inductor current ripple is determined in the last three time intervals t_5-t_8, and L_{eq3} and L_{eq7} determine the ripple value together.

$$\Delta i_{La} = \frac{\langle v_{La} \rangle_{T6}}{L_{eq3}} + \frac{\langle v_{La} \rangle_{T7}}{L_{eq7}} + \frac{\langle v_{La} \rangle_{T8}}{L_{eq3}}$$

For 0.75<D<0.1,

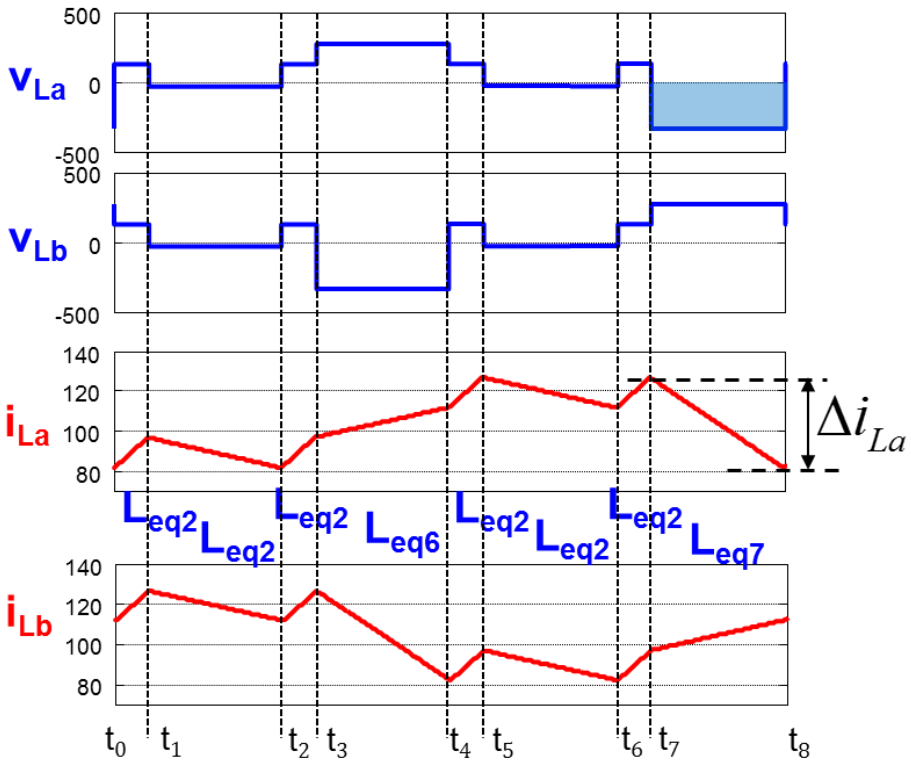

Figure A.4 Inductor current waveform with coupled inductors, 0.75<D<0.1

The inductor current ripple is calculated in the last time interval t_7-t_8, and only L_{eq7} determines the ripple value.

$$\Delta i_{La} = \frac{\langle v_{La} \rangle_{T8}}{L_{eq7}}$$

Note that L_{eq6} and L_{eq7} are two equivalent inductances existing in D>0.5 case only, and L_{eq4} and L_{eq5} only exist in D<0.5 case only.